MicroRNA-induced polarization of microglia and macrophages after focal cerebral ischemia

Inaugural-Dissertation

zur

Erlangung des Doktorgrades

der Mathematisch-Naturwissenschaftlichen Fakultät

der Universität zu Köln

vorgelegt von

Somayyeh Hamzei Taj

aus Tehran, Iran

MAX PLANCK INSTITUTE
FOR METABOLISM RESEARCH
COLOGNE

Köln, den 24. Mai 2016

Berichterstatter: PD. Dr. Heike Endepols

Prof. Dr. Wolfgang Walkowiak

Prof. Dr. Mathias Hoehn

Tag der mündlichen Püfung: 24. Mai 2016

Abstract……8

Kurzzusammenfassung……9

1.Introduction……11

1.1 Stroke……12

1.1.1 Pathophysiology……13

1.2 Cells of the nervous system and their function……14

1.2.1 The role of the immune cells in ischemic stroke……15

1.2.1.1 Microglia and Macrophages after CNS damage……16

1.2.1.2 Dynamic polarization of microglia and macrophages after CNS damage...18

1.2.2 The role of astrocytes in ischemic stroke……20

1.2.2.1 Phenotypic Polarization of astrocytes……21

1.2.3 Modulating the polarization of microglia and macrophages……22

1.2.4 The role of microRNAs on modulating the neuro-inflammation……24

1.2.4.1 The role of miR-124 on modulating the neuroinflammation……25

2.Material and Methods……26

2.1 Consumables……27

2.2 In-vivo experiments……28

2.2.1 Animal……28

2.2.2 Experimental groups……28

2.2.3 Middle cerebral artery occlusion (MCAO)……30

2.2.4 Intracranial injection of liposomated miR-124……31

2.2.5 Modified neurological deficit scores……..……..32

2.2.6 Magnetic resonance imaging……..……..33

2.2.6.1 Evaluation of lesion size and T2 time, based on T2 maps analysis……....33

2.3 Immunohistochemistry……..……..35

2.3.1 Quantitative immunohistochemical analysis of microglia/macrophages polarization……..36

2.3.2 Quantitative immunohistochemical analysis of glial scar……..37

2.4 Statistics……38

3.Results……39

3.1 In-vivo MR imaging……40

3.1.1 Characterization of ischemic lesion after MCAO……..……..40

3.1.2 Comparison of ΔT2 time and T2 lesion volume……41

3.2 Ex-vivo fluorescence imaging……..……43

3.2.1 Morphology and kinetics of microglia and macrophages after stroke……43

3.2.2 The effect of miR-124 on microglia and macrophages after stroke……..…45

3.2.2.1 The kinetics of microglia and macrophages……..45

3.2.2.2 The polarization of microglia and macrophages in the first experimental protocol – early injection and early observation……..47

3.2.2.3 The polarization of microglia and macrophages in the second experimental protocol – early injection and late observation……..……53

3.2.2.4 The polarization of microglia and macrophages in the third experimental protocol - late miR-124 injection……..……..57

3.2.2.5 Comparison of the ratio of pro-inflammatory (M1) to anti-inflammatory (M2) phenotype in all three experimental protocols……60

3.2.3 The effect of miR-124 on neuronal survival after stroke……62

3.2.3.1 Different morphology of NeuN positive cells after stroke……62

3.2.3.2 Different morphology of NeuN positive cells after stroke……63

3.2.3.3 The effect of the late intracranial injection of miR-124 on neuronal survival after stroke……65

3.2.4 The effect of miR-124 on the glial scar after stroke……67

3.2.4.1 Different morphology of the GFAP positive cells after stroke……67

3.2.4.2 The effect of intracranial miR-124 injection on the glial scar development after stroke……68

3.2.5 The effect of miR-124 on functional recovery after stroke……70

3.3 Correlation between the expression of M1/M2 markers by Iba-1+ cells and mNDS……72

3.4 Correlation between the expression of M1/M2 markers by Iba-1+ cells and neuronal survival……74

4.Discussion……76

4.1 miR-124 modulates the polarization of microglia and macrophages in the sub-acute phase of ischemic stroke……77

4.1.1 The effect of the early administration of miR-124……77

4.1.2 The effect of late administration of miR-124……81

4.2 miR-124 exerts a neuroprotective effect after ischemic stroke……82

4.3 miR-124 performs its neuroprotective effect via affecting the glial scar after ischemic stroke……85

5. Summary……87

6. Conclusion and outlook……88

References……89

Appendix……101

List of abrreviations……102

List of Figures……105

Publications……108

Acknowledgement……109

Declaration of Academic Honesty……110

Curriculum Vitae……111

Abstract

Stroke is the second-leading global cause of death and disability. The development of the stroke-induced damage is dramatically affected by the immune system. The CNS resident microglia and infiltrated macrophages are key players in the local and systemic inflammatory responses after stroke. Both microglia and macrophages exert a dual role on the development of the stroke-induced damage. These cells phagocytize the cell debris and promote the neuronal restorative process. They also can aggravate the tissue damage and prevent CNS repair. Polarization of microglia and macrophages toward different phenotypes at different stages of injury - generally defined as destructive phenotype (M1) and protective phenotype (M2) - is the reason of this dual role. Thus, the necessity of precise adjustment of the polarization of microglia and macrophages has been highlighted recently in the treatment of neurodegenerative disorders.

This dissertation aims to investigate the role of the brain specific miR-124 in modulating the polarization of microglia and macrophages at different time points after middle cerebral artery occlusion (MCAO) in mice. For this purpose, we investigated the effect of the early and late administration of liposomated miR-124, at day 2 or 10 after MCAO, respectively, on the polarization of microglia and macrophages. The early treatment of miR-124 resulted in significantly increased number of M2-like polarized microglia and macrophages compared to control groups. In parallel, the same treatment led to significantly decreased number of M1-like polarized microglia and macrophages. Importantly, both early and late treatments of miR-124 ended in significantly lower pro-inflammatory (M1) to anti-inflammatory (M2) ratio after stroke. Further important findings by the early treatment include: (i) significantly increased neuronal survival that was positively correlated to the number of M2-like polarized microglia and macrophages, (ii) improved functional recovery related to the observed modulation of neuroinflammation from the detrimental to the protective mode, and (iii) significantly decreased lesion core, demarcated by reactive astrocytes, over time.

The results presented in this dissertation show that miR-124 treatment represents a novel option for immunomodulation and neuroprotection after ischemic stroke.

Zusammenfassung

Der ischämische Schlaganfall ist nicht nur die zweithäufigste Todesursache weltweit, sondern auch eine der Hauptursachen für körperliche Beeinträchtigungen im Erwachsenenalter. Das Ausmaß der durch den Schlaganfall hervorgerufenen Gewebeschädigung ist stark durch das Immunsystem geprägt. Die im Zentralnervensystem (ZNS) ansässigen Mikroglia und die aus dem Blutsystem infiltrierenden Makrophagen sind die Schlüsselzellen der lokalen und systemischen Entzündungsantwort nach dem ischämischen Schlaganfall. Sowohl Mikroglia als auch Makrophagen spielen in der Entwicklung der Gewebeschädigung eine duale Rolle. Zum einen phagozytieren sie Zelltrümmer und unterstützen neuroregenerative Prozesse, zum anderen sind diese Zellen in der Lage den Zustand der Gewebsschädigung zu verschlimmern und einer Regeneration des ZNS entgegenzuwirken. Die Polarisierung der Mikroglia/Makrophagen hin zu verschiedenen Phänotypen ist abhängig von der jeweiligen Phase der Gewebeschädigung. Der destruktive, proinflammatorische Phänotyp (M1) steht dabei dem protektiven, antiinflammatorischen Phänotyp (M2) gegenüber. Die Notwendigkeit einer zielgerichteten Regulierung der polarisierten Mikroglia/Makrophagen zum protektiven M2-Phänotyp wurde bereits mehrfach im Zusammenhang mit der Behandlung von neurodegenerativen Erkrankungen erwähnt.

In der vorliegenden Dissertation soll die immunregulierende und neuroprotektive Wirkung der microRibonukleinsäure-124 (miRNA-124) in Bezug auf die Polarisierung von Mikroglia/Makrophagen zu verschiedenen Zeitpunkten nach Verschluss der Arteria cerebri media (ACM) im Gehirn von Mäusen gezeigt werden. Zu diesem Zweck wurde die liposomierte miRNA-124 zu einem frühen Zeitpunkt (Tag 2) und zu einem späten Zeitpunkt (Tag 10) nach Verschluss der ACM verabreicht. Die Behandlung mit der miRNA-124 zu einem frühen Zeitpunkt resultierte dabei in einem signifikanten Anstieg in der Anzahl der M2-positiven Mikroglia/Makrophagen im Vergleich zur Kontrollgruppe. Gleichzeitig nahm die Anzahl der M1-positiven Mikroglia/Makrophagen signifikant ab. Im Wesentlichen resultierte die Behandlung mit der miRNA-124 zu beiden Zeitpunkten in einem geringeren Verhältnis von proinflammatorischen (M1) zu antiinflammatorischen (M2) Mikroglia/Makrophagen. Zu den weiteren Erkenntnissen einer frühzeitigen Behandlung im

Rahmen dieser Dissertation gehören: (i) eine signifikante Zunahme des neuronalen Überlebens, das zudem positiv mit der Anzahl der M2-positiven Mikroglia/Makrophagen korreliert, (ii) eine verbesserte funktionelle Erholung, welche in Verbindung mit den veränderten neuroinflammatorischen Ereignissen steht und (iii) ein signifikant verkleinertes Läsionsareal, welches durch reaktive Astrozyten zum gesunden Gewebe hin abgegrenzt wird.

Die Ergebnisse dieser Dissertation zeigen, dass die Verabreichung von miRNA-124 eine neue Möglichkeit zur Regulierung der Immunantwort und der Neuroprotektion im Rahmen der Behandlung des ischämischen Schlaganfalls darstellt.

Chapter 1

Introduction

1. Stroke

Currently, around 15 million people suffer a stroke each year worldwide, and with about 5 million deaths, stroke is the second most leading cause of death and long-term disability (Macrez et al., 2011). Stroke is characterized by a sudden loss of cerebral blood circulation, which leads to severe oxygen and glucose deprivation and brain damage. There are two types of strokes: hemorrhagic and ischemic. Hemorrhagic stroke is caused by the rupture of a blood vessel in the brain parenchyma or in the subarachnoid space. Ischemic strokes are characterized by the occlusion of major cerebral arteries and account for up 80% of all stroke cases (Deb et al., 2010).

Stroke results in long-lasting neurological deficits including sensory and motor dysfunction, paralysis, aphasia and altered memory or mental conditions (Fatahzadeh and Glick, 2006). In the past decades, noticeable progress has been achieved in understanding the stroke pathophysiology, especially in ischemic stroke. These advances have resulted in more than 1,000 neuroprotective molecules from experimental models and in the application of more than 250 clinical trials (Young et al., 2007). However, the implementation into effective therapies has failed despite all of these efforts. It is worth mentioning that induced reperfusion by tissue plasminogen activator, tPA, is still the exclusive acute pharmacological therapy (Macrez et al., 2011) and can be applied only within a few hours after stroke onset (Gravanis and Tsirka, 2008). Therefore, stroke is still one of the severe and frequent diseases, where further studies are needed for more effective and safe stroke therapies.

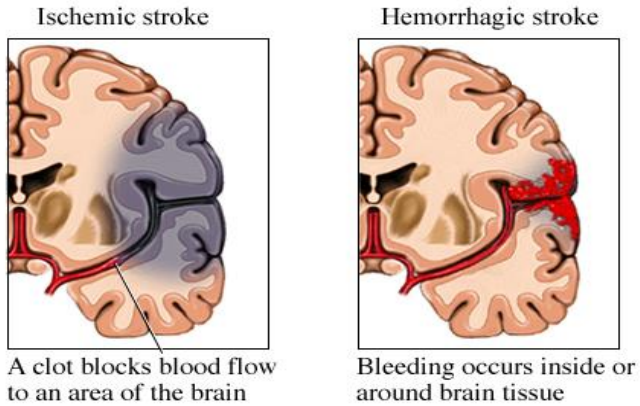

Figure 1.1 Different types of stroke. Schematic depiction of ischemic stroke (left), and hemorrhagic stroke (right), (Nucleus Communication., 2000).

1.1 Pathophysiology

The progressive loss of oxygen and glucose leads to a cascade of complex pathophysiological events, involving excitotoxicity mechanisms, oxidative stress, free radical production, ion imbalance, inflammatory processes and apoptosis (Figure. 1) (Deb et al., 2010). In addition, it results a deficit in the production of high energy phosphate compounds, such as ATP (Dirnagl et al., 1999). The failure of energy results in rapid anoxic depolarizations and irreversible cell death in the ischemic core (Mitsios et al., 2006). The collateral blood supply to the adjacent area preserves tissue from immediate cell death but this penumbra area is still vulnerable to later cell death. Incomplete restoration of ion gradients generates waves of peri-infarct depolarizations leading to excessive neurotransmitter release such as glutamate (Dirnagl et al., 1999). Excessive extracellular concentrations of glutamate, due to impaired glial re-uptake, triggers the accumulation of intracellular calcium (Iadecola and Anrather, 2011). Extreme intracellular calcium provokes several detrimental events as well as activation of lytic enzymes, mitochondrial dysfunction and oxidative stress (Moskowitz et al., 2010). Subsequent, free radicals are produced, which are strong destroyers of the cell membranes and DNA. Damaged endothelium breaks down the blood-brain barrier, leading to increased permeability and consequently to vasogenic edema (Durukan and Tatlisumak, 2007). Furthermore, neuronal cell death in the ischemic core triggers the specific recognition receptors such as toll like receptors, which recruit and activate over time the resident glial cells and cells of the peripheral immune system, including neutrophils, T cells, monocyte/macrophage cells and others ((Jin et al., 2010), (Kriz, 2006). Taking all together, the described events after stroke finally result in programmed cell death, apoptosis, which extends tissue damage in the ischemic penumbra ((Mitsios et al., 2006), (Ginsberg, 2003)).

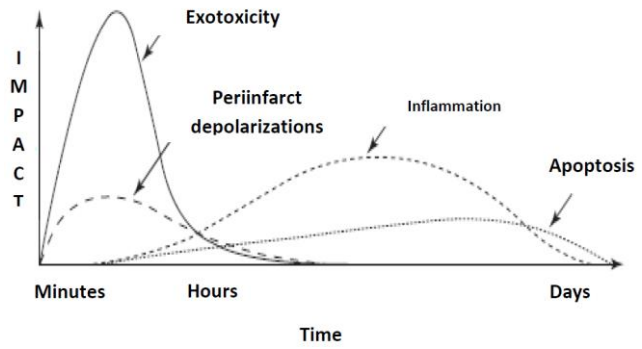

Figure 1.2 Events after cerebral ischemia. Excitotoxic mechanisms cause the lethal damage to neurons and glial cells in minutes after deficit in tissue perfusion. Following, the peri-infarct depolarization leads to enhanced tissue injury and promotes inflammation and apoptosis (Junior et al., 2014).

1.2 Cells of the nervous system and their function

The resident cells of the CNS, neurons and neuroglia, have a close interaction and do not act on their own (Burda and Sofroniew, 2014).

Neurons are the pivotal unit of the CNS. They have different morphology, electrical activation patterns, metabolic characteristics and neurotransmitter profiles. Based on these specificities they are categorized in interneurons, sensory and motor neurons, which exhibit distinct functions. Neurons connect to their surrounding environment in a network through synapses or gap junctions ((Shaham, 2005), (Paixao and Klein, 2010)).

Neuroglia, glia cells, are the most numerous cells of the CNS. According to morphological and molecular criteria, they are divided into: oligodendrocytes, astrocytes and microglia. Oligodendrocytes provide trophic support for neuron and equip the axons of neurons with myelin sheaths (Shaham, 2005). Astrocytes provide trophic support for neuron and have important role in neurotransmission, metabolite and electrolyte homeostasis, cell signaling, inflammation, and synapse modulation (Ricci et al., 2009). Microglia, the main resident immune cells of the CNS are involved in tissue homeostasis, developmental processes and neurodegenerative disorders (Benakis et al., 2014).

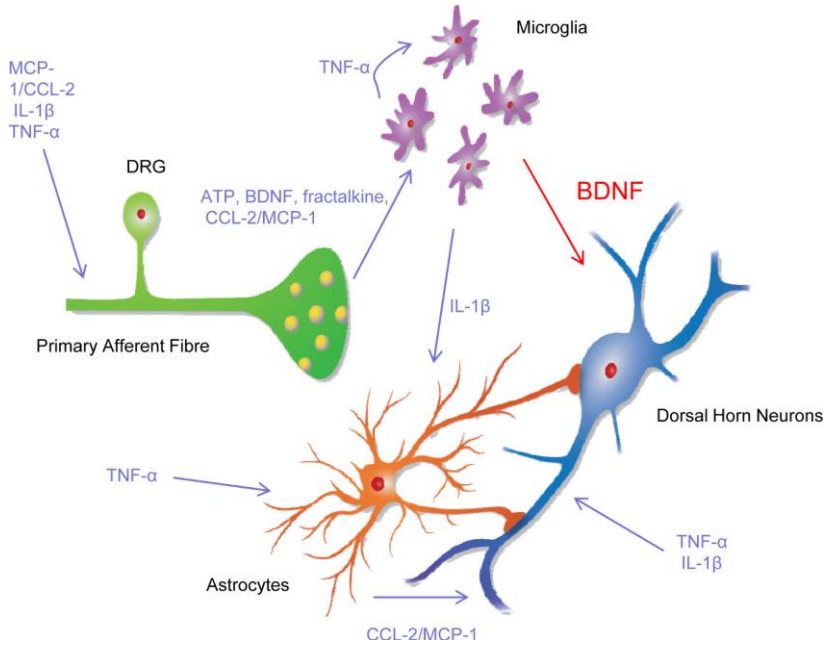

Figure 1.3 Interactions between neurons, microglia and astroctyes. The schematic diagram illustrates the complex relation of the cells of CNS in response to neurodegeneration. Degenerating neurons activate quiescent astrocytes and microglia. Reactive astrocytes and activated microglia secrete different factors, which could be either neuroprotective or neurotoxic. Reactive astrocytes may also affect the activation of microglia, and conversely (Biggs et al., 2010).

.

1.2.1 The role of the immune cells in ischemic stroke

Local and systemic immune responses play an important role after stroke and are involved in the primary and secondary extension of the lesion, as well as regeneration, recovery ((Kriz, 2006), (Macrez et al., 2011). Cerebral ischemia drives a time-dependent recruitment and activation of different types of immune cells, including resident microglia, neutrophils, T cells, blood-borne monocytes/macrophages via the damaged blood-brain barrier ((Burda and Sofroniew, 2014), (Jin et al., 2010)). Immune cells are attracted to the lesion site by a cocktail of molecules, the damage-associated molecular patterns (DAMPs), released by stressed and apoptotic cells ((Chen and Nunez, 2010), (Shichita et al., 2014)). Within minutes of ischemia onset, CNS resident microglia are activated and produce various pro-inflammatory or anti-inflammatory mediators (Jin et al., 2010)). Among several types of leukocytes, the neutrophils are the first infiltrating the lesion site (in 30 minutes to a few hours after ischemia) with the peak of recruitment between day one and three post ischemia (Amantea et al., 2009). The peripheral macrophages and dendritic cells infiltrate to the ischemic hemisphere within a few hours to a few days post ischemia ((Schilling et al., 2003), (Yilmaz et al., 2006)). Little is known regarding the accurate infiltration time of macrophages due to the lack of specific cell markers to distinguish these cells from resident CNS microglia (Jin et al., 2010), (Li et al., 2013), (Ritzel et al., 2015)).

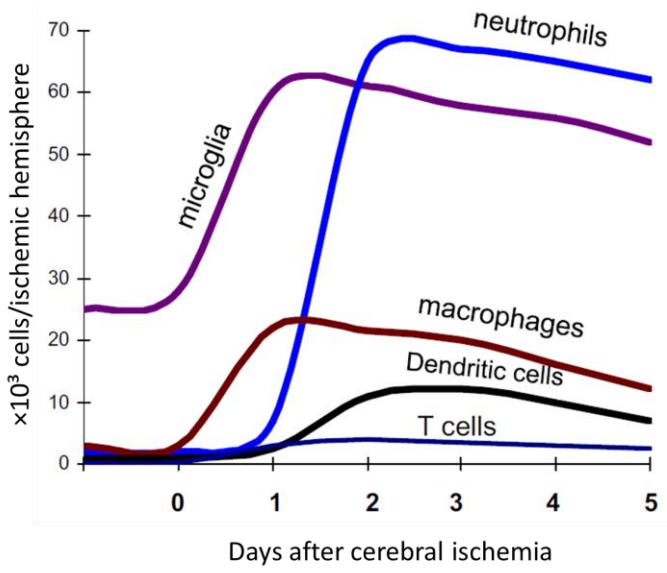

Figure 1.4 Time dependent recruitment of inflammatory cells into the brain following focal cerebral ischemia. The CNS resident microglia are the first cell type, which are activated within minutes of ischemia onset. Neutrophils, macrophages and DCs infiltrate the brain in 30 minutes to a few hours of ischemia (Jin et al., 2010).

.

1.2.1.1 Microglia and Macrophages after CNS damage

Microglia and blood-borne CNS-infiltrating macrophages are both myeloid cells. However, microglia originate from yolk sac progenitors during early embryogenesis and migrate as progenitors to the neuroepithelium and subsequently give rise to microglia, (Figure 1.5), (Ginhoux et al., 2010). Microglia are the first line of defense in CNS injury (Mizutani et al., 2012). Centralized intensive inflammatory reactions occur following CNS injury, which involve the activation of resident microglia, meningeal and perivascular macrophages of CNS and infiltrating macrophages from peripheral blood ((Popovich and Hickey, 2001), (Polfliet et al., 2001)).

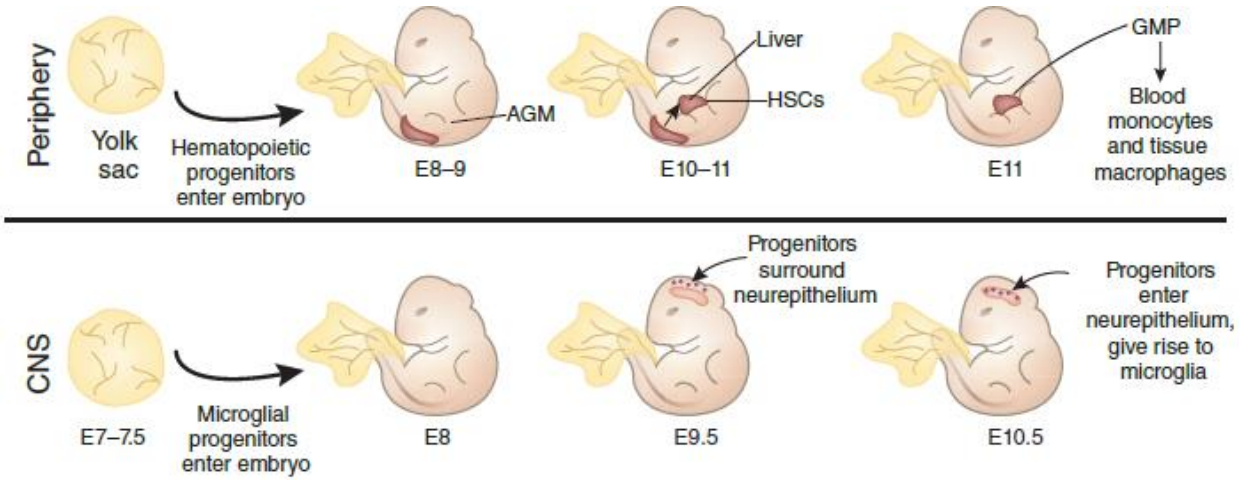

Figure 1.5 Embryonic origins of macrophages and microglia. Blood monocytes and tissue macrophages (top) arise from hematopoietic progenitors. They enter the embryo at embryonic day E8-9. There, the hematopoietic stem cells (HSCs) are accumulated in the fetal liver at E11. Then, they differentiate into granulocytic-myeloid progenitors (GMPs), to blood monocytes and finally to tissue macrophages. The CNS resident microglia arise from yolk sac progenitors (bottom) at embryogenic day E7–7.5. They enter the embryo at E8. They engulf the neuroepithelium at E9.5. The earliest microglia are detected in the neuroepithelium at E10.5 (Ransohoff, 2011).

Microglia and macrophages are indistinguishable by standard immunohistochemical techniques resulting in the common view of these cells as a functionally homogenous group ((Shechter et al., 2009), (Benakis et al., 2014)). However, microglia compared to macrophages are long-lived cells and have self-renewal potential (Gomez-Nicola and Perry, 2015). Microglia are functionally different from other immune cells in the CNS, such as

perivascular macrophages, supraependymal macrophages, epiplexus cells of the choroid plexus and meningeals ((Ransohoff et al., 2007), (Ransohoff and Perry, 2009)). In addition to their prominent role in CNS injury, they are actively involved in CNS homeostasis, normal development, connectivity and plasticity ((Benakis et al., 2014),(Lourbopoulos et al., 2015)). However, some studies demonstrated that microglia alone cannot cope with inflammatory processes after CNS injury. These findings emphasize the requirement of both microglia and macrophages for CNS repair following acute and chronic neurodegenerative disorders, (Figure 1.6), (Shechter et al., 2009).

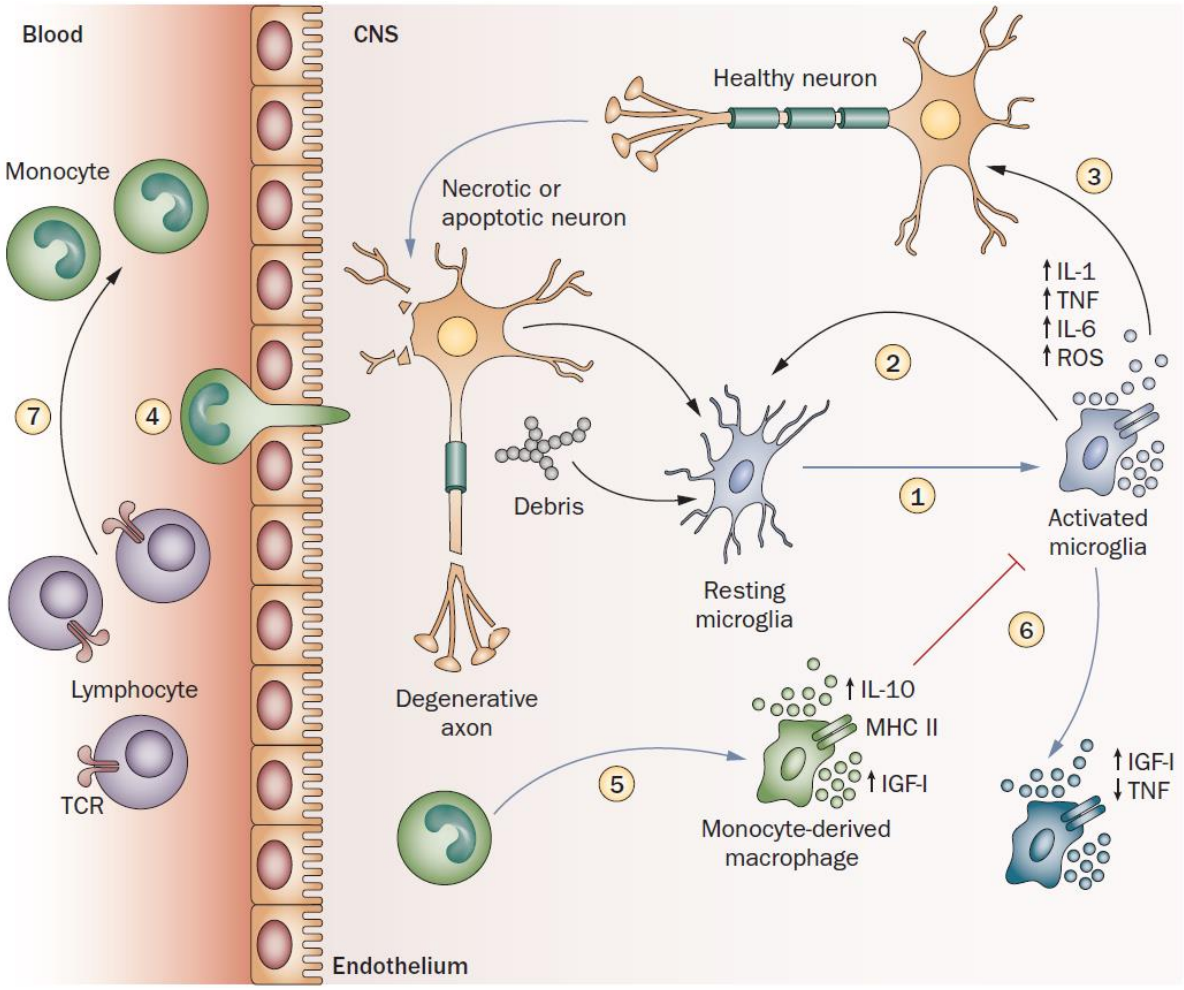

Figure 1.6 The microglia and macrophages interplay after CNS injury. Accumulation of cell debris activates resting microglia (1). They phagocytize cell debris and secrete pro-inflammatory cytokines. If the microglial reaction is prolonged, they can contribute to a neurotoxic cycle (3). At this point of local inflammation, macrophages infiltrate into the damaged tissue (4-5). They assist microglia to remove cell debris, secret anti-inflammatory cytokines and growth factors to indirectly modulating the function of microglia (6). T-helper lymphocytes recruit more monocytes to the damaged area (7), (Schwartz and Shechter, 2010).

1.2.1.2 Dynamic polarization of microglia and macrophages after CNS damage

Microglia and infiltrating macrophages are essential mediators of CNS repair as they acquire different beneficial or detrimental phenotypes and functions upon CNS damage. On the one hand, they promote CNS recovery by phagocytosis of cell debris, secreting various trophic factors and eliminating local inflammation ((Thored et al., 2009), (Kwon et al., 2013), (Miron et al., 2013)). On the other hand, over activation of these cells can aggarvate tissue damage and suppress regeneration ((Ekdahl et al., 2003), (Liu et al., 2007)). These contradictory phenotypes and functions are acquired in reaction to different microenviromental cues ((Shechter et al., 2009), (Schwartz and Shechter, 2010), (Hu et al., 2015). Classically activated microglia and macrophages, (M1), release pro-inflammatory molecules such as TNF-α, iNOS and interleukine-1. In contrast, alternatively activated microglia and macrophages, (M2), release several trophic factors and anti-inflammatory mediators, (Figure 1.7) ((Kriz, 2006), (Mosser and Edwards, 2008), (David and Kroner, 2011)).

The M1 and M2 classification is a useful concept in understanding the role of microglia and macrophages upon CNS damage (Boche et al., 2013). However, the application of this classification is an oversimplified conceptual framework that only shows two over activated conditions of microglia and macrophages. The in-vivo status of these immune cells is more complicated (Hu et al., 2015). For example, several sub-populations of M2 phonotype have been discovered, such as M2a, M2b, M2c and Mox. Each of these sub-populations have distinct physiological property and function ((David and Kroner, 2011), (Mosser and Edwards, 2008)).

It is worth to note that most of our knowledge of the polarization of microglia and macrophages is based on rodent experimental data, whereas the immune cells of humans display many differences with rodent (Smith and Dragunow, 2014). Although some in-vitro studies of human microglia and macrophages confirm the data derived from experiments on rodents (Durafourt et al., 2012), more studies using human immune cells are required.

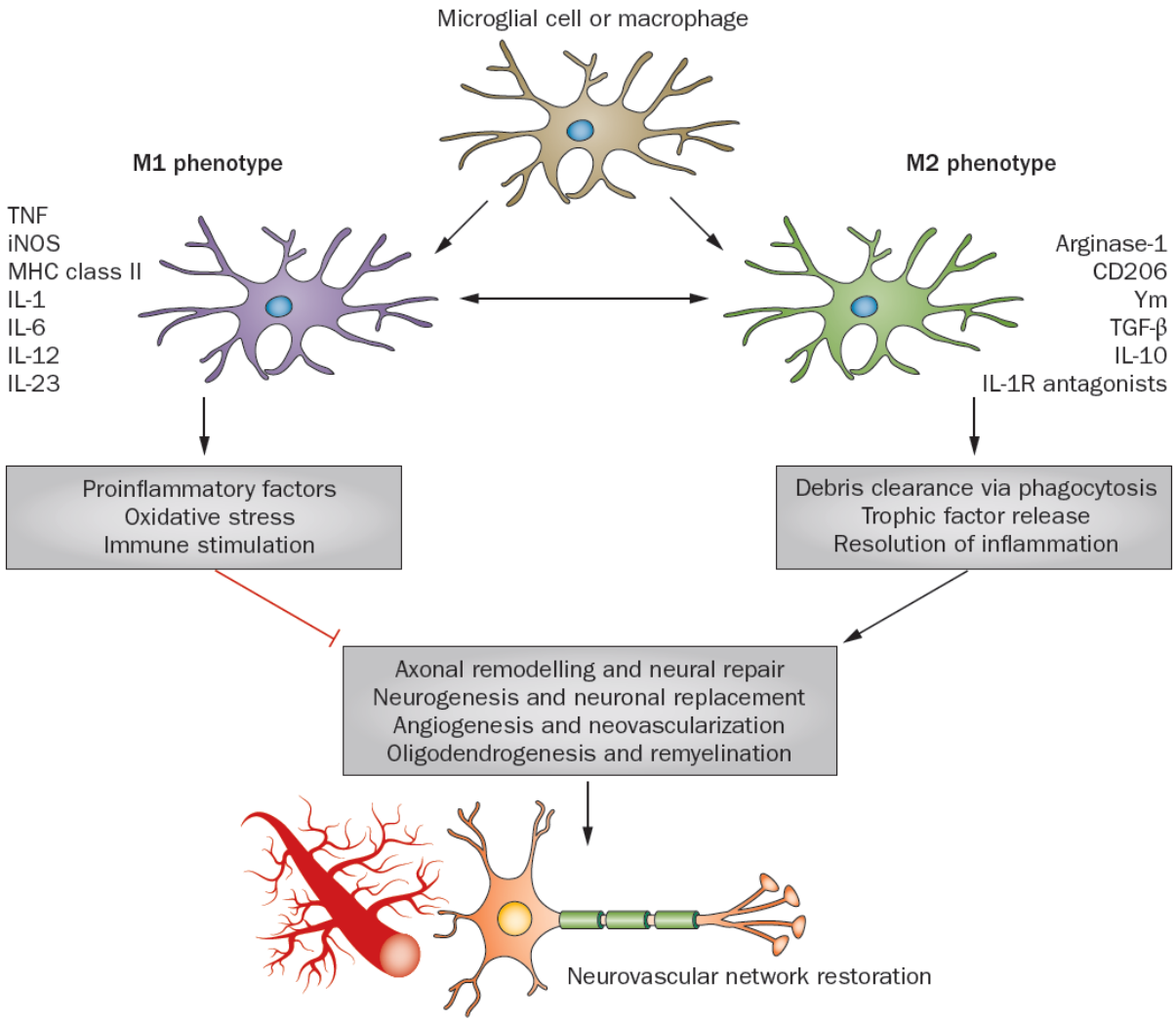

Figure 1.7 Polarization of microglia and macrophages. Following CNS damage, the microglia and macrophages are activated and are polarized towards M1 or M2 phenotypes. Depending on different phenotype, they represent distinct functions. The M1 polarized cells are characterized by releasing free radicals and expressing pro-inflammatory mediators such as TNF, iNOS and IL-6. These factors inhibit CNS repair and regeneration. In contrast, the M2 polarized cells are characterized by releasing trophic factors and expressing anti-inflammatory mediators such as arginase-1, CD206 and IL-10. These factors improve CNS repair and regeneration via phagocytosis of cell debris and resolving CNS inflammation (Hu et al., 2015).

1.2.2 The role of astrocytes in ischemic stroke

In the intact CNS, astrocytes are generally sub-divided into two major types: fibrous astrocytes in white matter detected predominantly in the corpus callosum and protoplasmic astrocytes in grey matter detected mostly in the cortex (Ding, 2014). In stroke, multiple signals from the damaged area induce temporal and spatial changes in the morphology and function of astrocytes (Ding, 2014), resulting in the formation of reactive astrocytes and the glial scar at the periphery of the ischemic area ((Faulkner et al., 2004), (Haupt et al., 2007; Hayakawa et al., 2010)). The glial scar is composed of reactive astrocytes, microglia, infiltrated macrophages, endothelial cells, fibroblasts and extracellular matrix molecules ((Rolls et al., 2009), (Pekny et al., 2014)). This physical barrier protects the healthy tissue from the spreading inflammatory factors of the ischemic core (Burda and Sofroniew, 2014).

Reactive astrocytes are characterized by the increased expression of glial fibrillary acid protein (GFAP) and the extended hypertrophic processes (Pekny et al., 2014). The dynamics of reactive astrocytes is subdivided into three phases: the acute, the sub-acute, and the chronic phase. In the acute phase, the hypertrophic astrocytes show a high proliferation rate and the cells represent stellate morphology. In the sub-acute phase, the proliferation rate decreases and the formation of a glial scar commences. In this phase, the cells become hypertrophic and show elongated processes pointing to the core of ischemia. In the chronic phase, the mature scar is formed and the cells further extend their processes toward the ischemic core (Figure 1.8).

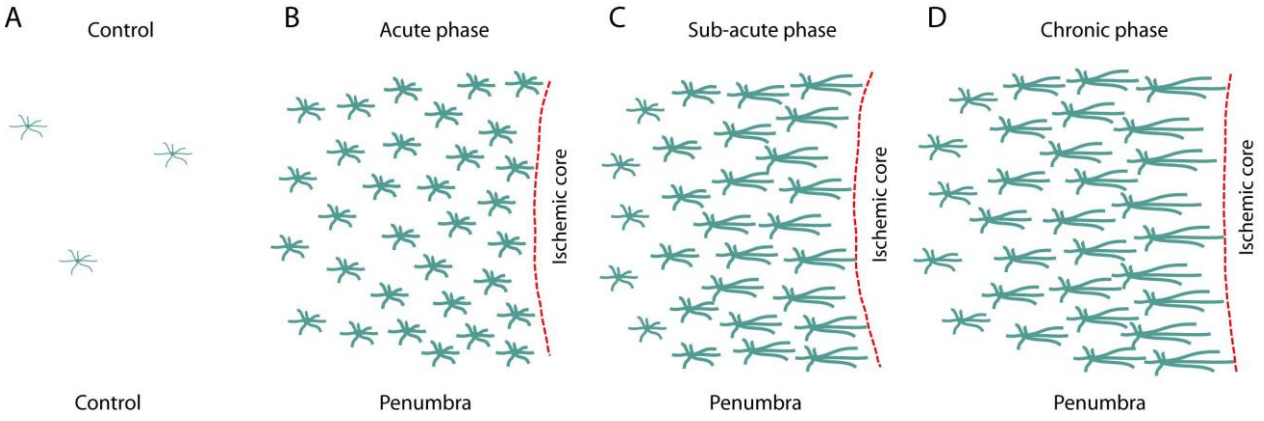

Figure 1.8 Dynamic reactive astrocytes in the penumbra at different stages after stroke. (A) In healthy conditions, few astrocytes are visible in CNS. (B) In acute phase, the stellate hypertrophic astrocytes show high proliferating rate. (C) In sub-acute phase, astrocytes with elongated processes are seen and a glial scar is formed. (D) In chronic phase, the mature glial scar is formed (Ding, 2014).

1.2.2.1 Phenotypic Polarization of astrocytes

Depending on the inflammatory microenvironment, astrocytes display neurotoxic or neuroprotective characteristics (Sofroniew and Vinters, 2010) and participate in immune responses (Farina et al., 2007). As an important part of neuro-inflammation, activated astrocytes show two phenotypes regarding the expression of pro- or anti-inflammatory cytokines/chemokines (John et al., 2003), the amount of GFAP and neurotoxic or neuroprotective activities (John et al., 2003). On the one hand, astrocytes secrete a variety of neurotrophic factors including insulin-like growth factors (IGFs), nerve growth factor (NGF), brain-derived growth factor (BDNF) and neurotrophin-3 (Rolls et al., 2009). On the other hand, they produce multiple detrimental mediators including IL-1β, iNOS, TNF-α in neurodegenerative disorders ((Li et al., 2011), (Akama and Van Eldik, 2000), (Lau and Yu, 2001)). However, polarization patterns including the regulatory mechanisms and the interplay with polarization of immune cells have not been clearly determined (Jang et al., 2013).

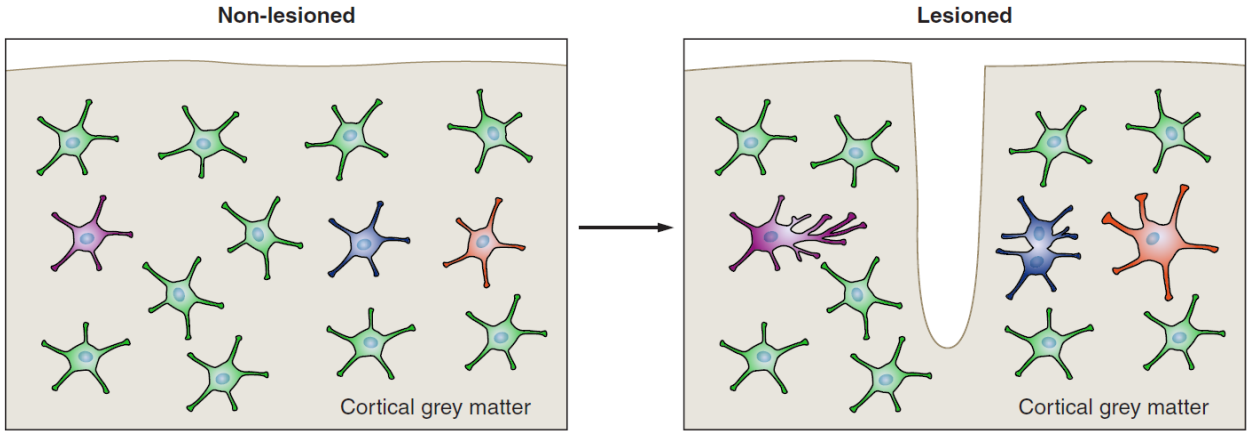

Figure 1.9 Astrocyte reactions after CNS injury. In the intact CNS, astrocytes are generally sub-divided in two major types: fibrous astrocytes discovered in the corpus callosum and protoplasmic astrocytes found in the cortex. Following CNS injury, activated astrocytes display different functional phenotypes undergoing hypertrophy of their cell body and processes, orange, polarization and extension of their processes, purple, and proliferation, blue, (Dimou and Gotz, 2014).

1.2.3 Modulating the polarization of microglia and macrophages

As discussed before, immune cells are activated and recruited to the CNS damage. Their polarization and subsequent function play an important role in the brain tissue repair. (Figure 1.10). The polarization into a more pro- vs. anti-inflammatory phenotype was neglected in the past by therapies directed towards a global down-regulation of the inflammatory reaction in clinical trials (Amantea et al., 2015). Therefore, a direct modulation of immune cell polarization is an attractive novel target. There is a rich literature on the molecular pathways of polarization ((Mosser and Edwards, 2008), (David and Kroner, 2011), (Boche et al., 2013).

The molecular cues derived from injured neurons or compromised endothelial cells are categorized as extracellular signals that trigger the phenotypic switch of immune cells. For example, the level of chondroitin sulphate proteoglycans (CSPGs), extracellular matrix proteins, increases strongly after CNS damage leading to more M2 polarization of microglia and macrophages ((Rolls et al., 2008), (Hu et al., 2015)). In addition, recruited peripheral immune cells, endothelial cells and astrocytes interact with microglia and macrophages and affect their polarization to either M1 or M2 phenotypes. For example, transfer of regulatory T lymphocytes at the early stage of ALS led to prolonged M2 phenotype of microglia and macrophages and improved functional recovery in mice ((Biswas and Mantovani, 2010), (Hu et al., 2015)). Moreover, the culture medium conditioned by type 1 T-helper cells, which is rich in LPS, IFN-γ and TNF-α, drives M1 polarization. In contrast, culture medium conditioned by type 2 T-helper cells, which is rich in IL-4, IL-13, IL-10 and TGF-β, induces M2 polarization ((Biswas and Mantovani, 2010), (Beers et al., 2011)).

The intracellular molecules, including the STAT family, the transcription factors PPARϒ and the interferon regulatory factors IRFs, have also been proven to regulate the polarization of microglia and macrophages ((Koscso et al., 2013), (Bouhlel et al., 2007), (Krausgruber et al., 2011)). Recently, the role of small non-coding RNAs on modulating the polarization of microglia and macrophages (microRNAs), as intracellular cues, has been discovered ((Graff et al., 2012), (Ponomarev et al., 2013)).

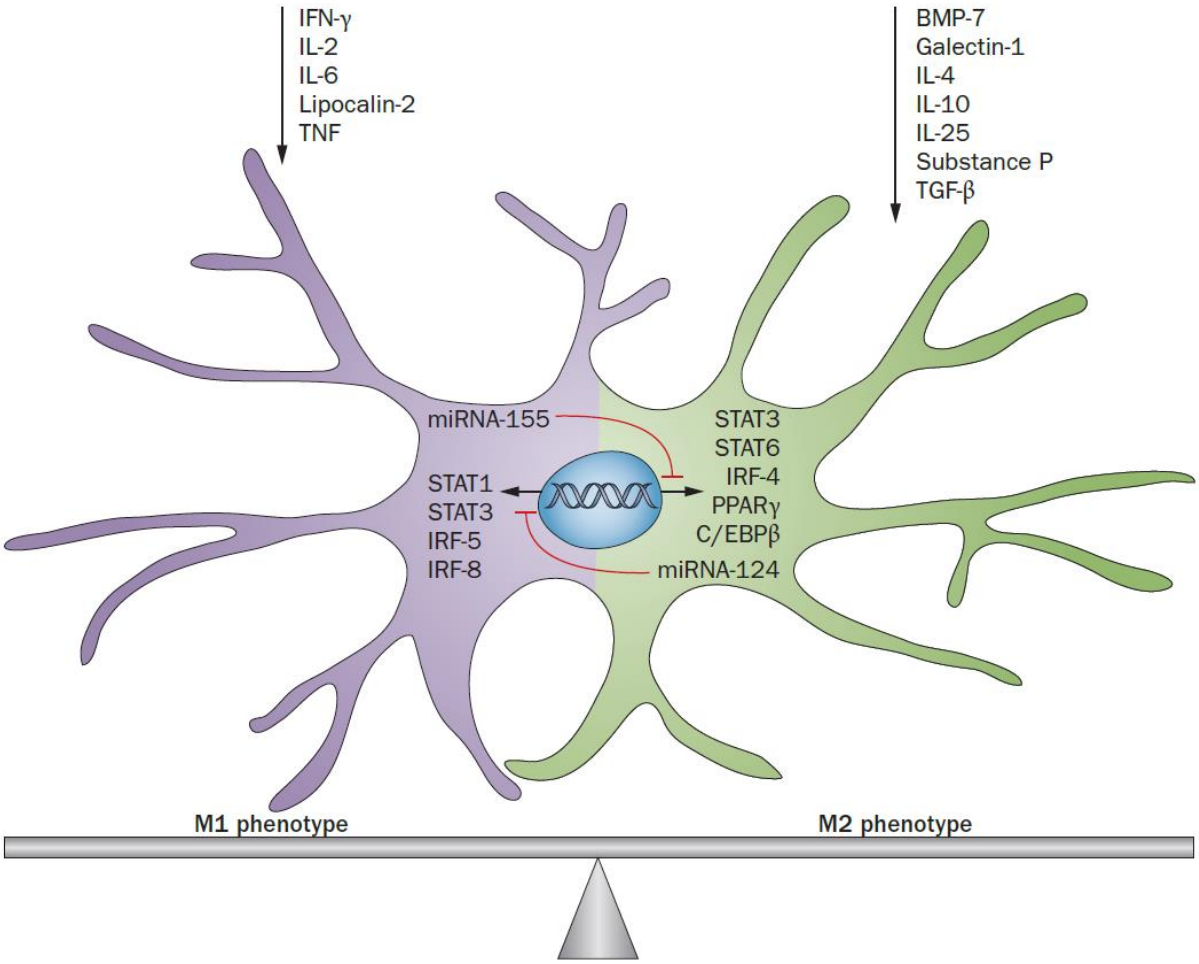

Figure 1.10 Factors involved in the polarization of microglia and macrophages. Both extracellular and intracellular molecules can switch the phenotype of microglia and macrophages, highlighting the importance of targeting the innate molecular cues (Hu et al., 2015).

1.2.4 The role of microRNAs on modulating the neuro-inflammation

MicroRNAs (miRNAs, miRs) belong to a small non-coding RNA family (21-23 nucleotides). They regulate the gene expression at the post-translational level by inhibiting protein translation or degrading the mRNA transcript (Ponomarev et al., 2013). A single miRNA can regulate the expression of multiple genes. They are involved in many biological processes, such as embryonic development, synaptic plasticity, apoptosis, immune function, and carcinogenesis ((Freilich et al., 2013), (Saugstad, 2015))

The role of miRNAs in the regulation of both innate and adaptive immune responses has been highlighted recently, (Figure 1.11), (Taganov et al., 2006). Multiple miRNAs play a key role in the development, differentiation, survival, and function of B and T lymphocytes, dendritic cells and macrophages ((Koralov et al., 2008), (Gracias and Katsikis, 2011)). Several miRNAs, such as miR-146a, miR-124, miR-125b, miR-155 and miR-9, regulate the inflammatory responses through regulating the activation of Toll-like receptors (TLR) ((Tili et al., 2007), (Bazzoni et al., 2009), (Jurkin et al., 2010)).

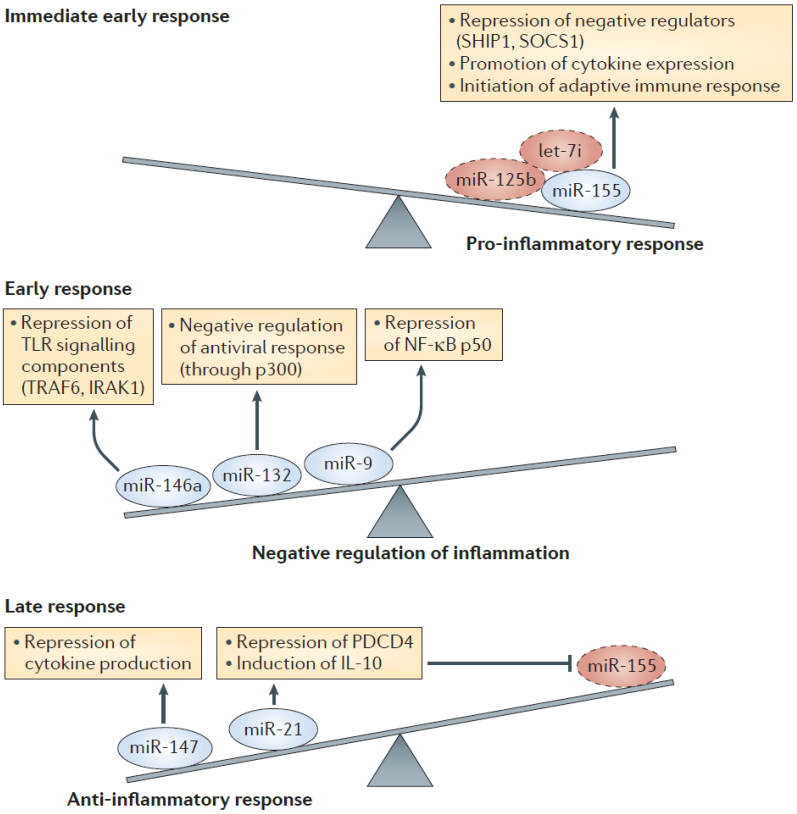

Figure 1.11 The role of miRNAs in the regulation of immune reactions. Inflammatory responses result in the sequential induction of several microRNAs (miRNAs) that could regulate the quality of the immune reactions. Inflammatory factors upregulate the expression of miR-155, and downregulate the expression of let-7i and miR-125b resulting in strongly enhanced pro-inflammatory response. Then, the upregulation of miR-146a and miR-9 can suppress the pro-inflammatory response. At later time points, upregulation of miR-21 and miR-147 can increase the anti-inflammatory response through the inhibition of miR-155, which results in decreased expression of pro-inflammatory cytokines (O'Neill et al., 2011).

1.2.4.1 The role of miR-124 on modulating the neuroinflammation

The brai-specific miR-124 has a key role in neurogenesis and neuronal differentiation ((Cheng et al., 2009), (Yu et al., 2008)). Recently, Ponomarev et al. reported high expression levels of miR-124 in CNS resident microglia. They also found the direct contribution of miR-124 on maturation of the progenitors of microglia and macrophages (Ponomarev et al., 2011). It is reported that miR-124 inhibits the M1 phenotype of microglia and macrophages resulting in down-regulation of M1-associated markers, such as IL-6, TNFα and iNOS. Moreover, it prolongs the M2 phenotype in those cells leading to up-regulation of M2-assoiciated markers, such as Arg-1, FIZZ1 and TGF-β ((Willemen et al., 2012), (Ponomarev et al. 2013)). Thus, miR-124 can be seen as a modulator of immune cells in CNS damage (Figure 1.12).

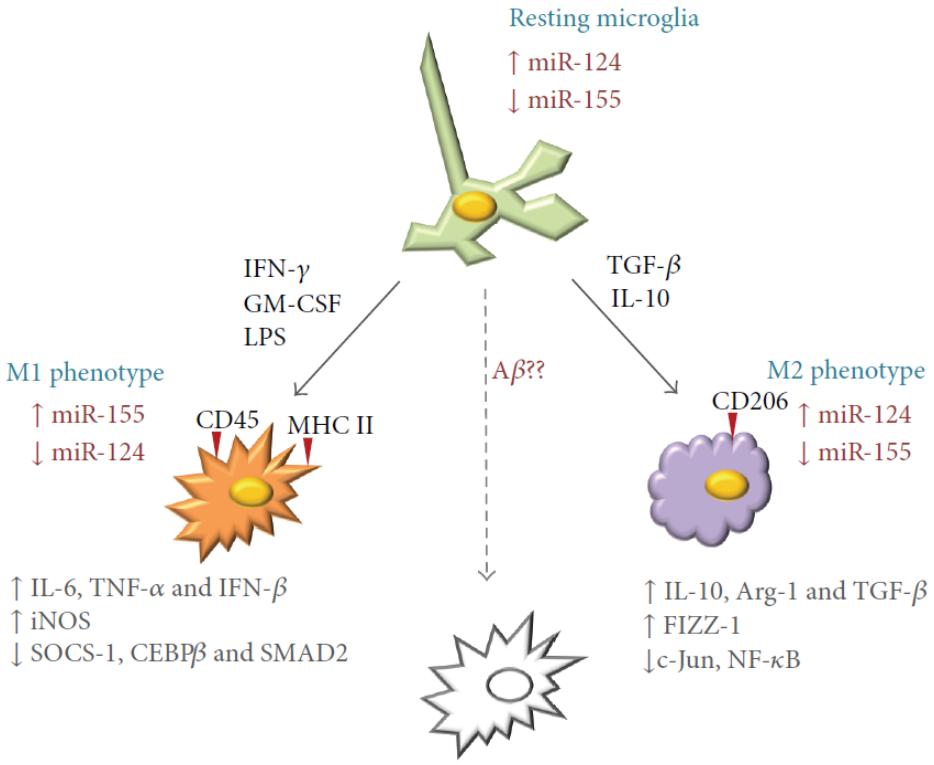

Figure 1.12 The role of miR-124 on modulating the polarization of microglia. Resting microglia express high levels of miR-124 and low levels of miR-155. The pro-inflammatory factors, such as IFN-Y, GM-CSF or LPS, induce M1 phenotype of microglia resulting in down-regulation of miR-124.In contrast, the anti-inflammatory factors, such as TGF-β or IL-10, induce the M2 phenotype of these cells (Guedes et al. 2013).

Chapter 2

Material and Methods

2.1 Consumables

Table 2.1: List of consumables

In-vivo experiment		
Name	**Product No.**	**Supplier**
Bepanthen eye cream	PZN: 01578681	Bayer
Carprofen	Rimadyl® 0110208	Pfizer
Isoflurane	PZN: 07253744	Actavis
Physiological saline	NaCl 0.9%	Braun
Silicon rubber-coated filament	7017PK5Re	Doccol Corporation
Suture silk	7/0 USP	Resorba
Opti-MEM	31985-062	Life technology
PBS with Mg2+/Ca2+	H15-001	PAA
miRNA Mimic, has-miR-124-3p	MC10691	Life technology
Hamilton syringe 26G needle	7732-06	Hamilton
Hamilton syringe	7634-01	Hamilton
Syringes and needles	Various	Braun
Surgical instruments (scissors, forceps)	Various	Braun
Histology		
Name	**Product No.**	**Supplier**
Aceton	1.00014.2500	Merk
Tri-Sodium citrate	S4641-500G	Sigma
potassium dihydrogen orthophosphate (KH2PO4)	60220	Fulka
Di-potassium phosphate (K2HPO4)	105104	Merck
Sodium chloride (NaCl)	71300	Sigma
PFA	0335	Roth
Entellan	1.07961.0500	Merck
Microscope slides	J1800AMNZ	Thermo Scientific
DAKO pen	S2002	DAKO
Triton X-100	3051.3	Carl Roth

2.2 In-vivo experiments

2.2.1 Animals

All animal experiments followed the guidelines established by the German Animal Welfare Act, according to the European Council Directive 2010/63/EU, which were approved by the Landesamt für Natur, Umwelt und Verbraucherschutz North Rhine-Westphalia on the subject of animal rights. All animals were housed for 2 weeks before starting any experiments under fixed circadian rhythm with ad libitum access to food and water. All surgical and scanning procedures were performed under isoflurane anesthesia and body core temperature control.

2.2.2 Experimental groups

A total of 34 adult C57BL6/N male mice (11-12 weeks, 21-25 g; Janvier, Saint Berthevin Cedex, France) were randomly assigned to three experimental protocols of different treatment and survival times (Figure 2.1). Stroke was induced in all mice through the middle cerebral artery occlusion (MCAO) model (see chapter 2.3.3). The anatomical location and the size of the ischemic lesions were verified by MR scans 48 hour after MCAO, at day 6 and day 14.

In the first experimental protocol with short survival time, MCAO was induced in fifteen mice that were perfused 6 days later divided into three following groups: control mice only exposed to stroke (n=5), miR-124 treated group that received an intracranial injection of liposomated miR-124 48 hours after MCAO (n=5), and the negative control mice that received liposomated negative control of miR, random primer, 48 hours after MCAO (n=5).

In the second experimental protocol with long survival time, MCAO was induced in thirteen mice that were perfused 14 days later. These were divided in the three following groups: control mice only subjected to stroke (n=5), miR-124 treated group that were injected 48 hours after MCAO (n=6), and the negative control group that were injected 48 hours after MCAO (n=3).

In the third experimental protocol with long survival time, MCAO was induced in ten mice that were perfused 14 days later. These were divided in the two following groups:

control mice only subjected to stroke (n=5), and miR-124 treated mice that received liposomated miR-124 at day 10 after MCAO (n=5).

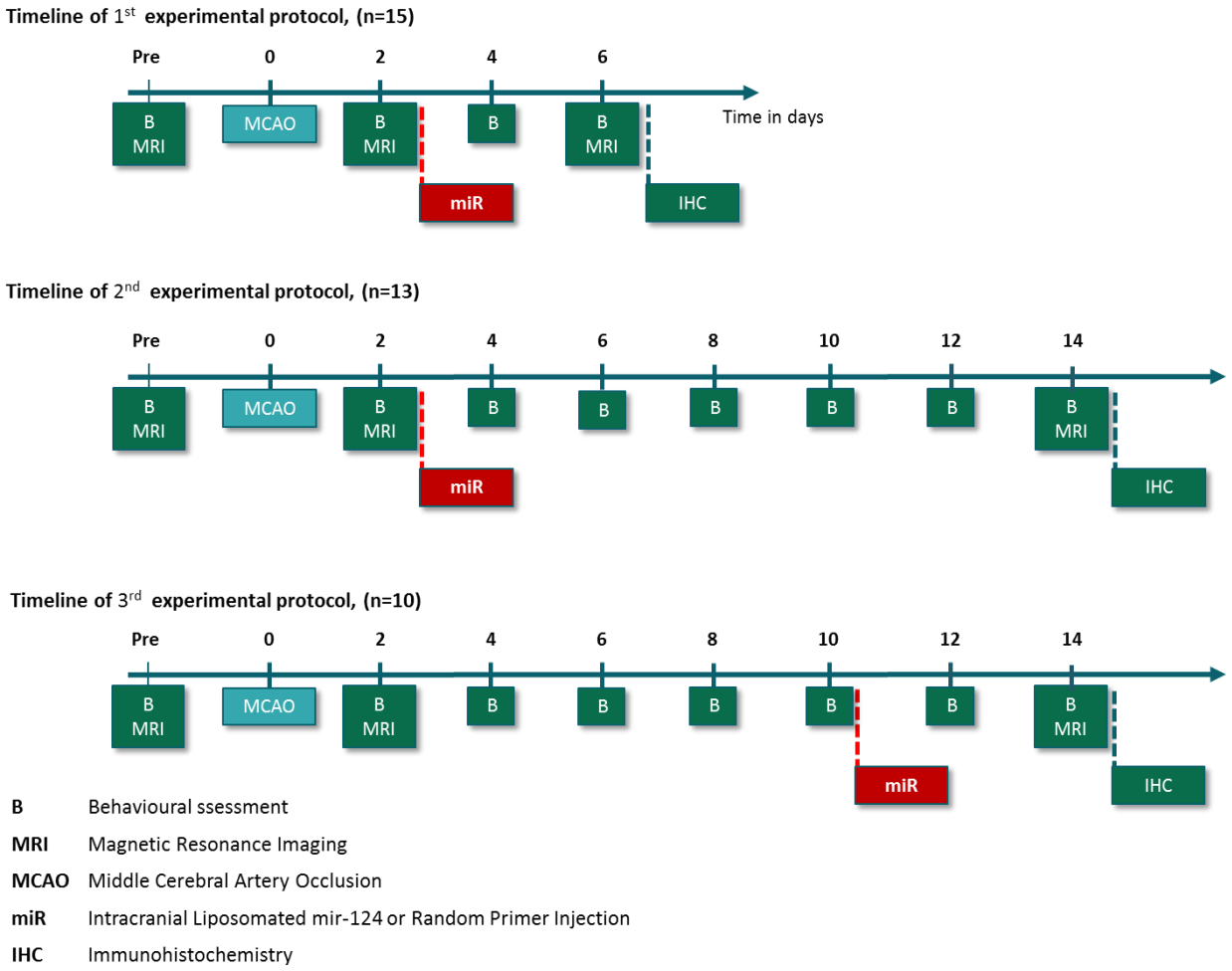

Figure 2.1 Timelines of the experimental protocols. Stroke was induced in all mice via the middle cerebral artery occlusion (MCAO) model, and all mice were scanned by MRI 48 hours after MCAO. At the first experimental protocol, miR-124 was injected at day 2 after MCAO and animals were sacrificed at day 6. In the second experimental protocol, miR-124 was injected at day 2 and animals were sacrificed at day 14 after MCAO. And at the third experimental protocol, miR-124 was injected at day 10 and the animals were sacrificed at day 14.

2.2.3 Middle cerebral artery occlusion (MCAO)

Transient occlusion of the right middle cerebral artery (MCAO) was induced via the intraluminal filament model as described previously (Adamczak et al., 2014). Briefly, mice were anesthetized with 2% Isoflurane (O_2:N_2O, 30:70 %) and subcutaneously injected with 4mg/kg Carprofen (Pfizer, Berlin, Germany). The body core temperature was controlled during surgery by a temperature-regulated heating pad (Medres, GmbH, Cologne). Blood flow was monitored via laser doppler flowmetry (Perimed, Järfälla, Sweden) fixed on the right foramen ovale of the skull. The right common carotid artery (CCA), external carotid artery (ECA), and internal carotid artery (ICA) were revealed. A silicon rubber-coated filament with a tip diameter of 170 µm and a length of 20 mm (7017PK5Re, Doccol Corporation, Sharon, USA) was inserted and forwarded into the ICA lumen until the tip blocked the origin of MCA, resulting in blood flow secession to the related brain regions (Figure 2.2). The mice were allowed to recover in a controlled heating box during 30 min occlusion time. Afterwards, the animals were re-anesthetized, the reperfusion was started by filament withdrawal, and the CCA was ligated. Following surgery, 1 ml NaCl was subcutaneously injected in all animals twice daily until stabilization of body weight. Only the mice with cortico-striatal lesion, observed by MRI 2 days after MCAO, were selected for further experiments in order to have homogenous groups.

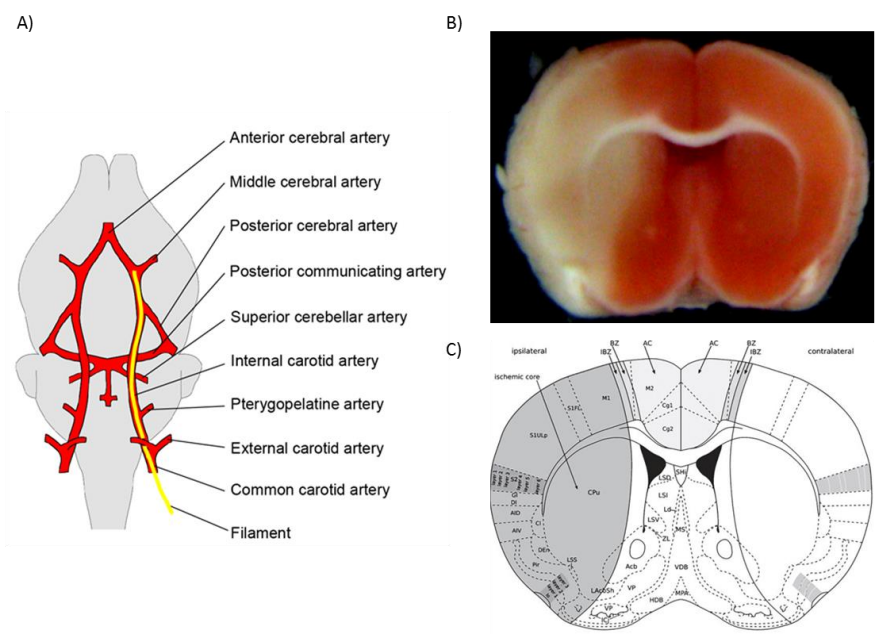

Figure 2.2 Middle cerebral artery occlusion model. a) Schematic depiction of major arteries of circle of Willis (left). A silicon rubber-coated filament (yellow) is inserted into the internal carotid artery (ICA) lumen until it blocks the origin of the middle cerebral artery (MCA) (Adamczak et al., 2014). b) TTC staining shows the ischemic cortico-striatal lesion after 30 minutes MCAO. C) Corresponding brain section selected from the mouse brain atlas (Mammele et al., 2015)

2.2.4 Intracranial injection of liposomated miR-124

To determine the implantation coordinates, T2-weighted MRI was performed in all mice 48 hours after MCAO. At the transplantation day the miR-124 (2 µg in 50 µl PBS, PM10691 Applied Biosystems, Carlsbad, CA, USA) or the random primer (2 µg in 50 µl PBS, AM17110; Applied Biosystems) was mixed with the transfection reagent, Lipofectamine 2000 (Invitrogen, Paisley, UK). Intracranial injections into the right striatum ipsilateral to the ischemic lesion were performed (Figure 2.3) as described previously (Aswendt et al., 2012). Briefly, mice were anesthetized with isoflurane (O_2:N_2O, 30:70 %), received a subcutaneous (s.c.) injection of 4 mg/kg Carprofen as analgesic agent and were fixed in a stereotactic frame throughout the surgery (Stoelting, Dublin, Ireland). The body core temperature was monitored with a rectal probe and maintained constant by a feedback control heating pad (Medres, GmbH, Cologne). A volume of 2.0 µl of the suspensions containing 100 ng of miR or random primer was injected with a Hamilton syringe (26G needle) in flow rates: 1500 nl/min for withdrawal, and 500 nl/min for the actual injection at the following coordinates relative to bregma: AP +0.5; ML +1.4; DV -2.4. The syringe was kept in location for 5 more minutes, before needle removal.

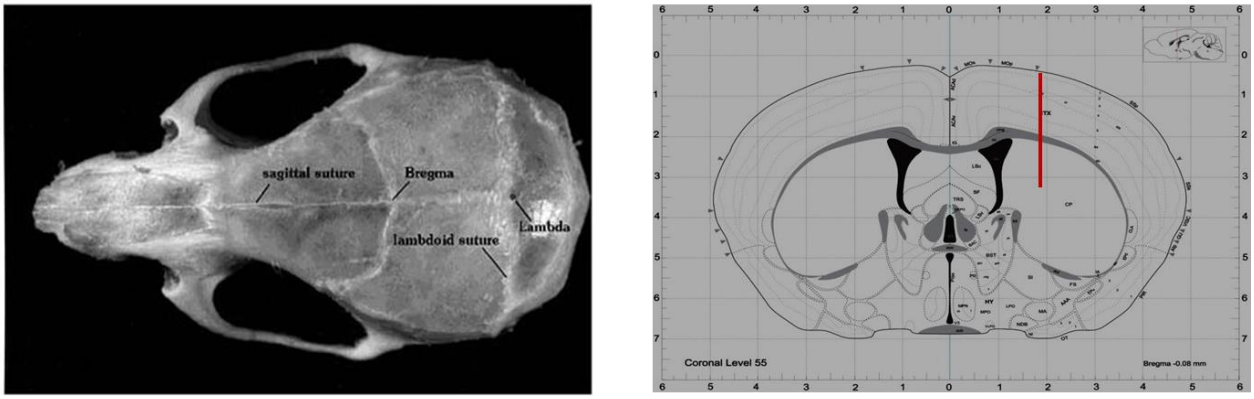

Figure 2.3 Schematic representation of the mouse brain in stereotaxic coordinates. a) Location of bregma and lambda. b) Using a stereotaxic atlas to inject the miR-124 (or random primer, resp.) in the striatum close to lesion (Paxinos, 2001).

2.2.5 Modified neurological deficit scores

To observe the different aspects of neurological function loss and recovery, behavioral tests were performed in all mice, before and every 2 days after MCAO. The modified neurological deficit scores (mNDS) was used, which is a modification of a previously published test (Chen et al., 2001). The modified NDS (mNDS; Table 1) includes assessment of general health, a set of motor tests (i.e., muscle status and abnormal movement), sensory test (i.e., tactile, and proprioceptive), and reflexes on a total scale of 0-16. One point is given for the loss of a tested reflex or a failure of performed test. Accordingly, the higher score indicates higher severity of ischemia.

Table 2.2 Modified Neurological Deficit Score	Points
General Health	1
Weight Loss	3
Less than 5%	1
Between 5%-15%	2
Between 15%-20%	3
Motor tests	
Raising mouse by tail	3
Flexion of forelimb	1
Flexion of hindlimb	1
Head moved >10° to vertical axis within 30 s	1
Placing mouse on floor	2
Normal walk	0
Inability to walk straight	1
Circling toward paretic side	2
Sensory tests	
Proprioceptive test (deep sensation, pushing the paw against the table edge to stimulate limb muscles)	2
Reflexes absence	
Pinna reflex (head shake when auditory meatus is touched)	2
Whisker reflex (head shake when whiskers is slightly touched with cotton)	2
Startle reflex (motor response to a brief noise)	2
Maximun points	16

One point is given for the failure of a performed test or for the loss of a tested reflex: 11–16, severe injury; 6–10, moderate injury; 1–5, mild injury.

2.2.6 Magnetic resonance imaging

MRI was performed on a 9.4 T Biospec animal scanner system with a 20 cm horizontal bore magnet (Bruker BioSpin, Ettlingen, Germany) equipped with actively shielded gradient coils (BGA9S, 750 mT/m, Bruker BioSpin), using the ParaVision 5.1 software. Radio frequency (RF) transmission and reception were carried out by a 112/72 mm od/id resonator and a mouse surface coil (Bruker), respectively. Mice were anesthetized with 2% Isoflurane in a 30:70 oxygen/air mixture and fixed in an animal holder (Bruker) using tooth and ear bars to prevent movement artefacts from breathing. Respiration rate was monitored via a pressure sensitive pad placed on the back of the mice. Body core temperature was followed via a rectal probe and maintained at 37 ± 1.0 °C with a temperature control unit (medres, GmbH, Cologne), by adjusting the temperature of the circulating warm water within the warming pad. The physiological status of the animal was monitored with DASYlab software (National Instruments, Austin, TX, USA). Tripilot Gradient-echo scans were performed to position the mouse head in the magnet. Images were acquired with a multi slice multi-echo spin-echo (MSME) sequence, (TR/TE = 5000 ms/10 ms, 16 echoes, 10 coronal slices, slice thickness 0.5 mm, FOV 2.5 × 2.5 cm^2, matrix 256 × 256, resolution 98 × 98 mm^2, bandwidth 75 kHz), for T2 evaluation and lesion extent visualization.

2.2.6.1 Evaluation of lesion size and T2 time, based on T2 maps analysis

After image acquisition, quantitative T2 maps were calculated using the IDL software (Version 6.4, Exelis Visual Information Solutions, Boulder, CO, USA), by fitting pixel intensities to a mono-exponential decay curve, on a pixel-by-pixel basis. To determine the infarct volume, the MR images were further analyzed with ImageJ based on T2 maps (U. S. National Institutes of Health, Bethesda, Maryland). A T2 threshold above normal value was determined according to the average T2 of two same sized regions in the cortex and striatum of the intact hemisphere across all animals. The threshold was set to two standard deviations above the average T2 value (39 + 2.4 ms). Further, the areas of infarcted slices were delineated with the exclusion of ventricles, and the lesion volume was calculated

according to slice thickness. To measure the water content of brain after stroke, ΔT2 times in the cortico-striatal lesion components of the T2 images were determined by subtracting the T2 value of the healthy contralateral side from T2 value of the ischemic ipsilateral hemisphere.

2.3 Immunohistochemistry

At the end of the individual survival period, animals were transcardially perfused under profound Isoflurane anesthesia with 20 ml cold PBS followed by 20ml 4% PFA at day 6 or 14 after MCAO. Afterwards, brains were fixed in 4% PFA overnight and then were cryo-protected by immersion in 30% sucrose solution for the next 2 days at 4 °C. Following, the brains were frozen in -60 °C cold 2-methylbutane (Sigma-Aldrich, Taufkirchen, Germany) and subsequently stored at -80 °C. The cerebral tissue was cut into 10 µm coronal slices using a cryostat (Leica Microsystems, Wetzlar, Germany), and was directly mounted on slides and stored at -20 °C until the staining.

The cryosections were kept at room temperature for 30 minutes at the day of immunostaining. To gain favorable antigen retrieval for Iba-1 the acetone -20 °C pre-treatment was performed for 20 min. To prevent non-specific binding of antibodies, the sections were pre-incubated in 5% normal serum and 0.25% Triton X-100, in KPBS for 60 min at room temperature. The treated sections were incubated overnight at 4 °C with subsequent primary antibodies. Secondary antibodies were applied for 2 h at room temperature (list of used antibodies Table 2.4). Hoechst solution was added to the secondary antibody solution, for nuclear staining, at the same time of secondary antibody addition. For arginase-1 staining, a pretreatment with citrate buffer (0.01mol/L; pH 6.0) for 30 minutes was necessary to gain optimal antigen retrieval. Sections serving as negative control were included with identical preparation, aside from primary antibodies. Slides were coverslipped with mounting medium (Entellan,Merck, Darmstadt, Germany) and kept overnight at room temperature .

For each region of interest (ROI) three sections per mouse were imaged with a fluorescent microscope (BZ-9000 Keyence, Osaka, Japan) at 4, 20 and 40x magnification. To be able to quantify the immunohitochemical staining of the sections, care was taken to acquire microscopy images with a constant exposure time across all sections. Analysis involved 6 different ROIs in each brain section in the ipsilateral and contralateral hemispheres; a) four ROIs at the border and the core region of the ischemic hemisphere in both cortex and the striatum, and b) two ROIs in the cortex and striatum of the intact hemisphere.

Table 2.3 List of antibodies used for IHC

	Antibody	Species	Dilution ICC/ IHC	Supplier
1st	anti-Iba-1	Rabbit	1:1000	WAKO
	anti-Iba-1	Goat	1:100	Novus Biological
	anti- MMR/CD206	Mouse	1:200	R&D
	anti-CD16/32	Rat	1:200	Biolegend
	anti-Arginase-1	Rabbit	1:200	GenTex
	anti-GFAP	Mouse	1:400	Sigma
	anti-NeuN	Mouse	1:500	Chemicon
2nd	Cy5-anti rabbit	donkey	1:200	Jackson Immuno Research
	Cy3-anti goat	donkey	1:200	Jackson Immuno Research
	Cy3-anti mouse	donkey	1:200	Jackson Immuno Research
	Cy3-anti rat	donkey	1:200	Jackson Immuno Research
	Cy5-anti mouse	donkey	1:200	Jackson Immuno Research
	Hoechst	----	1:1000	Sigma

2.3.1 Quantitative immunohistochemical analysis of microglia/macrophage polarization

To observe the activation and polarization of microglia and macrophages after stroke, immunofluorescence images were acquired of either M1 or M2 representative markers double stained with Iba-1. Images were quantified using ImageJ for Preprocessing and TissueQuest 4.0 (TissueGnostics, Vienna, Austria) for quantitative cytometry analysis. Cells were identified based on the nuclei staining (nuclei size, staining intensity and discrimination by area set manually) followed by the analysis of specific staining. The background threshold was always kept constant. The cut offs were defined for each ROI individually to distinguish the misleading signal, due to the overlapping of Iba-1 cell ramification with neighbor cells nuclei. Scattergrams were created to visualize the corresponding positive cells in the source ROI via the real-time back gating component. Intensities and the number of Iba-1 positive cells co-expressed with CD206, arginase-1 and CD16/32 were obtained. The mean values were determined from analyses of three brain sections per mouse in each group. For each ROI, the following parameters were quantified: (a) total cell density according to the nuclei staining, (b) Iba-1+ microglia/macrophage cell density, (c) total CD206+ cell number and the cell density relative to Iba-1+ cells, (d) total

CD16/32+ cell number and the cell density relative to Iba-1+ cells, and (e) total arginase-1+ cell number and the cell density relative to Iba-1+ cells.

2.3.2 Quantitative immunohistochemical analysis of glial scar

In order to analyze the glial scar, the 4 fold magnification image of GFAP stained sections were taken. ImageJ was used to measure the glial scar area and the necrotic core relative to the size of the whole ischemic hemisphere, as both areas are delineated by the GFAP positive cells. The necrotic ischemic core was taken as the volume inside the glial scar with no infiltration of GFAP positive cells (Figure 2.4). The following formulas were used to calculate the percentage of glial scar and necrotic area (Kho, 2015):

$$\text{Percentage of glial scar area} = \frac{(\text{outer glial scar border} - (\text{lesion core} + \text{ventricle}))}{\text{Ipsilateral hemisphere}} \times 100$$

$$\text{Percentage of lesion size area} = \frac{\text{Lesion size}}{(\text{Ipsilateral hemisphere} - \text{ventricle})} \times 100$$

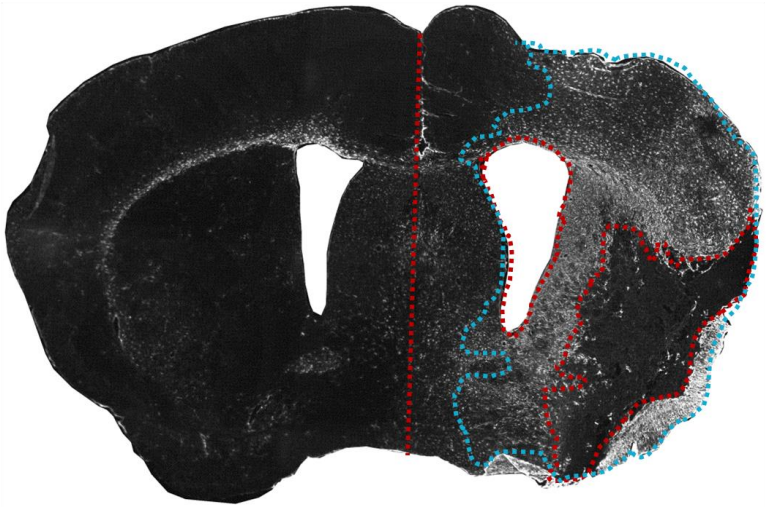

Figure 2.4 Schematic representation of glial scar and lesion size area. The drawn lines represent the ROIs used for calculation of the percentage of glial scar area in the ipsilateral hemisphere. The GFAP stained area is visible in gray-white, the lesion core is the separated black area within the glial scar. The ventricle was subtracted from the calculation of the tissue sizes. 4x magnification.

2.4 Statistics

All acquired data were analyzed by SPSS version 22 (IBM SPSS statistics, Ehningen, Germany). The Normality test and homogeneity of variances were evaluated for all data.

The nonparametric Kruskal-Walis H test was performed for mNDS data.

IHC data of single early time point injection of liposomated miR-124 at day 2 after MCAO were tested for significant changes between the 3 groups using one-way analysis of variance (ANOVA) with Bonferroni corrected *posthoc* comparisons. Using an independent one-tailed Student's *t*-test, the data of late liposomated miR-124 injection at day 10 were analyzed to observe the significant changes between the stroke and the treated group.

The IHC results are represented by box-and-whisker plots, wherein each box represents the central 50% of the data points, the interquartile range (IQR), a horizontal line in each box indicates the median, and the vertical bars reflect the spread of 1.5 × IQR. Dots display outliers, which were included in calculations of significance. The box-and-whisker plots were generated by SPSS version 22.

The number of Iba-1+ cells expressing M1 or M2 markers correlated with neurological deficit scores measured by mDNS. Regression was done via considering the Iba-1+ cell number expressing M1 or M2 markers as the independent variable and mNDS as the dependent variable.

Also correlations have been made by the number of M1 or M2 fraction of the Iba1+ cells versus the total number of neurons. Via considering the Iba-1+ cell number expressing M1 or M2 markers as independent variable and the number of surviving neurons as dependent variable, regression was done. A p-value ≤ 0.05 was considered to be statistically significant.

Chapter 3

Results

3.1 In-vivo MR imaging

3.1.1 Characterization of ischemic lesion after MCAO

Occlusion of the middle cerebral artery resulted in elevated T2-values in the ischemic regions, representing the augmented tissue water content. In order to follow the ischemic lesion location, size and development, quantitative MRI T2 maps were calculated from MSME images before MCAO, at day 2, 6 and 14 after stroke (Figure3.1). As expected, T2 maps showed no signs of ischemic lesion before MCAO, and both hemispheres represented equal T2 intensities. In contrast, strongly increased T2 values were detected 2 days after MCAO, which represents the vasogenic edema in sub-acute phase of stroke. The lesion merged with healthy tissue through a thin border of slightly elevated T2 values. Two characteristic lesion types were present: 1) lesions restricted to the striatum and 2) lesions involving both striatum and cortex. The cortico-striatal ischemic mice were used for this experiment to have more homogenous groups. A gradual decrease in infarct volume was visible in all animals at day 6 and day 14 (Figure 3.1 A-B).

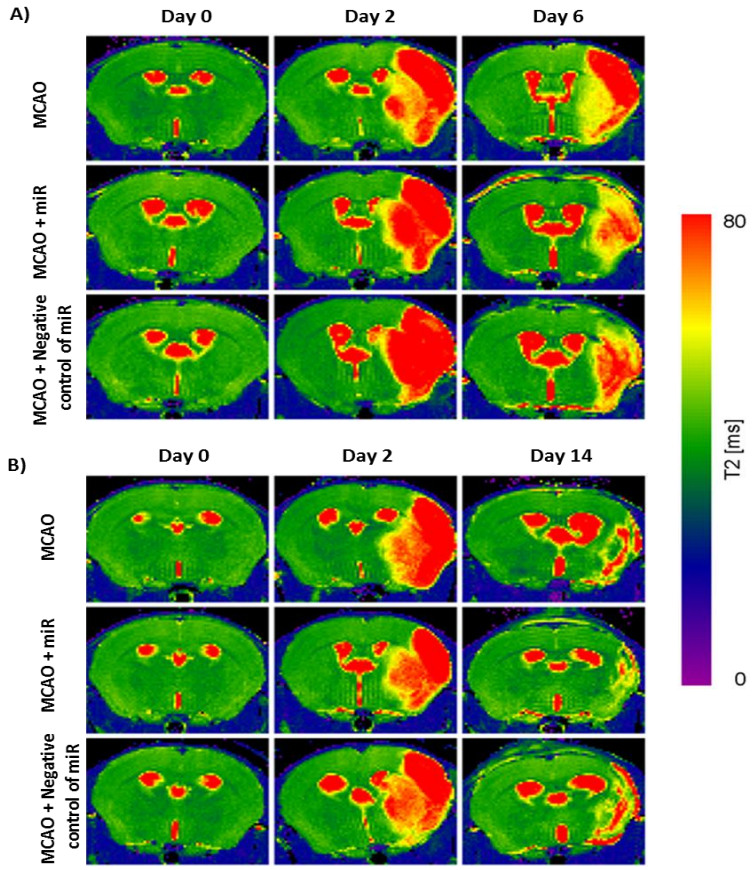

Figure 3.1 Characterization of the development of ischemic lesion after MCAO. A) survival time 6 days, and b) 14 days. Representative time series of T2maps of one animal per group. T2 maps are shown as coronal brain sections. T2 maps of intact subjects, 1 week before MCAO, show symmetrical intensity distribution in both hemispheres. The T2 values increased noticeably 48 hours later in the target area of the occluded vessel. The cortico-striatal lesions are visible in the right hemisphere. A gradual shrinkage of volume of infarcted area was visible at day 6 and day 14, when comparing to day 2, showing the reduction of vasogenic edema after stroke.

3.1.2 Comparison of ΔT2 time and T2 lesion volume

The ΔT2 times, subtracted T2 value of healthy contralateral hemisphere from T2 value of ischemic ipsilateral hemisphere, and T2 based lesion volume were analyzed at day 2, day 6 or day 14 after MCAO. In all later time points (6 or 14 days after MCAO), the ΔT2 decreased compared to day 2 in all groups (Figure 3.2 A-C).

In the first experimental protocol, the ΔT2 time decreased more in miR treated and negative control groups at day 6 post MCAO, when compared to day 2, but not significantly (Figure 3.2 A). In the second experimental protocol, the miR treated group had pronounced reduction in ΔT2 relaxation time at day14 (p = 0.035), representing less water content in the ischemic hemisphere at this group (Figure 3.2 B). Following the late injection of miR-124 in the third experimental protocol, no significant difference was seen between the miR treated and the stroke only groups (Figure 3.2 C).

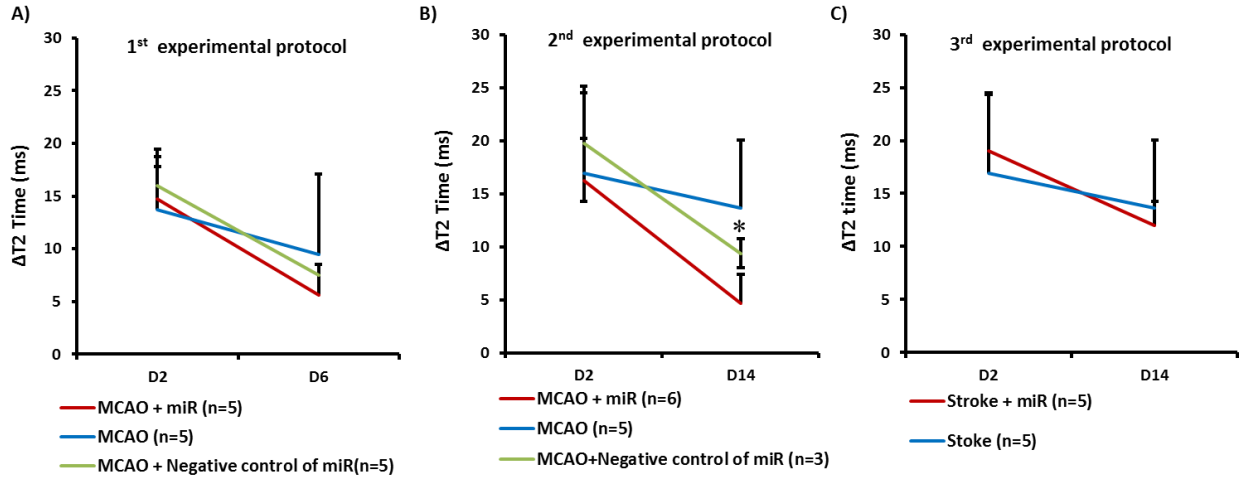

Figure 3.2 Comparison of ΔT2 time in three experimental protocols at day 2, 6 and 14 after MCAO. (A) In the first experimental protocol, the animals had MCAO with a treatment time point of 48h after stroke and a survival time of 6 days, (B) In the second experimental protocol, the animals had MCAO with a treatment time point of 48h after stroke and a longer survival time of 14 days after MCAO, and (C) in the third experimental protocol, the animals had MCAO with a treatment time point at 10 days after stroke and a survival time of 14 days after MCAO. ΔT2 time decreased in all groups from day 2 comparing to day 6 or day 14 after MCAO. In the miR treated group a significant decrease of ΔT2 time was observed at day 14 after MCAO (B), representing less vasogenic edema. Bars represent mean ± S.D. * indicates statistical significance $P < 0.05$ using non parametric Kruskal-Walis H test.

The lesion volume was determined according to a T2 threshold of 39 + 2.4 ms (See chapter 2.3.6.1). In all animals, the lesion volume decreased at day 6 and 14 in comparison to day 2 after MCAO. In the first experimental protocol, the decrease of lesion volume showed no difference between the groups at day 6 (Figure 3.3 A). In the second experimental protocol, the T2 lesion volume shrank considerably in miR treated group at day 14, although not significantly (Figure 3.3 B). The late injection of miR-124 in the third experimental protocol, 10 days after MCAO, showed no significant difference between the groups at day 14 (Figure 3.3 C).

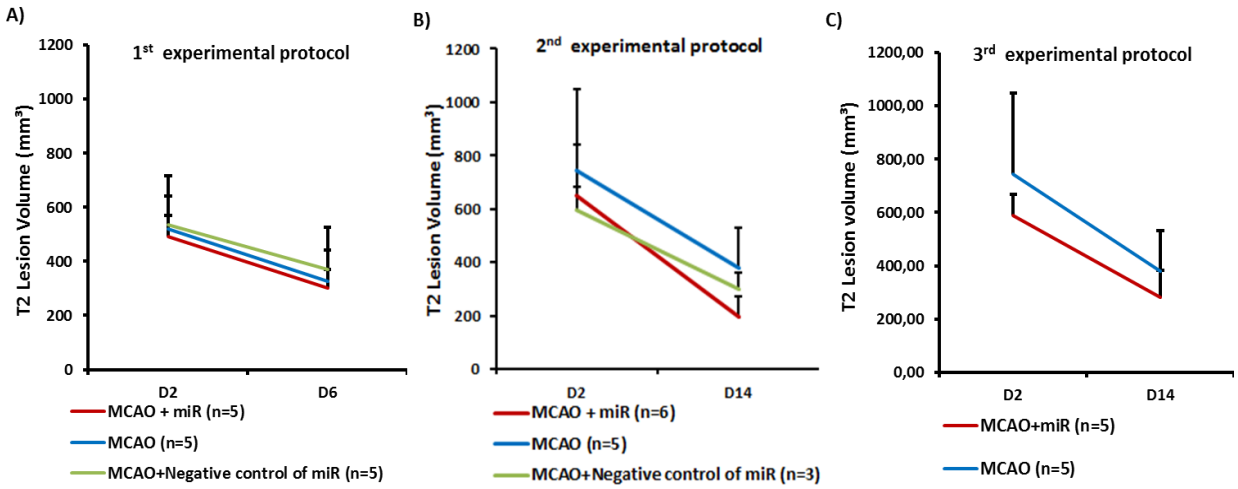

Figure 3.3 Comparison of T2 lesion volume in three experimental protocols at day 2, 6 and 14 after MCAO. (A) In the first experimental protocol, the animals had MCAO with a treatment time point of 48h post stroke and a survival time of 6 days, (B) In the second experimental protocol, the animals had MCAO with a treatment time point of 48h post stroke and a longer survival time of 14 days after MCAO, and (C) in the third experimental protocol, the animals had MCAO with a treatment time point at 10 days post stroke and a survival time of 14 days after MCAO. The lesion volume decreased in all groups from day 2 comparing to day 6 or day 14 after MCAO. Bars represent mean ± S.D.

3.2 Ex-vivo fluorescence imaging

3.2.1 Morphology and kinetics of microglia and macrophages after stroke

The ionized calcium-binding adapter molecule 1, Iba-1, was used to stain the resident microglia of the CNS and infiltrating monocyte-derived macrophage cells in the brain. I have focused on characterizing Iba1$^+$ cells in the stroke core, border of the ischemic tissue and healthy tissue.

The Iba-1$^+$ cells were visible in both intact and ischemic hemisphere, although with various morphology and distribution. They were intensely localized inside the ischemic hemisphere and aligned as a dense boundary around the lesion (Figure 3.4 A). Different phenotypes of microglia and macrophages were found. The ramified type with small cell bodies and long thin branching processes was mostly observed in the contralateral and in the healthy part of the ipsilateral ischemic hemisphere. In the peri-infarct area, the majority of Iba-1$^+$ cells were observed as intermediate morphology with short or long swollen processes and amorphous larger cell bodies. In contrast, the amoeboid and round shape Iba-1$^+$ cells were exclusively found in the ischemic core (Figure 3.4 B-C).

Furthermore, the density of the Iba-1$^+$ cells varied in different regions. The ischemic border had the highest density of Iba-1$^+$ cells, followed by the core regions, whereas the contralateral hemisphere had the lowest cell density with only scattered Iba-1$^+$ cells.

Quantitatively higher Iba-1$^+$ cells density was observed in the striatal regions at day 6, in comparison to day 14 post MCAO, emphasizing the increased early stage proliferation of Iba-1$^+$ cells after stroke, especially in the striatum (Figure 3.4 D).

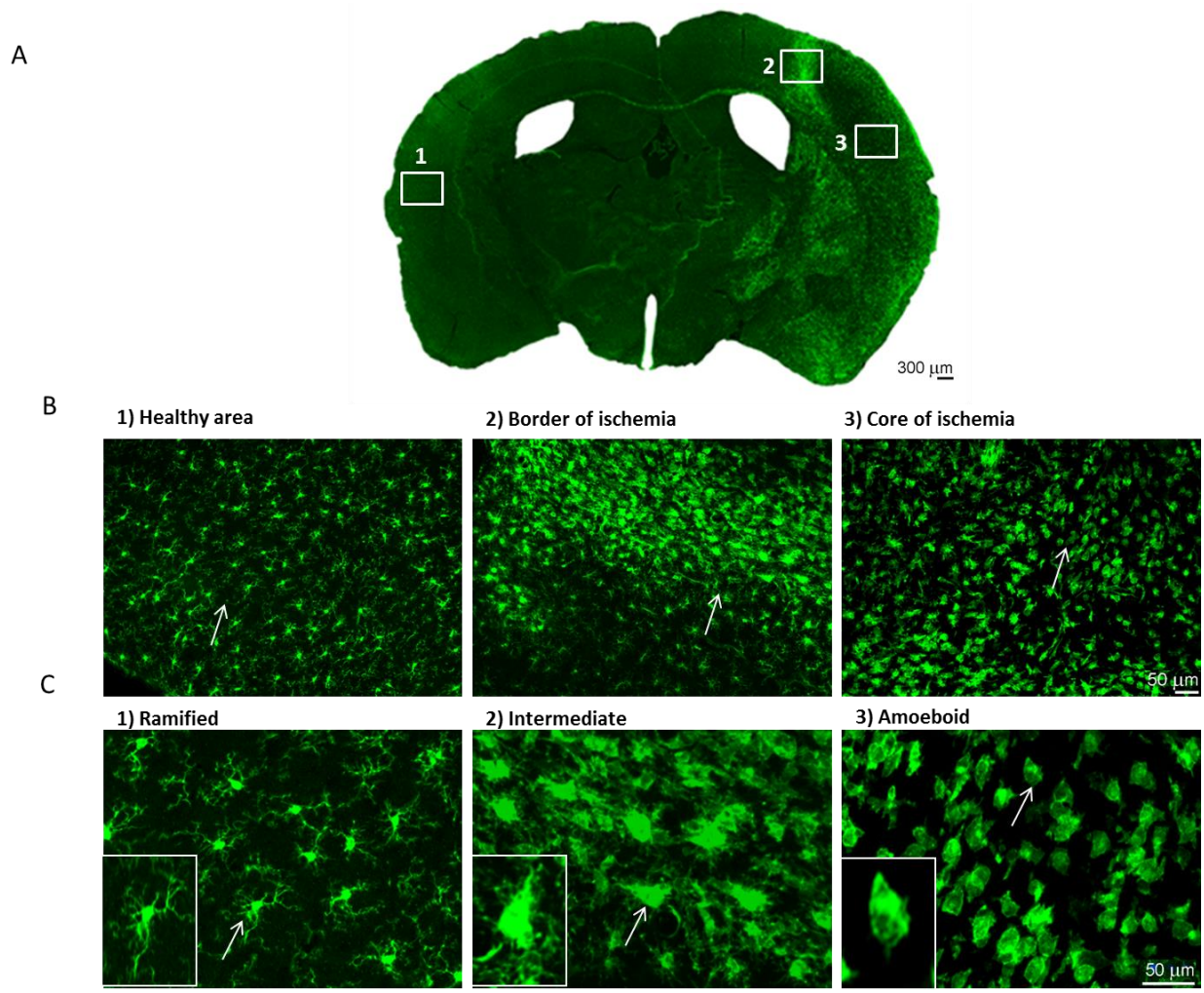

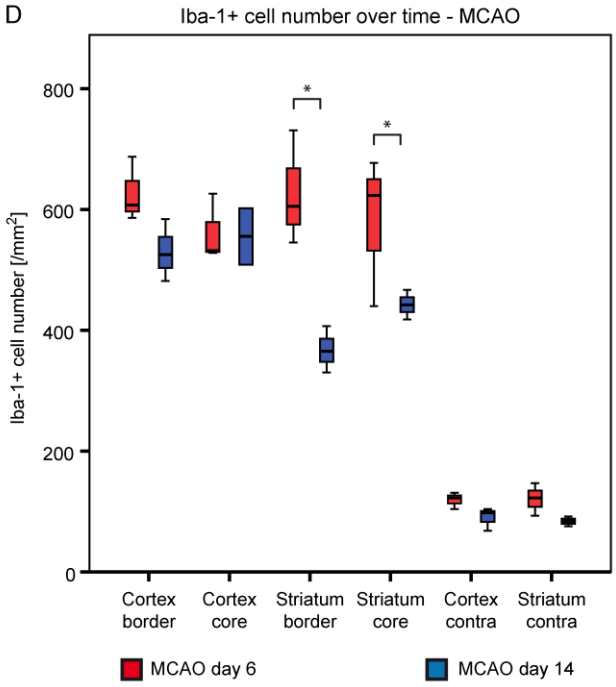

Figure 3.4 Different morphology and kinetics of microglia and macrophages after stroke. The photomicrograph shows the localization of Iba-1⁺ cells at the ipsilateral ischemic hemisphere at day 6 after stroke in 4X magnification (A). Following stroke, different morphologies of the microglia and macrophages can be detected: ramified, intermediate, amoeboid or round phenotype (B). The ischemic border showed the highest density of Iba-1+ cells, followed by the core region, whereas the contralateral hemisphere had the lowest cell density with only scattered Iba-1⁺ cells (C). The Box plot shows the number of Iba-1+ cells in the core and border zone of cortex and striatum at day 6 in comparison to day 14 after MCAO (D). A significant increase of Iba-1⁺ cells in striatal regions was detected at day 6 after MCAO, when compared to day 14. n=5 mice in each time point. *P<0.05 at Student's T-test).

3.2.2 The effect of miR-124 on microglia and macrophages after stroke

3.2.2.1 The kinetics of microglia and macrophages

To investigate the contribution of liposomated miR-124 to the dynamic response of microglia and macrophages after stroke, the expression of Iba-1 at different post stroke time was evaluated.

In the first experimental protocol, intracranial injection of miR-124 at day 2 after MCAO led to a significant increase in Iba-1$^+$ cells number in the ipsilateral ROIs, both cortical ($p = 0.002$ and $p = 0.026$) and striatal ($p = 0.032$ and $p = 0.042$), when compared to the stroke only and negative control groups at day 6 post MCAO (Figure 3.5 A). In these ROIs the interquartile ranges of Iba-1$^+$ cells number in miR treated group are in clear contrast to both control groups, the stroke only and negative control groups. Notably, the differences in Iba-1$^+$ cells distribution are pronounced in the cortical lesion border. In the cortical ROIs of the contralateral hemisphere, a slight increase in the Iba-1$^+$ cells number was detected in the miR treated group, but not significantly. No significant difference in the number of Iba-1$^+$ cells was found between the stroke only and negative control groups (Figure 3.5 A).

To observe the long-term effect of miR-124 on the microglia and macrophages kinetics after stroke, Iba-1$^+$ cells number were analyzed in second experimental protocol at day 14. The density of Iba-1$^+$ cells decreased in all three groups, especially in striatal ROIs, in comparison to day 6 post MCAO (Figure 3.5 A-B). No significant differences in Iba-1$^+$ cells number were observed between the miR treated group and both control groups in the ipsilateral ROIs at this time point (Figure 3.5 B). However, the miR treated group displayed a higher distribution range of the Iba-1$^+$ cells, with a trend towards a higher Iba-1$^+$ cells number.

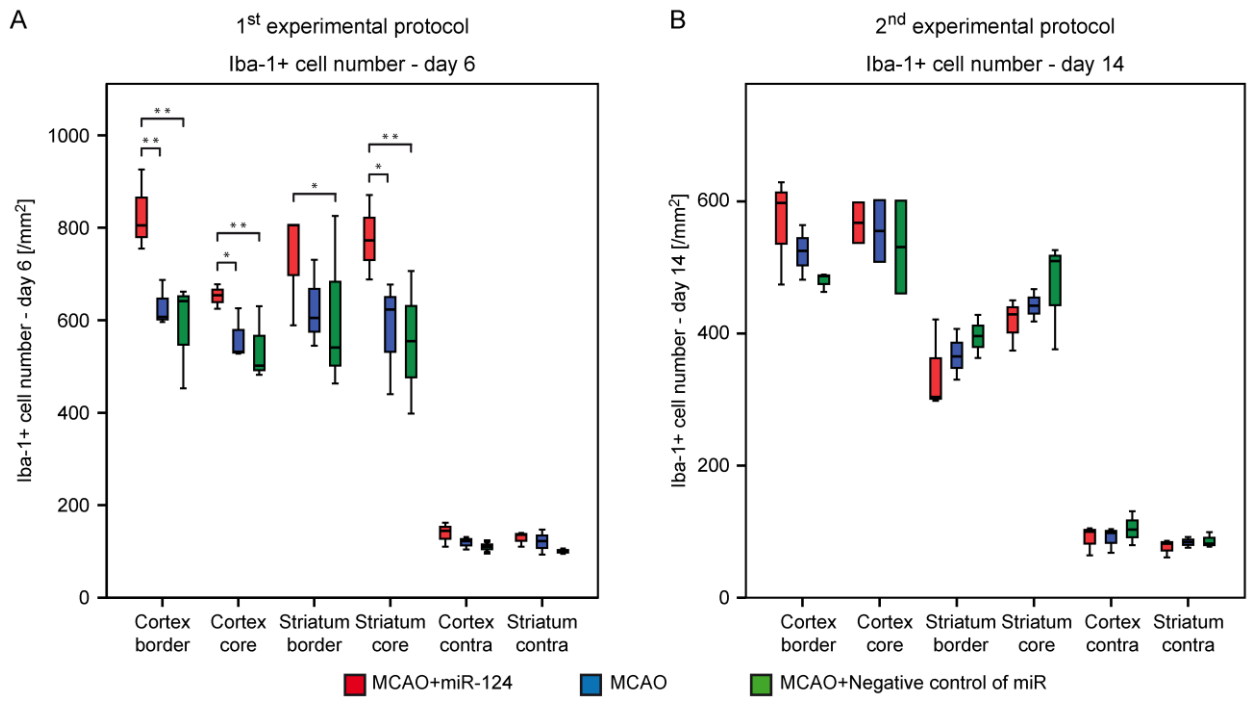

Figure 3.5 Dynamic proliferation of Iba-1⁺ cells after intracranial injection of miR-124 in stroke model. The density of Iba-1⁺ cells in the border and core regions of cortex and striatum at day 6 (A) and day 14 after MCAO (B). Significant increases in the Iba-1⁺ cells number in miR treated mice were detected at day 6 after stroke. No significant difference in number of Iba-1⁺ cells was found between the groups at day 14 after stroke. n=5-6 mice in each time point. Median and minimum/maximum values are shown; *P<0.05, **P<0.01 at one-way ANOVA (with Bonferroni's post hoc test).

3.2.2.2 The polarization of microglia and macrophages in the first experimental protocol – early injection and early observation

The various morphologies of microglia and macrophages after stroke are correlated to their dynamic polarization over time, transforming from an alternative activated M2 phenotype to a classical activated M1 phenotype. The characteristic polarization of microglia and macrophages was evaluated, using the representative M1-associated (CD16/32) or M2-associated (CD206 and Arginase-1) markers in double immunofluorescent staining with Iba-1 in the ischemic territory (See Figure 3.6, 3.7 and 3.8).

In the stroke only group the expression of the M1 marker CD16/32 by Iba-1$^+$ cells was high at day 6 after MCAO and remained elevated until day 14 (See Figure 3.8). In contrast, the immunofluorescence of the M2 markers CD206 and Arg-1 was slightly decreasing over time from day 6 until day 14 after MCAO (See Figure 3.6 and 3.7).

Intracranial administration of 100 ng miR-124 at day 2 after MCAO resulted in a significant increase of Iba-1$^+$ cells expressing CD206 at day 6 post stroke (In Cortex border: $p = 0.021$ and $p = 0.002$, Cortex core: $p = 0.014$, Striatum border: $p = 0.006$ and $p = 0.001$, and striatum core: $p = 0.008$ and $p = 0.001$ respectively; Figure 3.6 D), in comparison to both control groups. At this time point, the miR treated group showed the maximum CD206 positive cells number at around 600 cells/mm^2 in the border region of both cortical and striatal lesions. On the other hand, the control groups showed the maximum of CD206 positive cells number at around 300 cells/mm^2 (Figure 3.6 D). Interestingly, the border regions in comparison to core regions in the miR treated group, showed higher M2 marker expression. This trend of higher M2 marker expression in border regions of lesion emphasizes the more anti-inflammatory effect of miR-124 in the penumbra. The CD206 expression by Iba-1$^+$ cells showed no differences in both control groups at day 6 after MCAO.

The intracranial administration of miR-124 at day 2 after MCAO resulted in a significant increase of Iba-1$^+$ cells expressing Arg-1 in all ipsilateral selected regions at day 6 post MCAO (In Cortex border: $p = 0.0$ and $p = 0.0$, Cortex core: $P = 0.001$ and $p = 0.002$, Striatum

border: p = 0.026, and striatum core: p = 0.019 respectively; Figure 3.7 D). The increase of Arg-1 expression by Iba-1$^+$ cells in miR treated group was especially pronounced in the cortical regions of the lesion, with the maximum Arg-1$^+$ cells number at around 140 cells/mm^2 in the core of cortical region. On the other hand, the control groups showed the maximum of Arg-1$^+$ cells number at around 80 cells/mm^2. Interestingly, by comparing the core and border regions of the lesion, it is remarkable that in all three groups, but especially in the miR treated one, the Arg-1 expression by Iba-1$^+$ cells tends to be higher in the core regions than in the border (Figure 3.7 D). This underlines that Arg-1 is mostly expressed by strongly activated microglia and macrophages, since those are reported to accumulate mostly in the core regions of the lesion in neurodegenerative disorders (Lourbopoulos et al., 2015). The Arg-1 expression by Iba-1$^+$ cells showed no difference in the contralateral ROIs of all three groups.

On the other hand, intracranial injection of miR-124 at day 2 after MCAO led to a significant decrease in Iba-1+ cells expressing the M1 marker CD16/32 in all ipsilateral ROIs (In Cortex border: p = 0.006 and p = 0.012, Cortex core: p = 0.007, Striatum border: p = 0.039, and striatum core: p = 0.004 respectively; Figure 3.6 D), when compared to both control groups at day 6 after MCAO. In these ROIs, almost all the relevant 50th percentile, and interquartile ranges of the Iba-1+ cells expressing CD16/32 in the miR treated group were in clear contrast to both control groups. Thus, a clear trend towards less Iba-1+ cells expressing CD16/32 emphasizes a noticeably lesser pro-inflammatory environment in the miR treated group (Figure 3.8 D). No significant difference in the number of CD16/32 expressed by Iba-1+ cells was found between the stroke only and negative control groups. The CD16/32 expression by Iba-1+ cells showed no difference in the contralateral ROIs of all three groups.

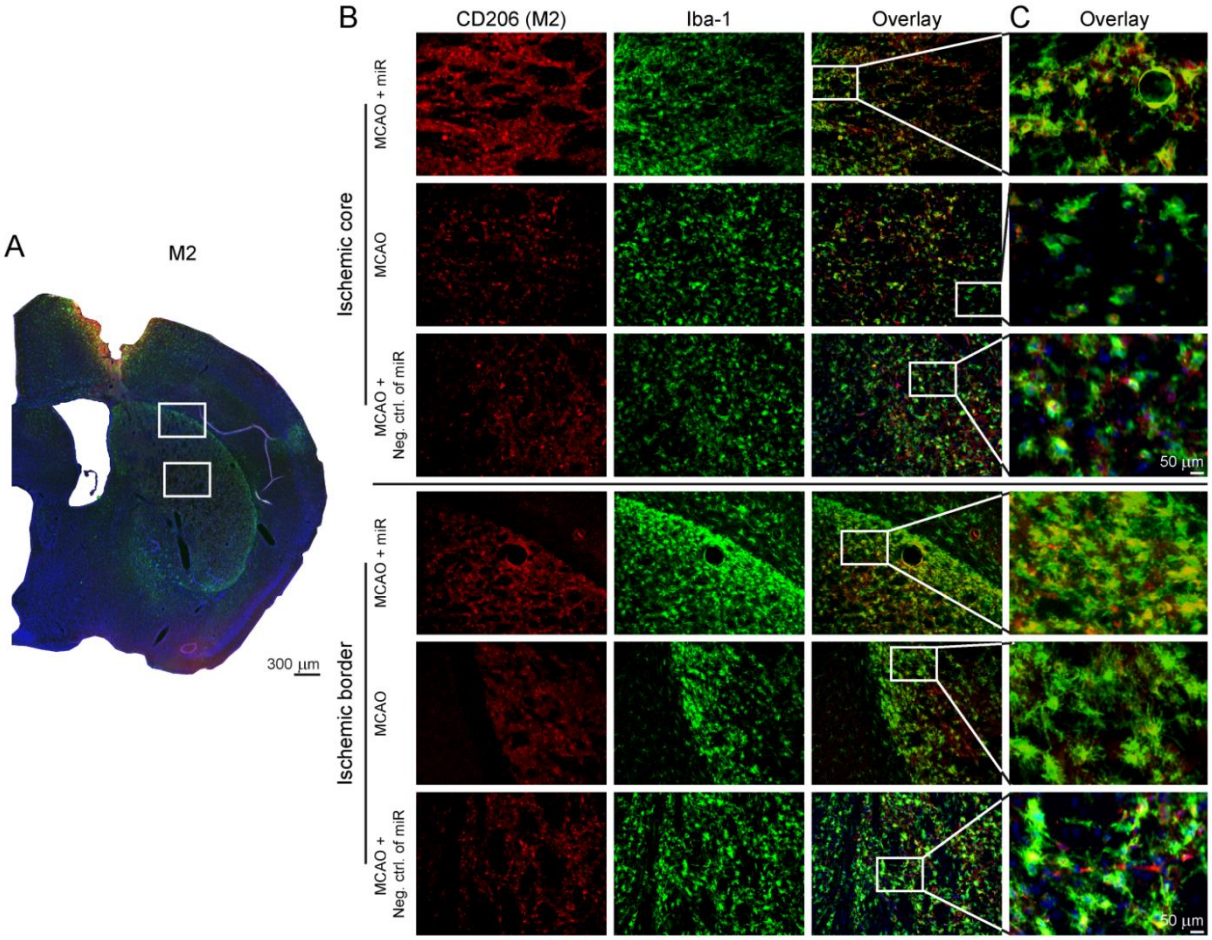

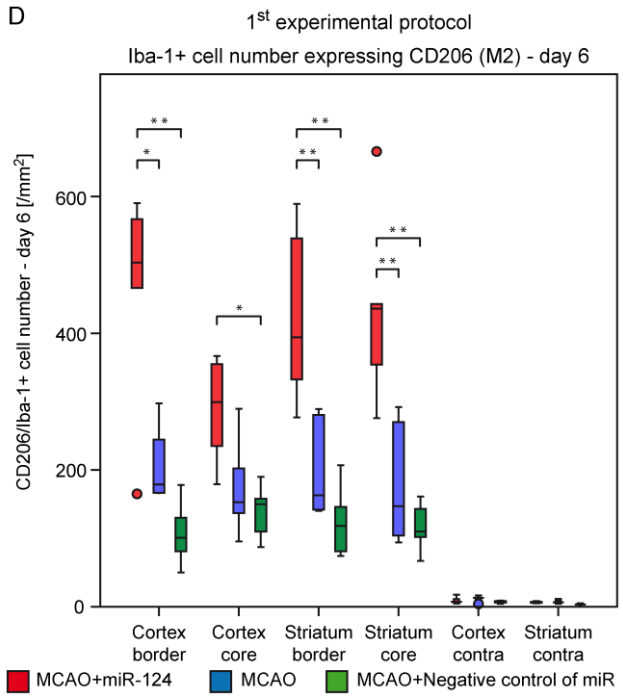

Figure 3.6 Effect of miR-124 on M2 phase of Microglia and macrophages. Photomicrographs show the examples of double-staining immunofluorescence of CD206 and Iba-1 on brain sections of ischemic core and border zones acquired from the first experimental protocol at 6 days after stroke. Illustrative 4X and 20X close-up magnification visualizes the changes in CD206 expression by Iba-1⁺ cells (A-C). Scale bar: 50 µm. Boxplots show the number of Iba-1⁺ cells expressing CD206 at the first experimental protocol (D). All ipsilateral ROIs clearly showed a significant increase in the number of Iba-1⁺ cells expressing CD206 in the miR treated group at day 6 after stroke (D). n=5 mice in each group. *P<0.05, **P<0.01 at one-way ANOVA (with Bonferroni's post hoc test).

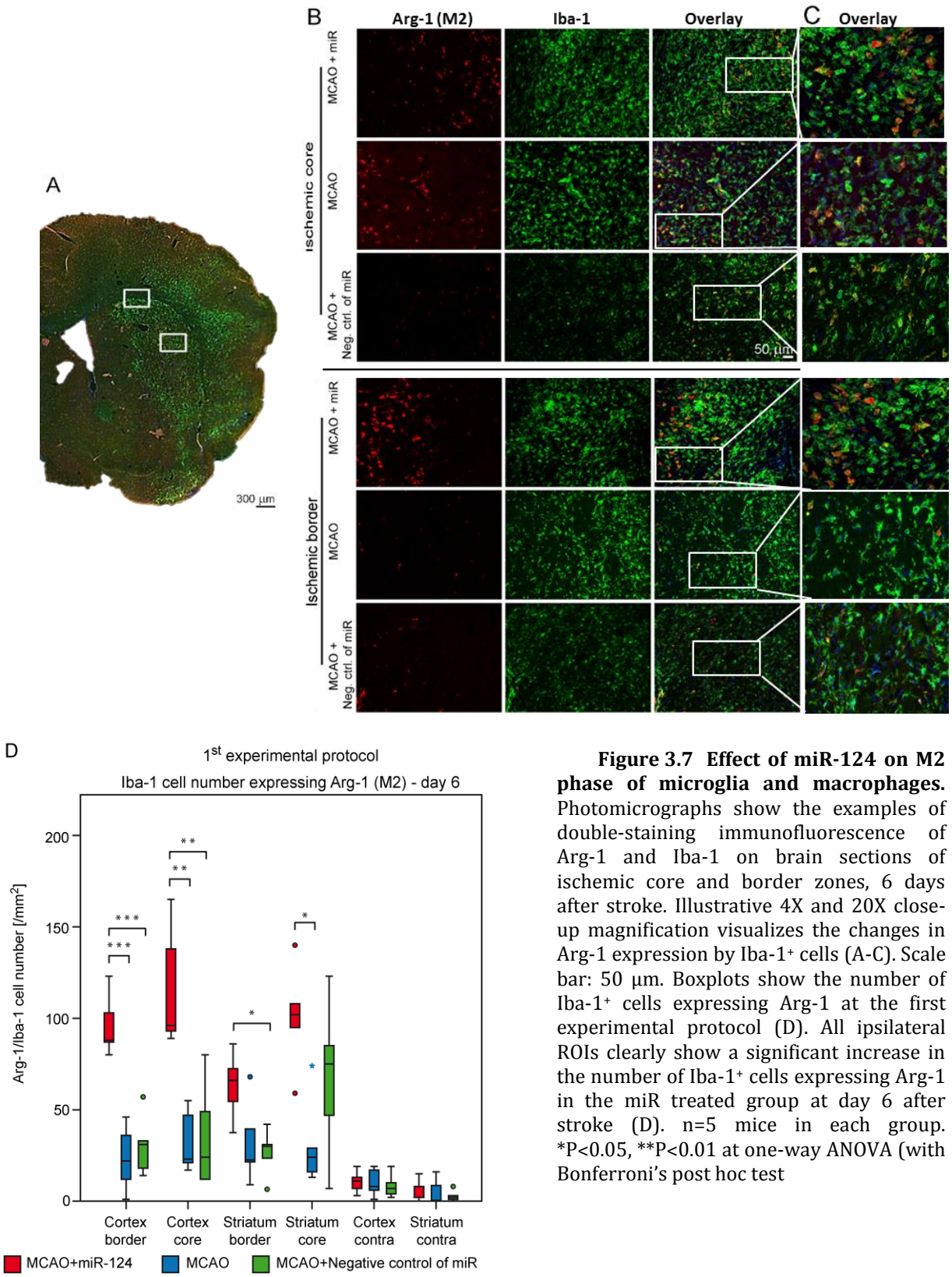

Figure 3.7 Effect of miR-124 on M2 phase of microglia and macrophages. Photomicrographs show the examples of double-staining immunofluorescence of Arg-1 and Iba-1 on brain sections of ischemic core and border zones, 6 days after stroke. Illustrative 4X and 20X close-up magnification visualizes the changes in Arg-1 expression by Iba-1⁺ cells (A-C). Scale bar: 50 µm. Boxplots show the number of Iba-1⁺ cells expressing Arg-1 at the first experimental protocol (D). All ipsilateral ROIs clearly show a significant increase in the number of Iba-1⁺ cells expressing Arg-1 in the miR treated group at day 6 after stroke (D). n=5 mice in each group. *P<0.05, **P<0.01 at one-way ANOVA (with Bonferroni's post hoc test

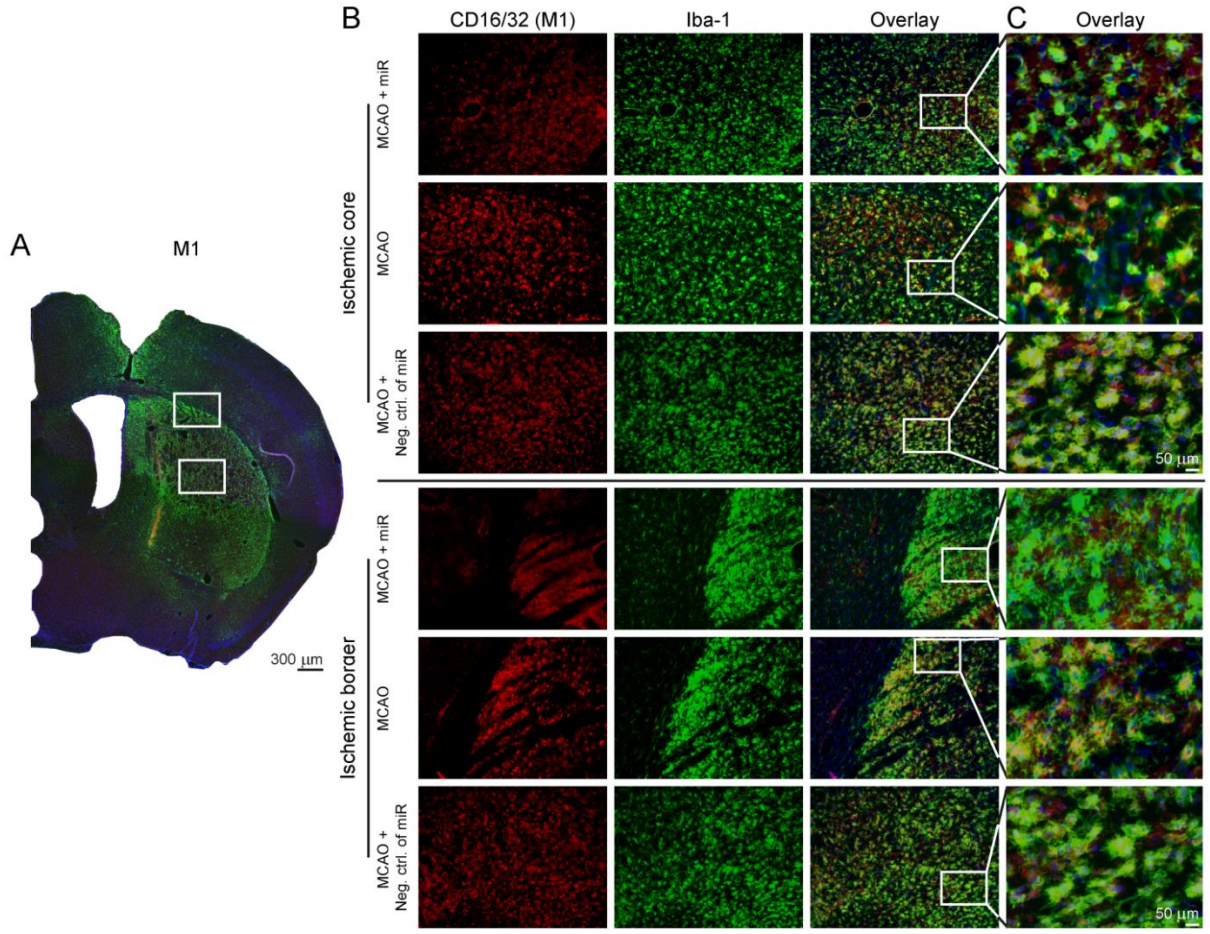

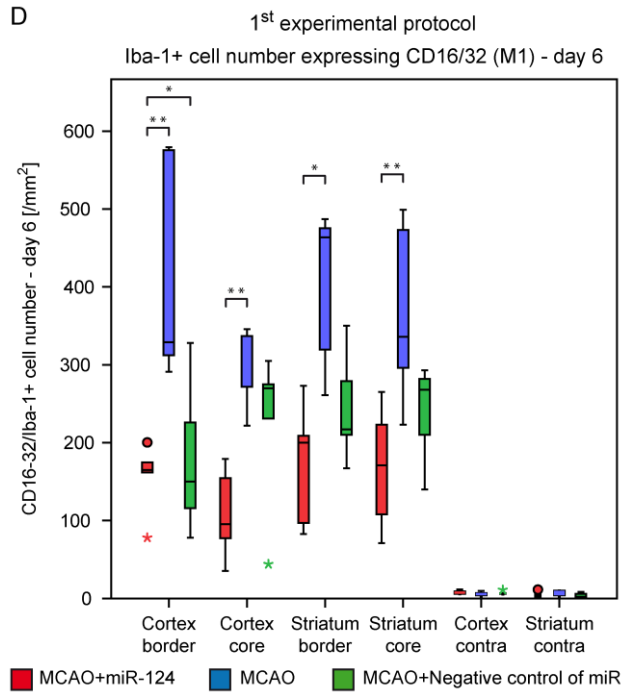

Figure 3.8 Effect of miR-124 on M1 phase of microglia and macrophages. Photomicrographs show the examples of double-staining immunofluorescence of CD16/32 and Iba1 on brain sections of ischemic core and border zones, 6 days after stroke. Illustrative 4X and 20X close-up magnification visualizes the changes in CD16/32 expression by Iba-1⁺ cells (A-C). Scale bar: 50 µm. Boxplots show the number of Iba-1⁺ cells expressing CD16/32 in the ipsilateral and contralateral ROIs of cortex and striatum at first experimental protocol (D). The results confirms that the intracranial injection of miR-124 at day 2 after MCAO results in a significant decrease of the number of Iba-1+ cells expressing CD16/32 monitored at day 6 post stroke (d). n=5 mice in each group. *P<0.05, **P<0.01 at one-way ANOVA (with Bonferroni's post hoc test).

The results of the first experimental protocol clearly show that the early treatment with miR-124, 2 days after MCAO, had an strong effect on the polarization of microglia and macrophages at the first week after stroke. The miR-124 strongly increased the M2 protective markers, CD206 and Arg-1, and decreased the M1 marker, CD16/32. This modulation was particularly evident in the border regions of the stroke, emphasizing the more anti-inflammatory effect of miR-124 in the penumbra. Moreover, the strong modulation of the M1 and M2 markers expression in the microglia and macrophages was associated with an increase in the Iba-1^{+} cells number in the same ROIs (See Figure 3.5 A). Thus, the miR-124 not only skewed the microglia and macrophages towards a more pronounced M2 phenotype, but also led to an increased proliferation of immune cells.

3.2.2.3 The polarization of microglia and macrophages in the second experimental protocol – early injection and late observation

Long-term effect of the miR-124 injection were observed, when the mice received intracranial injection of miR-124 or the random primer 2 days after MCAO and were sacrificed at day 14 after MCAO.

Concerning the expression of CD206 by Iba-1$^+$ cells, no significant difference was detected at day 14 after MCAO, when comparing the three groups of this experimental protocol. In the cortical lesion ROIs, the miR treated group showed a larger interquartile range compared to both control groups, with the middle 50% of the Iba-1$^+$ cells expressing CD206 reaching up to 350 cells/mm^2. Thus, it indicates a trend towards a higher amount of CD206 expression by Iba-1$^+$ cells in the cortical regions of miR treated group at day 14 after MCAO (Figure 3.9 B). In the border of striatum, almost all three groups showed the same interquartile range. In the core of striatum, both the miR treated and the negative control groups displayed somehow a similar larger range of Iba-1$^+$ cells expressing CD206 in comparison to the stroke only group, however not significantly (Figure 3.9 B). This increase might be induced by the injection procedure and not by the miR-124 treatment. No differences were detected in the ROIs of the contralateral hemisphere.

Regarding the Arg-1 expression by Iba-1$^+$ cells, no significant difference was detected between the three groups at day 14 after MCAO (Figure 3.10 B). In the border of the cortical region, both the miR treated and the negative control groups displayed almost a similar Iba-1$^+$ cells number expressing Arg-1. This increase might be induced by the injection procedure. In the border of striatal region, the miR treated group displayed a larger interquartile range, compared to both control groups, with the middle 50% of the Iba-1$^+$ cells expressing Arg-1 reaching up to 40 cells/mm^2. On the other hand both control groups displayed smaller interquartile ranges. The stroke only group showed the lowest amount of Iba-1$^+$ cells expressing Arg-1 at this time point (Figure 3.10 B). No difference was detected in the ROIs of the contralateral hemisphere.

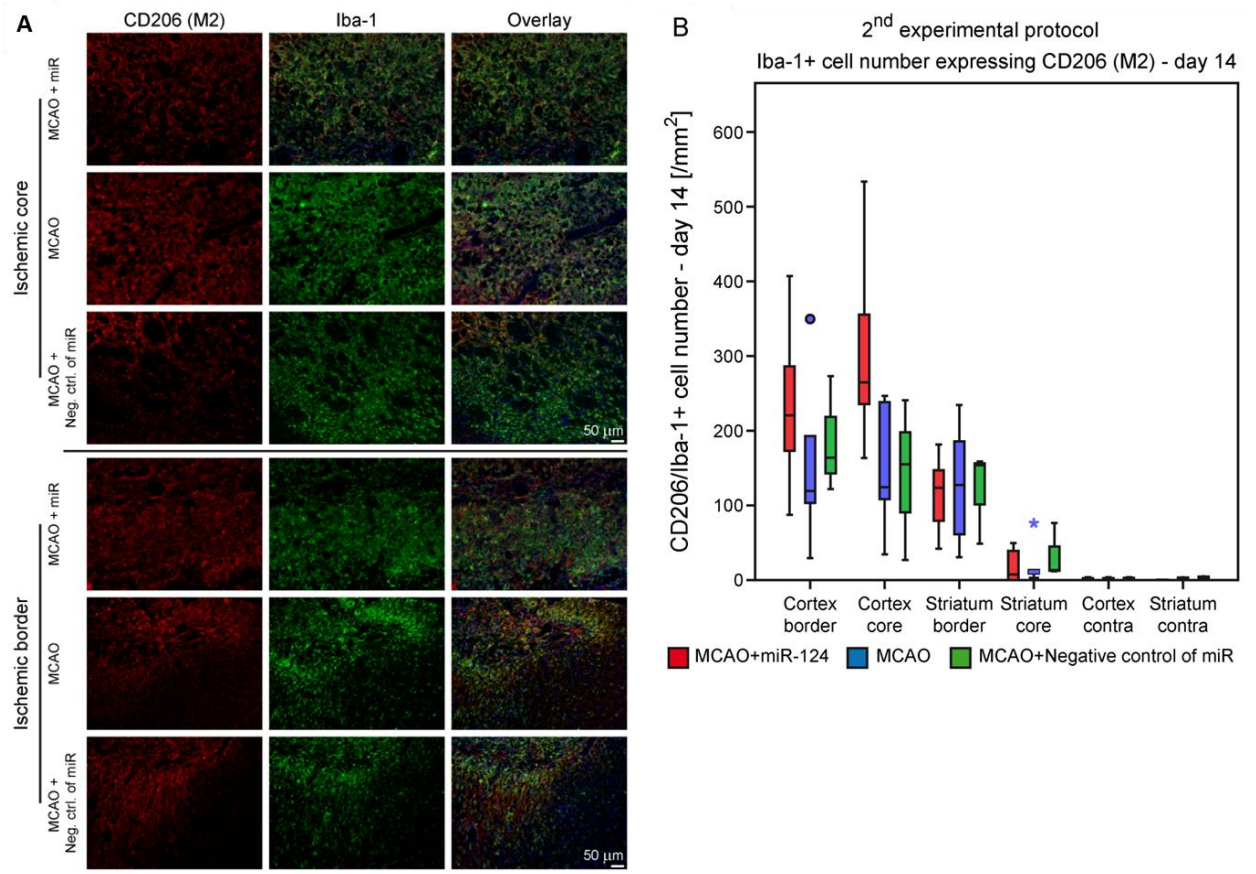

Figure 3.9 Effect of miR-124 on M2 phase of microglia and macrophages at day 14 after stroke of second experimental protocol. Photomicrographs show the examples of double-staining immunofluorescence of CD206 and Iba-1 on brain sections of ischemic border zones acquired at day 14 after stroke (A). Scale bar: 50 µm. Boxplots show the number of Iba-1⁺ cells expressing CD206 in the ipsilateral and contralateral ROIs of cortex and striatum at day 14 after stroke (B). The results show no difference in comparison of three groups. n=3-6 mice.

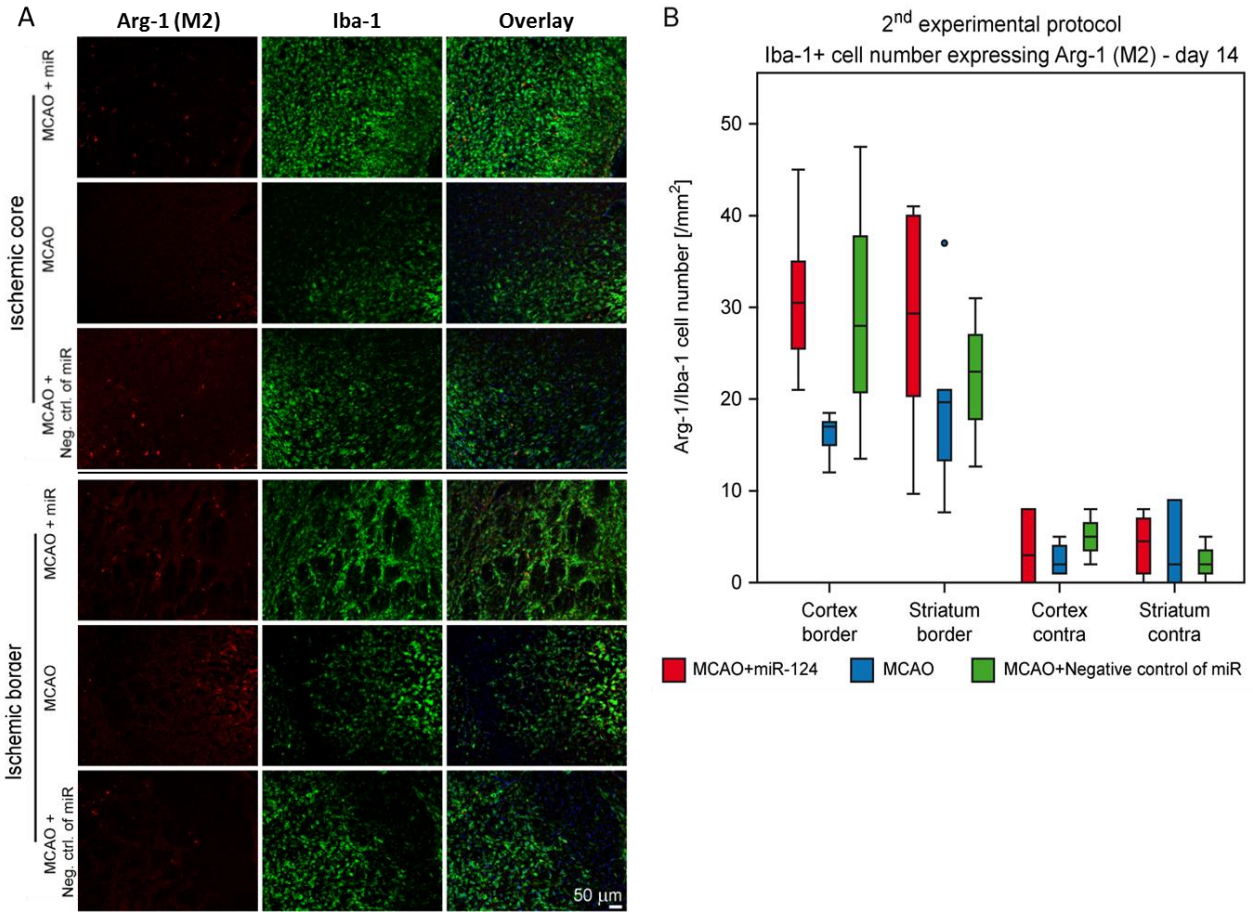

Figure 3.10 Effect of miR-124 on M2 phase of microglia and macrophages at day 14 after stroke of second experimental protocol. Photomicrographs show the examples of double-staining immunofluorescence of Arg-1 and Iba-1 on brain sections of ischemic border zones acquired at day 14 after stroke (A). Scale bar: 50 µm. Boxplots show the number of Iba-1$^+$ cells expressing Arg-1 in the ipsilateral and contralateral ROIs of cortex and striatum at day 14 after stroke (B). The results show no difference in comparison of the three groups. n=3-6 mice.

Regarding the long-term effect of early miR-124 injection on the M1 marker expression, CD16/32, no significant effect was detected between the three groups at day 14 after MCAO. In the cortical border region, the miR treated group showed higher CD16/32 expression by Iba-1$^+$ cells, compared to both control groups. However, in the cortical core region the median was lower in miR treated group (Figure 3.11 B). In the striatal regions, in the proximity of the injection channel, the median of both border and core regions was lower in the miR treated group, showing a trend towards a lower amount of CD16/32 expression by

Iba-1⁺ cells, compared to both control groups. No difference was detected in the ROIs of the contralateral hemisphere (Figure 3.11 B).

On the one hand, the M1 response increased strongly in the miR treated group from day 6 to day 14 after MCAO, showing a decreasing effect of miR-124 at the longer time (12 days vs. 4 days) after intracranial injection. On the other hand, the lower M1 marker expression in striatal region of the miR treated group showed that the anti-inflammatory effect of miR-124 was not completely lost at the latter time point.

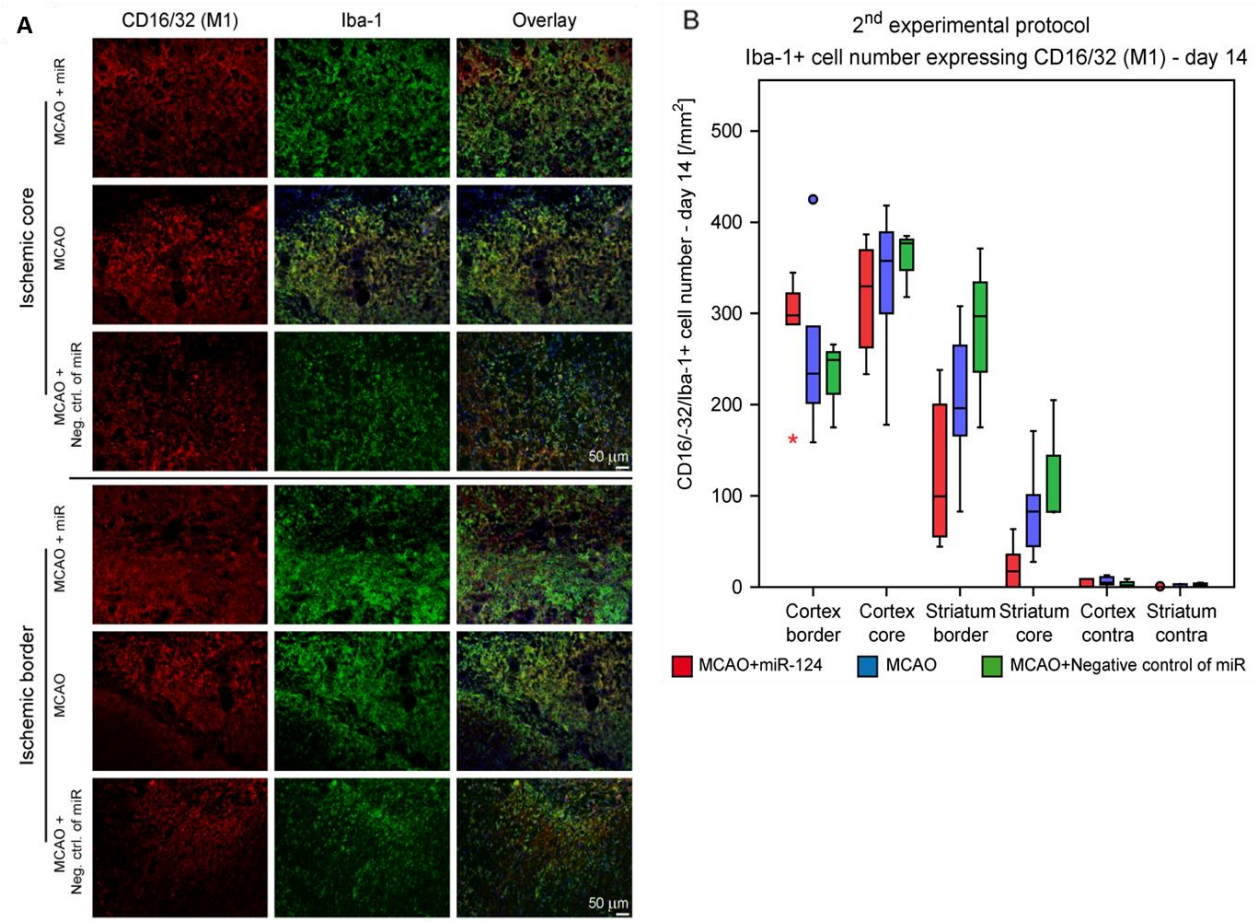

Figure 3.11 Effect of miR-124 on M1 phase of microglia and macrophages at day 14 after stroke of second experimental protocol. Photomicrographs show the examples of double-staining immunofluorescence of CD16/32 and Iba-1 on brain sections of ischemic core and border zones at day 14 after stroke (A). Scale bar: 50 µm. Boxplots show the number of Iba-1⁺ cells expressing CD16/32 in the ipsilateral and contralateral ROIs of cortex and striatum at day 14 after stroke of second experimental protocol (B). No difference in comparison of three groups was seen. n=3-6 mice.

3.2.2.4 The polarization of microglia and macrophages in the third experimental protocol - late miR-124 injection

To survey the effect of intracranial injection of miR-124 at a later stage of ischemia, when M1 polarization dominates, 100 ng of miR-124 was injected 10 days after MCAO. The induced changes in the polarization of Iba-1$^+$ cells were analyzed 4 days later. It is worth mentioning that there were no significant difference in the results of the first and the second experimental protocols between both control groups, the negative control and stroke only groups. Thus, in our study the third experimental protocol lacks a negative control group.

In this experiment, no significant difference in Iba-1$^+$ cells number expressing M2 marker CD206 was detected between the miR treated and the stroke only group. In the cortical regions, both miR treated and stroke only groups showed approximately the same amount of CD206 expression by Iba-1$^+$ cells. As regards, in the striatal regions a trend of higher CD206$^+$ cell number was detected in the miR treated group (Figure 3.12 B). It is worth to note, both interquartile range and the 50th percentile of CD206 expression by Iba-1$^+$ cells in the striatal core region were at higher values than the stroke only group, showing the increased M2 marker expression by Iba-1$^+$ cells adjacent to the injection channel at this time point. No differences were detected in the ROIs of the contralateral hemisphere (Figure 3.12 B).

The number of Iba-1+ cells expressing Arg-1 was higher in the miR treated group, especially in the striatal border region, although not significantly (Figure 3.12 D). In the cortical border region, the variation in the Iba-1$^+$ cells expressing Arg-1 in the miR treated group was very high, with an interquartile range from 8 to 53 cells/mm^2, indicating a higher Arg-1 expression in some animals. The Arg-1 expression by Iba-1$^+$ cell did not cross a value above 20 cells/mm^2 in the stroke only group.

Interestingly in this experimental protocol, pronounced decline in M1 marker expression of Iba-1$^+$ cells was visible in the miR treated group, particularly in the border and core regions of striatum. The coherent interquartile range and the 50th percentile of all

ipsilateral ROIs in miR-124 treated group are in remarkably lower values confirming the reduced M1 expression (Figure 3.13 B).

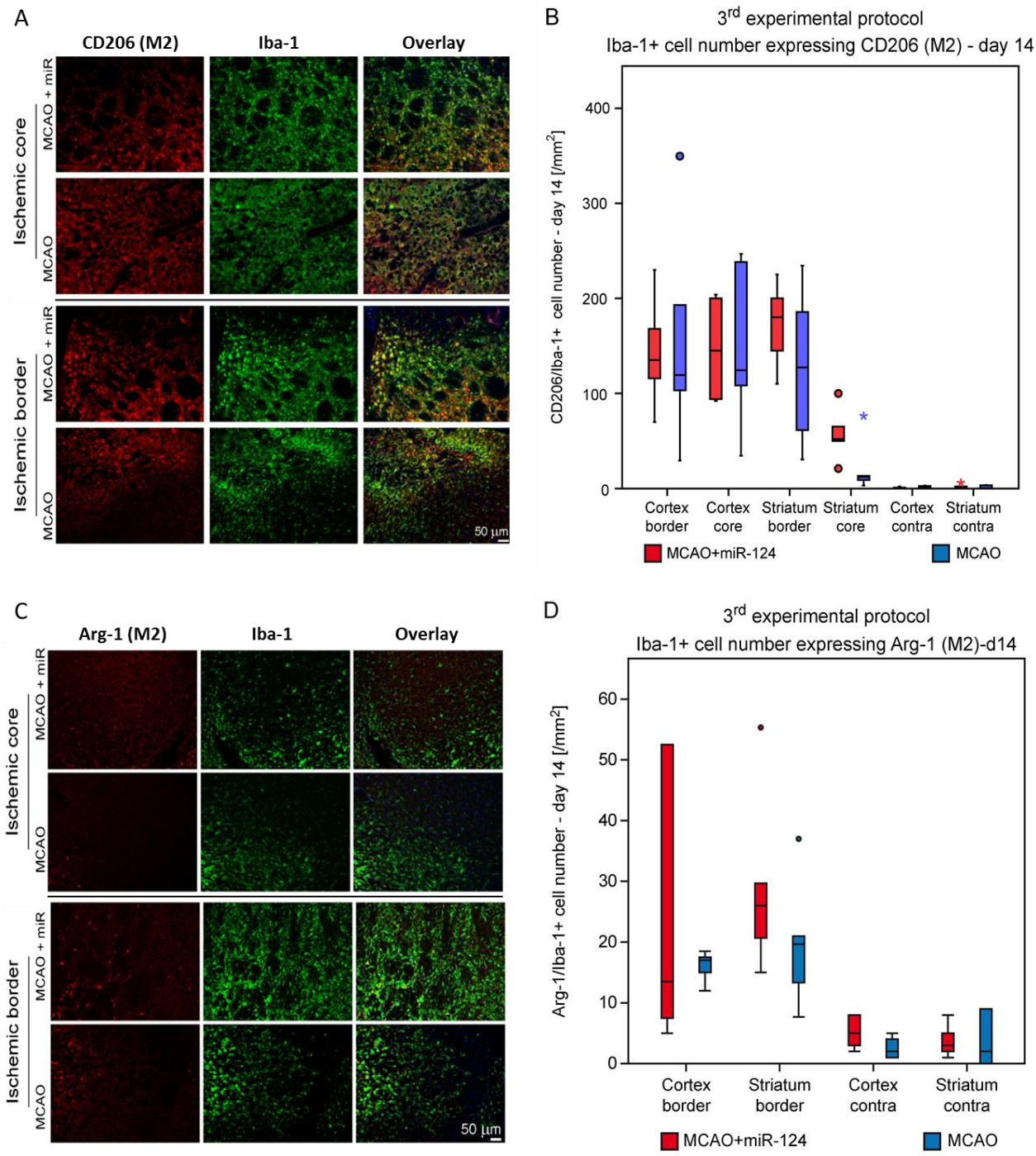

Figure 3.12 Effect of delayed miR-124 injection on M2 phenotype of microglia and macrophages. Photomicrographs show the examples of double-staining immunofluorescence of CD206 expression (A) and Arg-1(C) by Iba-1⁺ cells on brain sections of ischemic core and border zones acquired from third experimental protocol, where miR-124 was injected 10 days after MCAO and the mice were perfused 4 days later. Scale bar: 50 µm. Boxplots show the number of Iba-1⁺ cells expressing M2 markers in the ipsilateral and contralateral

ROIs of cortex and striatum at the third experimental protocol (B and D). The results show no difference in comparison of two groups. n=5 mice in each group. P<0.05, at independent one-tailed Student's t-test.

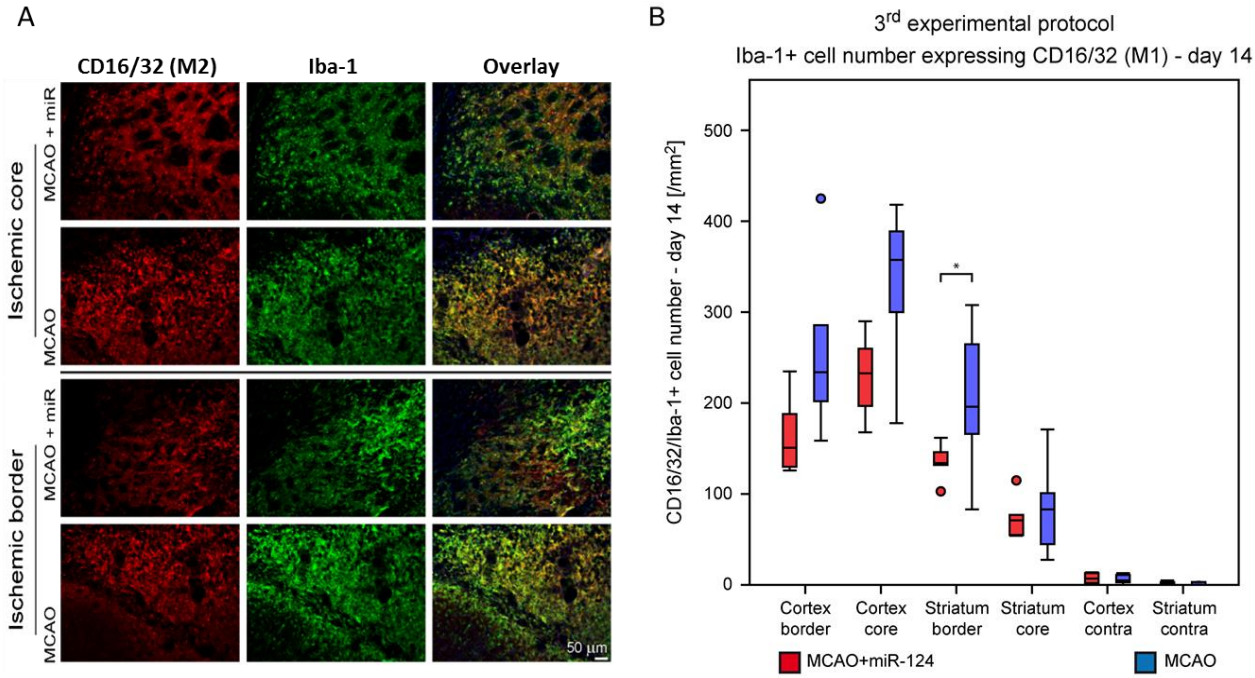

Figure 3.13 Effect of delayed miR-124 injection on M1 phenotype of microglia and macrophages. Photomicrographs show the examples of double-staining immunofluorescence of CD16/32 expression by Iba-1⁺ cells (A) on brain sections of ischemic core and border zones acquired from third experimental protocol, where miR-124 was injected 10 days after MCAO and the mice were perfused 14 days after MCAO. Scale bar: 50 µm. Boxplots show the number of Iba-1⁺ cells expressing M1 marker in the ipsilateral and contralateral ROIs of cortex and striatum at day 14 after stroke of the third experimental protocol (B). The results show that the intracranial injection of miR-124 at day 10 after MCAO led to a significant decrease of Iba-1⁺ cells expressing CD16/32 in striatal border region monitored at day 14 post stroke (d). n=5 mice in each group. *P<0.05, at independent one-tailed Student's t-test.

3.2.2.5 Comparison of the ratio of pro-inflammatory (M1) to anti-inflammatory (M2) phenotype in all three experimental protocols

To determine the efficiency of miR-124 in providing the anti-inflammatory environment after ischemic stroke, we analyzed the ratio of pro-inflammatory (M1) to anti-inflammatory (M2) phenotype of Iba-1$^+$ cells for all experimental protocols (Figure 3.14 and 3.15).

In the border region of striatal lesion of the first experimental protocol, the miR-124 administration resulted in a significant decrease of M1:M2 ratio in the miR treated group, in comparison to both control groups at day 6 after stroke, ($p = 0.019$ and $p = 0.021$), (Figure 3.14 A). Both a noticeable decrease of the number of Iba-1$^+$ cells expressing M1 marker and a significant increase of the number of Iba-1$^+$ cells expressing M2 marker were the reason of the lower M1:M2 ratio at this experimental protocol. From day 6 to day 14 in the second experimental protocol, the effect of miR-124 administration on modulating the polarization of Iba-1$^+$ cells gradually decreased. However, the ratio of M1:M2 was at about 1.04, showing the presence of the same amount of both pro-inflammatory (M1) and anti-inflammatory (M2) phenotype of Iba-1$^+$ cells, which confirms the persistent anti-inflammatory effect of the miR-124 still at day 14 after stroke. In addition, the shift in M1:M2 ratio remained significantly different in the miR treated group compared to the negative control group at this protocol, ($p = 0.016$), but not to the stroke only group (Figure 3.14 B). Interestingly, in the third experimental protocol, the result of the late miR-124 injection showed significant decrease of M1:M2 ratio, in comparison to the stroke only group ($p = 0.013$), (Figure 3.14 C).

The same comparison was made for the M1:M2 ratio of the border region of cortical lesion. In the first experimental protocol, the miR-124 administration resulted in a significant decrease of M1:M2 ratio in the miR treated group, in comparison to both control groups at day 6 after stroke, ($p = 0.023$ and $p = 0.047$, respectively), (Figure 3.14 A). No significant difference was detected in the M1:M2 ratio at day 14 after stroke in this region between the groups of the second experimental protocol (Figure 3.15 B). The late miR-124 injection in the third experimental group resulted in a lower M1:M2 ratio in the miR treated group compared to the stroke only group, but not significantly (Figure 3.15 C).

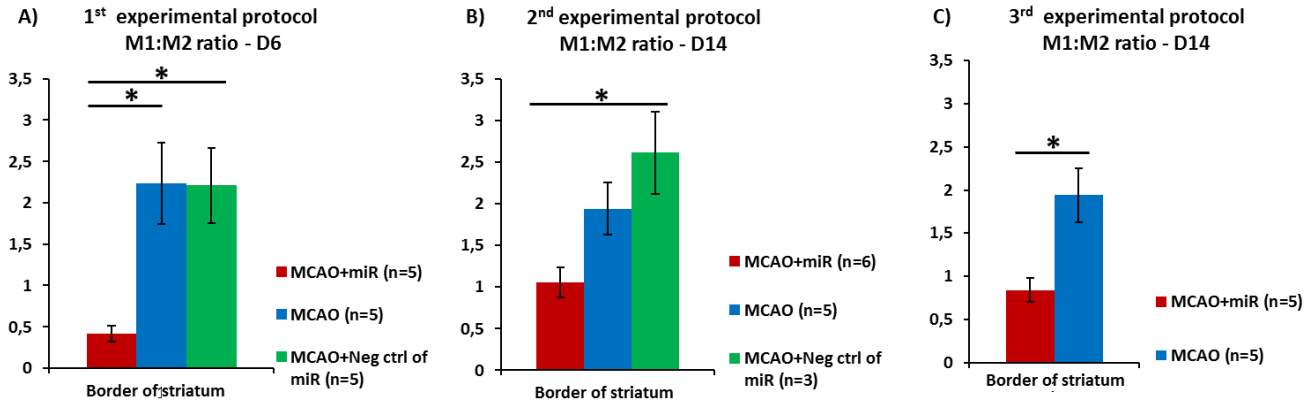

Figure 3.14 Effect of miR-124 on the M1:M2 ratio of microglia and macrophages in the border region of striatal lesion. The graphs show the M1:M2 ratio at day 6 (A), and at day 14 related to early injection of miR-124 (B) or to late injection of miR-124 (C). n=5-6 mice in each group and each time point. Mean ± SEM values are shown. *P<0.05 at one-way ANOVA with Bonferroni's post hoc test for three groups of the first and second experimental protocols and independent t-test for two groups in the third experimental protocol.

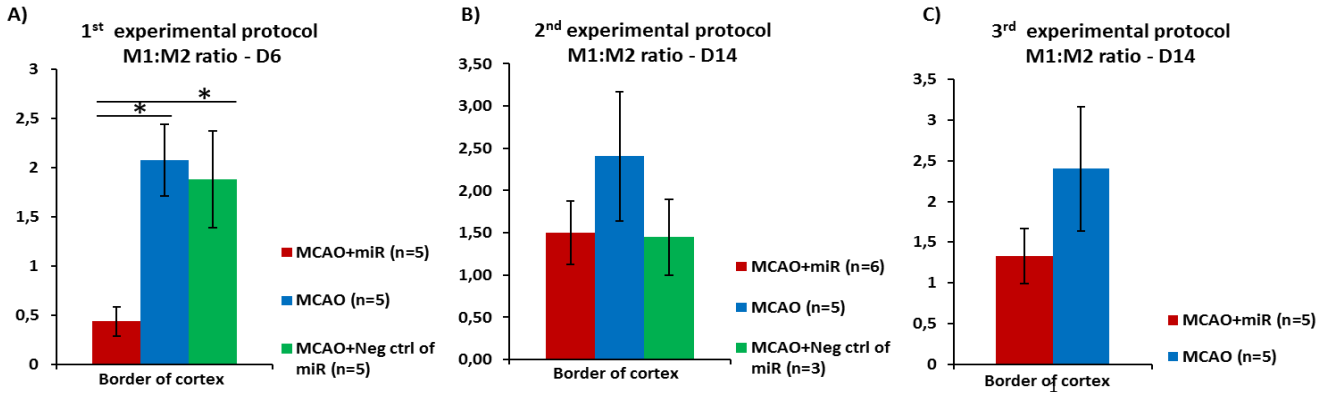

Figure 3.15 Effect of miR-124 on the M1:M2 ratio of microglia and macrophages in the border region of cortical lesion. The graphs show the M1:M2 ratio at day 6 (A), and at day 14 related to early injection of miR-124 (B) or to late injection of miR-124 (C). n=5-6 mice in each group and each time point. Mean ± SEM values are shown. *P<0.05 at one-way ANOVA with Bonferroni's post hoc test for three groups of the first experimental protocol.

3.2.3 The effect of miR-124 on neuronal survival after stroke

3.2.3.1 Different morphology of NeuN positive cells after stroke

The NeuN antibody, which represents the neuron-specific nuclear protein, was used for the detection of neurons. NeuN positive cells were visible in both, the intact and ischemic hemispheres, although with various morphology and distribution in the ischemic core and the surrounding regions. The round shape NeuN$^+$ cells were intensely localized in the healthy area, which could hardly be detected in the lesion core (Figure 3.16 A). In the core of the lesion NeuN$^+$ cells had smaller, more shrunken cell bodies (Figure 3.16 C) and were widely scattered compared to the border of the lesion or the healthy area that were densely covered with positive cells (Figure 3.16 B). In the border of the lesion, a mixture of swollen and healthy round shape NeuN$^+$ cells were detected with lower density, in comparison to the healthy hemisphere.

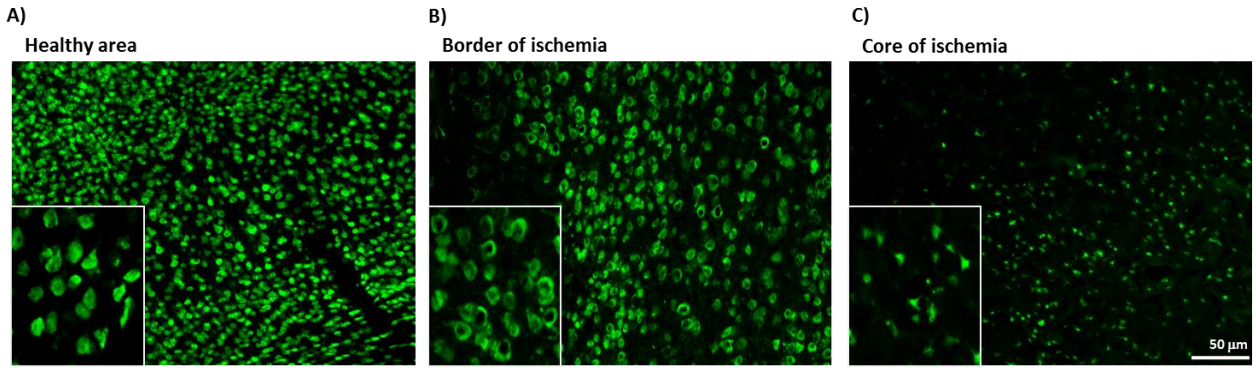

Figure 3.16 Different morphology of NeuN positive cells after stroke. The photomicrographs show the localization of NeuN$^+$ cells at healthy hemisphere (a), border of the lesion (b) and core of the lesion (c) at day 6 after stroke in 20X magnification. Following stroke the different morphology of NeuN positive cells was detected; round shape cells with high intensity in the healthy area, small shrunken cells in the core and swollen ones in the border region (a-c).

3.2.3.2 The effect of early injection of miR-124 on neuronal survival after stroke

To investigate the contribution of liposomated miR-124 to neuronal survival after stroke, the expression of NeuN at different time points after MCAO, day 6 and 14, was evaluated (Figure 3.17 A-C).

Intracranial injection of miR-124 at day 2 after MCAO led to a significant increase of $NeuN^+$ cells number in the ipsilateral ROIs at day 6 after MCAO compared to the stroke only and negative control groups (Figure 3.18 A). The increased neuronal survival was especially pronounced in the border region of cortex in miR treated group. In this region, the boxplots clearly show the middle 50% of $NeuN^+$ cells number, interquartile range, was more than twice as high than in the both control groups. Also, in the border region of striatum, the interquartile ranges of $NeuN^+$ cells number of miR treated group were in clear contrast to both control groups. Generally, there was lower number of neurons in the striatal regions in comparison to cortical regions in all three groups, which could be due to the general different distribution of neurons in various regions of brain (Figure 3.18 A).

Regarding the long-term effect of miR-124 on neuronal survival, the neuroprotective effect of the early intracranial injection of miR-124 was not detectable at day 14 after MCAO (Figure 3.18 B). In all three groups, less neurons were detected in both cortical and striatal regions than in the contralateral ROIs. In the border region of the cortical lesion, almost all three groups displayed similar amounts of neurons. In the border region of the striatal lesion, the amount of neurons was clearly higher in the stroke only group, which could be due to the implantation procedure and the associated wounds in both injected groups. Therefore, the neuroprotective effect of early miR-124 injection, 2 days after MCAO, decreased to a non-significant level 12 days after injection.

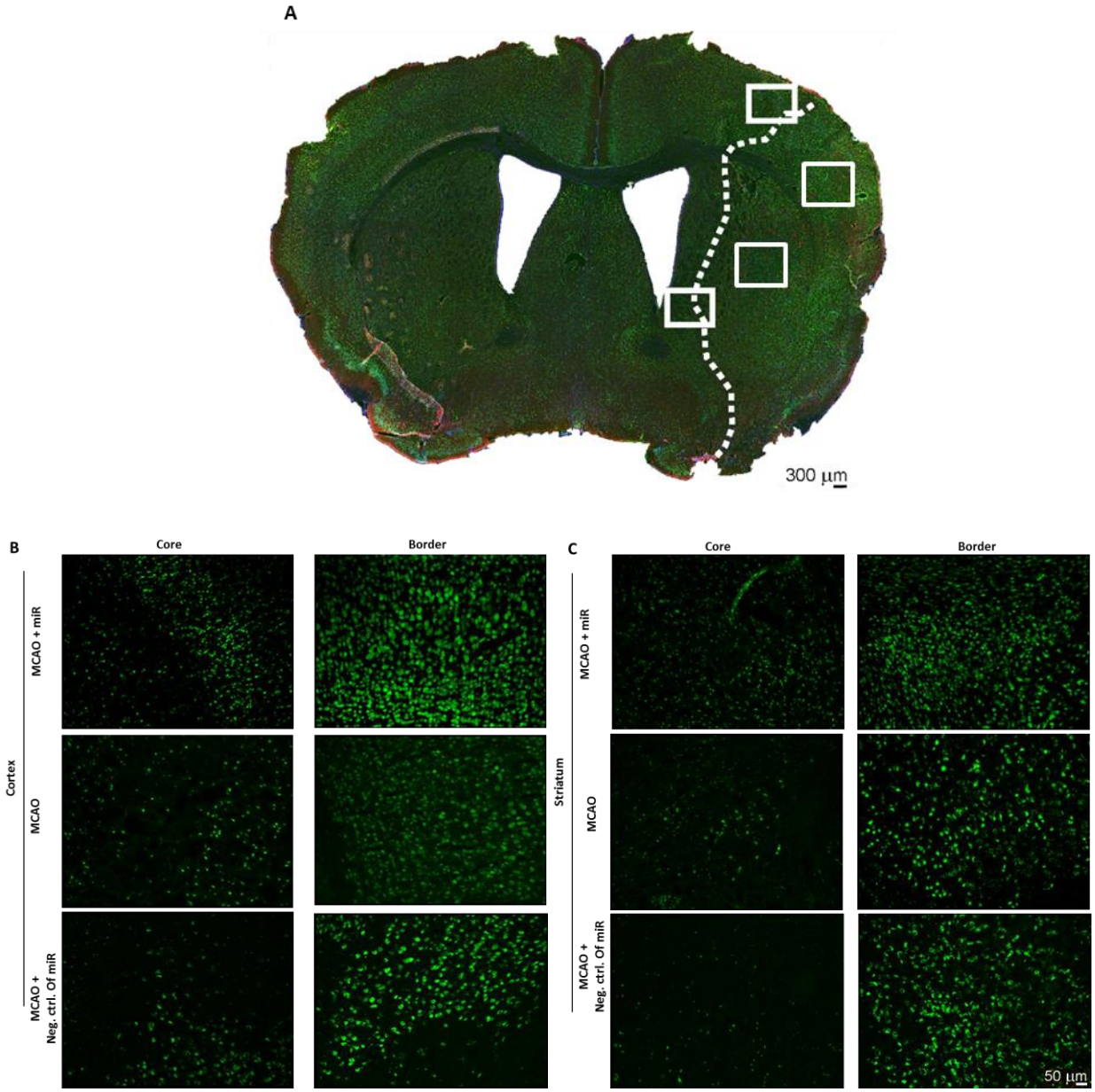

Figure 3.17 Effect of early intracranial injection of miR-124, day 2 after MCAO, on neuronal survival. Photomicrographs show the examples of staining immunofluorescence of NeuN on brain sections of ischemic border and core of cortical and striatal regions, acquired from first experimental protocol at 6 days after stroke (B-C). Illustrative 4X and 20X magnification visualize the changes in NeuN positive cells number (A-C). Scale bar: 50 µm.

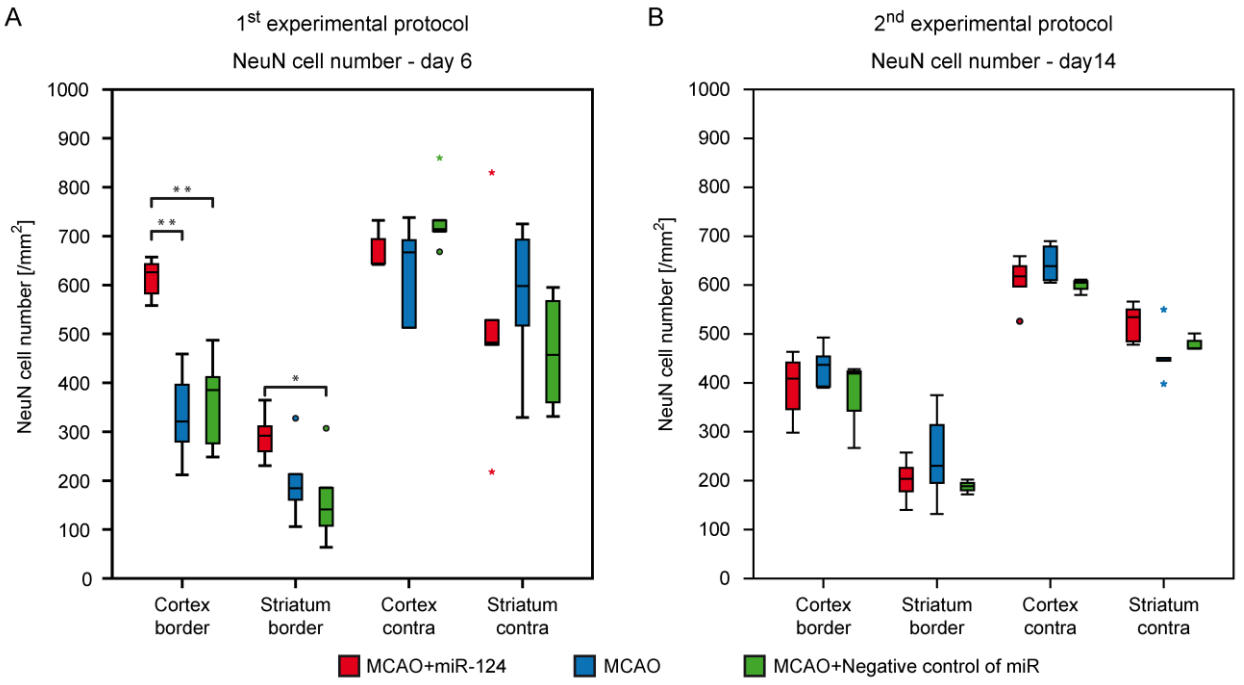

Figure 3.18 The effect of early intracranial injection of miR-124, at day 2 after MCAO, on neuronal survival at day 6 after MCAO. Boxplots shows the number of NeuN⁺ cells at the first experimental protocol (A) and the second experimental protocol (B). The ipsilateral ROIs of first experimental protocol clearly show a significant increase of NeuN⁺ cells in the miR treated group at day 6 after stroke (A). n=5-6 mice in each group. *P<0.05, **P<0.01 at one-way ANOVA (with Bonferroni's post hoc test).

3.2.3.3 The effect of the late intracranial injection of miR-124 on neuronal survival after stroke

To survey the effect of intracranial injection of miR-124 at the late stage of stroke, miR-124 was injected 10 days after MCAO and the neuronal survival was analyzed 4 days later.

At this point, no significant difference between the miR treated group and the stroke only group were found in the total number of neurons (Figure 3.19 C). However, it is worth to note that the miR treated group displayed a slightly higher neuronal survival in the border of the striatal region, when compared to the NeuN⁺ cells number of the second experimental protocol (See Figure 3.19 B). The interquartile range of the border of striatal region was from 120 to 220 cells/mm^2 in the second experimental protocol (See Figure 3.18 B), while in the third experimental protocol it was from 110 to 320 cells/mm^2 at this ROI (See Figure 3.19 C). This finding indicates that a late miR-124 treatment could lead to an increased neuronal survival in the close proximity of the injection site.

As regards, significantly increased NeuN+ cells were only observed 6 days after MCAO, the treatment with miR-124 needs to take place within a specific time window early after stroke onset.

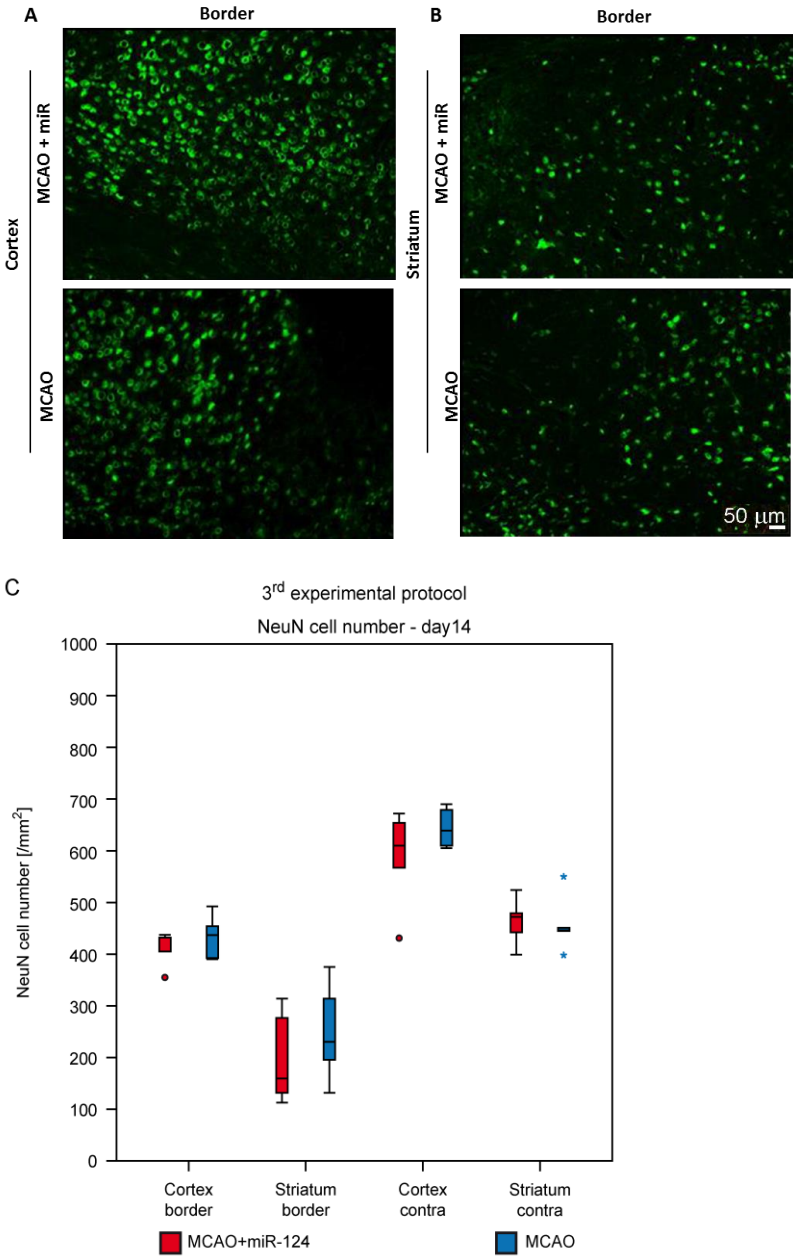

Figure 3.19 The effect of late intracranial injection of miR-124, 10 days after MCAO, on neuronal survival. Photomicrographs show examples of staining immunofluorescence of NeuN on brain sections of ischemic border of cortical and striatal regions acquired from third experimental protocol at 14 days after stroke (A-B). Scale bar: 50 µm. Boxplots show the number of NeuN+ cells in third experimental protocol (C). No significant difference between the miR treated group and the stroke only group was found in the total number of neurons at this time point. n=5 mice in each group.

3.2.4 The effect of miR-124 on the glial scar after stroke

3.2.4.1 Different morphology of the GFAP positive cells after stroke

Immunohistochemistry staining against the glial fibrillary acid protein (GFAP) was used to observe reactive astrogliosis and scar formation 6 and 14 days after MCAO. The GFAP positive cells were visible in both intact and ischemic hemisphere, although with various localization and morphologies. Astrocytes were widely scattered in the healthy area of the brain (Figure 3.20 A). In contrast to the healthy area, the density of astrocytes in stroke border was much higher. After stroke onset, astrocytes proliferated and continued to gradually accumulate more at the lesion border. In this region, the accumulated astrocytes demarcated the lesion area and displayed a hypertrophic morphology with swollen cell bodies and elongated thickened processes that often pointed towards the lesion core (Figure 3.20 B). Over time, a dense "wall" of astrocytes demarcated the lesion core (Figure 3.20 C).

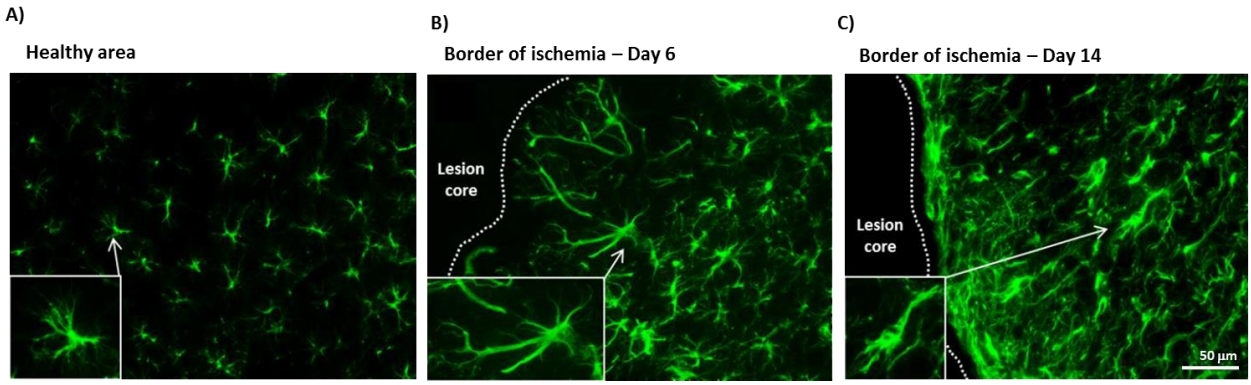

Figure 3.20 Reactive astrogliosis and the scar formation over time. The photomicrographs show the localization of GFAP positive cells at the healthy area close to the lesion (a), at the border of ischemia on day 6 (b) and at the border of ischemia on day 14 (c). In the healthy area, the astrocytes had small cell bodies and short processes. At the stroke border of day 6 after MCAO, the astrocytes developed long processes and their cell bodies were swollen. At the stroke border of day 14 after MCAO, the astrocytes built up a strong border to demarcate the lesion (Kho, 2015).

3.2.4.2 The effect of intracranial miR-124 injection on the glial scar development after stroke

To analyze the development of the glial scar after miR-124 injection in our stroke model, the percentage of the glial scar area and the lesion area in the ipsilateral hemisphere were calculated (see chapter 2.3.2), regarding the demarcated region by reactive astrocytes. Measurement of the glial scar area at the two different survival times revealed that the proliferation of astrocytes was directed towards the lesion center as the total affected area, delineated by the outer glial scar border (Figure 3.21).

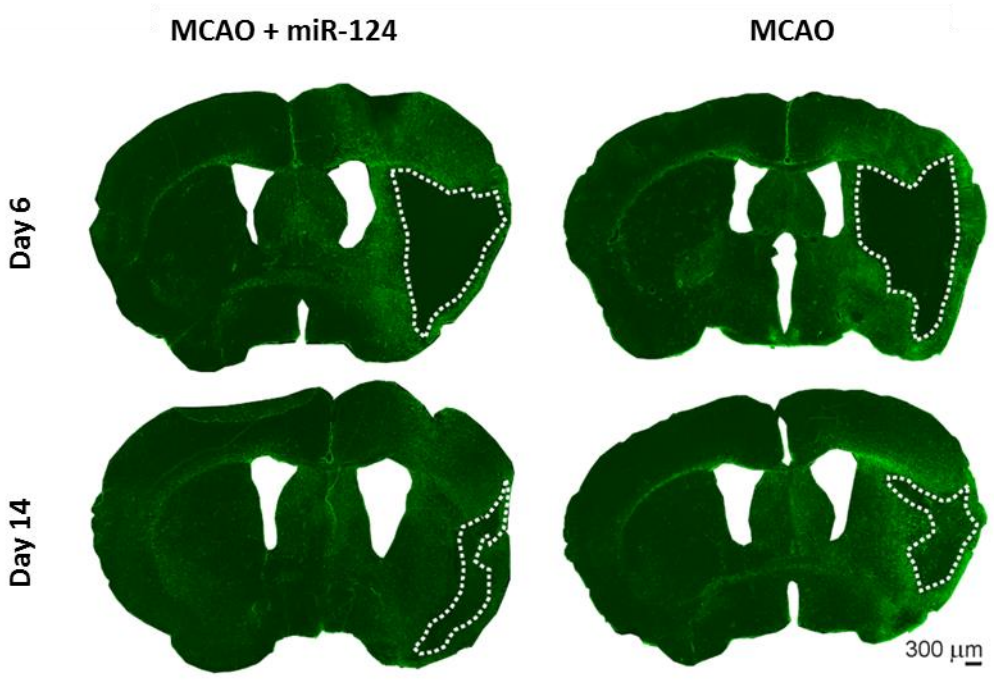

Figure 3.21 The effect of miR-124 on reactive astrocytes and the glial scar development. The development of the glial scar from 6 to 14 days after MCAO was similar between miR treated group and the stroke only group. The white dashed lines delineate the inner glial scar border surrounding the necrotic area demarcated by the astrocytes (Kho, 2015).

The comparison of the area of the outer glial scar showed no difference in all groups, neither among the groups at one time point, nor within individual groups over time. In contrast to the unchanged outer glial scar border, the lesion area (necrotic area), delineated by the inner glial scar border, diminished significantly over time in the miR treated group, in comparison to both control groups ($p = 0.001$ and $p = 0.037$, respectively), (Figure 3.22

B). However, no significant difference was observed between the groups at the third experimental protocol, when miR-124 was injected 10 days after MCAO.

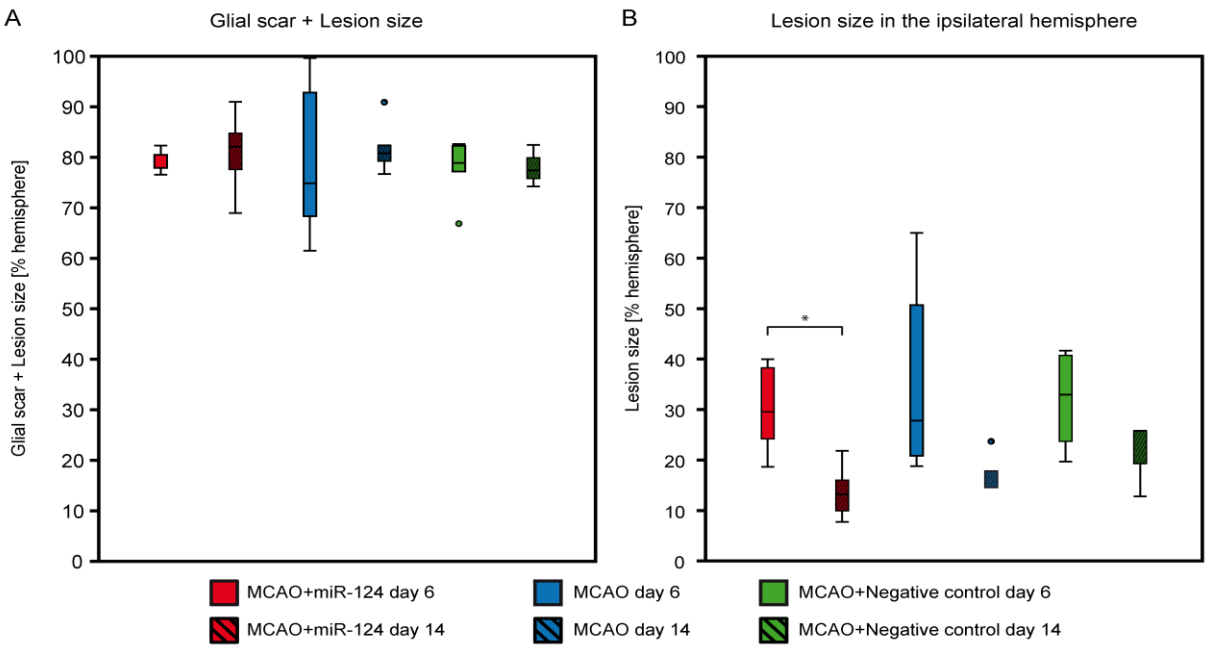

Figure 3.22 The effect of miR-124 on reactive astrocytes and the glial scar development. A) The percentage of the glial scar area within the ischemic hemisphere neither changed within the groups of the early or late observation time point, nor over time. B) Measurement of the lesion area delineated by the glial scar (dashed lines in Figure 3.21) revealed that the percentage of the lesion area within the ischemic hemisphere was reduced significantly in the miR-124 treated animals over time, *P<0.05

3.2.5 The effect of miR-124 on functional recovery after stroke

To analyze whether intracranial liposomated miR-124 improves motor and sensory performance after stroke, the animals were tested and ranked according to the modified Neurological deficit scores (mNDS) once before MCAO (baseline) and every 2 days after MCAO until the day of perfusion. In all groups, the neurological deficit scores increased at day 2 after MCAO compared to baseline, indicating the impaired motor and sensory functions due to the stroke (Figure 3.23 A-B).

With the early intracranial injection of miR-124 at day 2 after MCAO, animals performed significantly better on day 4 (p = 0.025 and p = 0.018, respectively) and 6 (p = 0,011 and p = 0,043, respectively) after MCAO (Figure 3.22 A, B), compared to the stroke only and the negative control groups. Slight differences were observed between both control groups; however the differences were not significant (Figure 3.23 A-B).

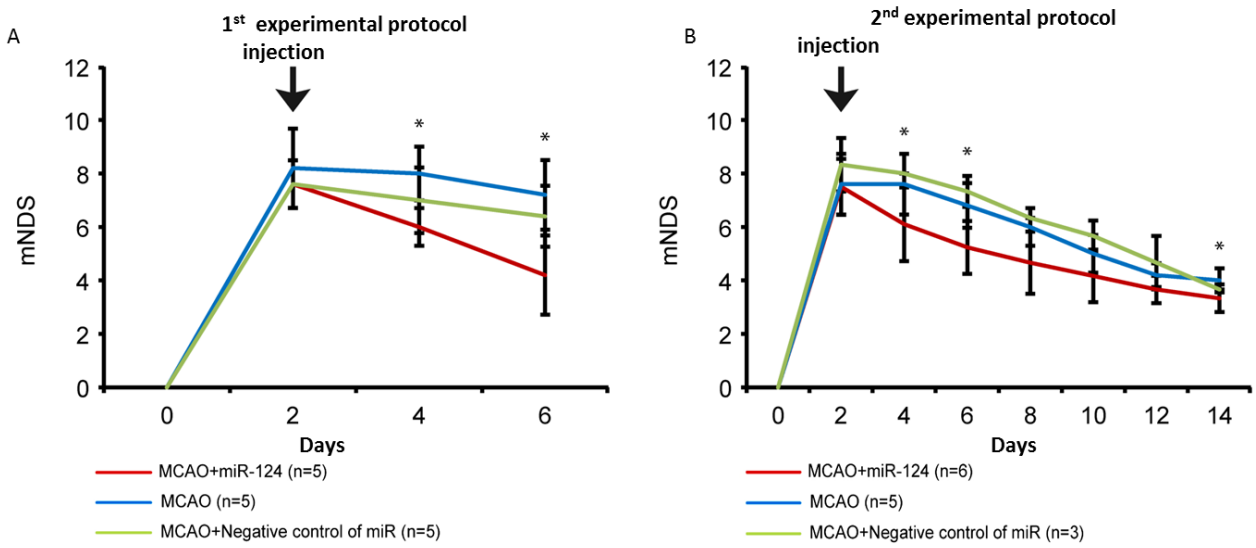

Figure 3.23 The effect of early intracranial injection of miR-124 on functional recovery after stroke. Behavioral functional test was evaluated by the modified Neurological deficit scores (mNDS) before and after MCAO. The graphs represent the functional recovery of the groups of the first (A) and second (B) experimental protocols subjected to miR transplantation at day 2 after MCAO that were perfused at day 6 or day 14, respectively. miR-124 treatment at day2 after MCAO significantly improved the functional recovery at day 4 and day 6 (A, B). n=5-6 mice in each group and each time point. Values are mean±SD. *P<0.05, as compared with control groups using non parametric Kruskal-Walis H test for each time point.

With the late intracranial injection of miR-124, at day 10 after MCAO, no significant difference was observed between the miR treated group and the stroke only group (Figure 3.24). In summary, the analysis of the neurological deficit scores after MCAO showed that early treatment with miR-124 after MCAO could improve the functional recovery after stroke.

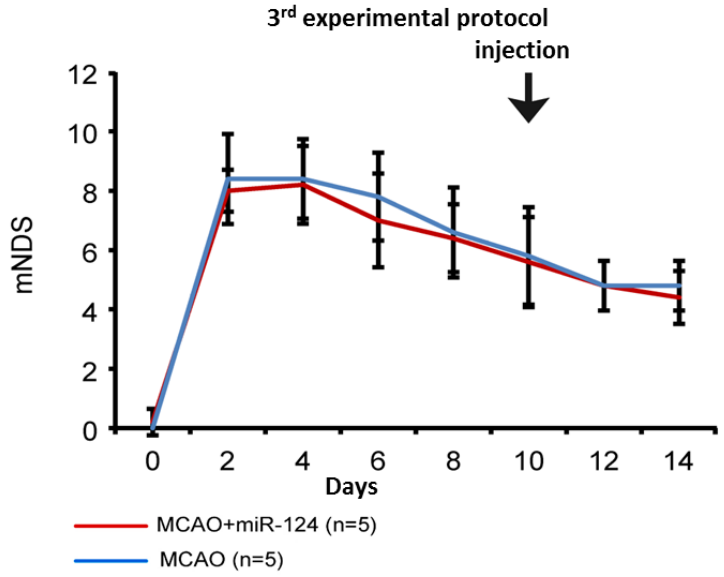

Figure 3.24 The effect of late intracranial injection of miR-124 on functional recovery after stroke. The graph represents the functional recovery of the groups of the third experimental protocol subjected to miR transplantation at day 10 after MCAO that were perfused 4 days later. No significant difference was seen among the miR treated group and the stroke only group. n=5 mice in each group. Values are mean±SD. *P<0.05, as compared with control groups using the non parametric Mann Witteney U test.

3.3 Correlation between the expression of M1/M2 markers by Iba-1⁺ cells and mNDS

The Spearman correlation analysis was performed between the M1/M2 markers expressed by Iba-1⁺ cells and the mNDS (Figure 3.25). Liposomated miR-124 treatment resulted in improved functional recovery, which was paralleled by the observation of decreased M1 marker, CD16/32, and increased M2 markers, CD206 and Arg-1, expression by microglia and macrophages.

A negative linear correlation was found between CD206 expression by Iba-1⁺ cells and increased neurological deficit score at day 6 after stroke ($r^2 = 0.425$, $p = 0.041$), (Figure 3.25 A). Also, a negative linear correlation was found between Arg-1 expression by Iba-1⁺ cells and increased neurological deficit score at day 6 after stroke ($r^2 = 0.489$, $p = 0.024$), (Figure 3.25 B). There was no correlation between the mentioned M2 markers expression and mNDS at day 14 after stroke.

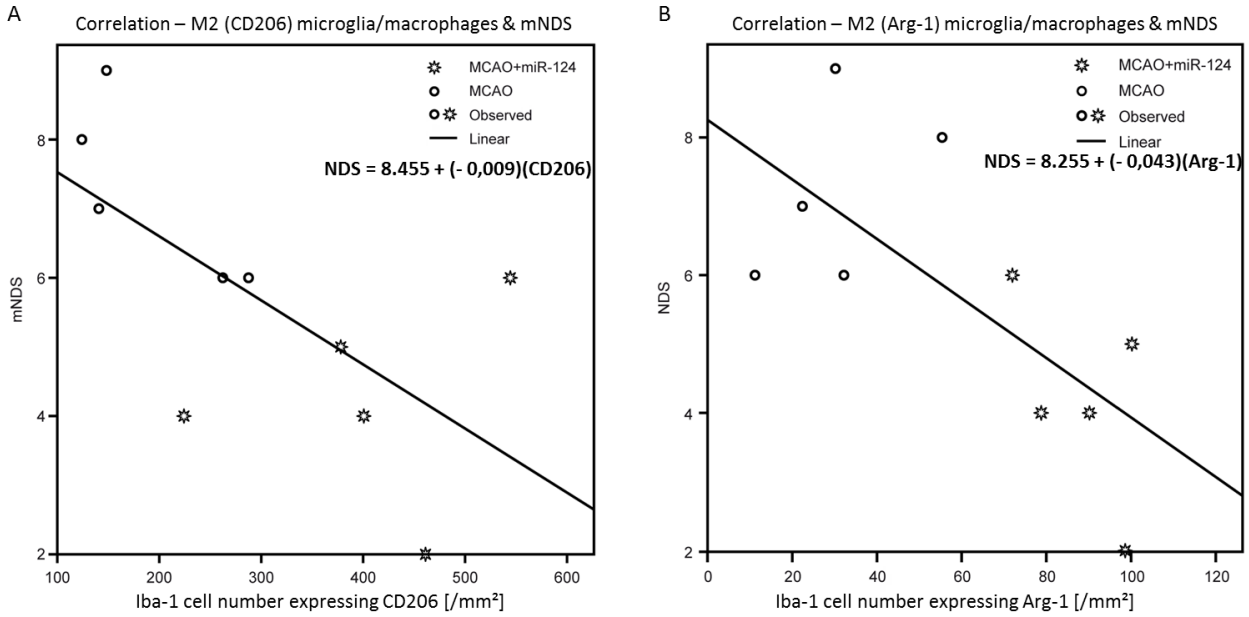

Figure 3.25 Correlation between M2 markers expression and mNDS. The graphs show the correlation between CD206 expression and mNDS (A), and Arg-1 expression and mNDS (B) of the groups of the first experimental protocol. n=5 mice in each group. Changes of CD206 expression within the ischemic hemisphere inversely were correlated to mNDS changes (Spearman r2 = 0.425, p = 0.041) (A). Changes of Arg-1 expression within the ischemic hemisphere inversely were correlated to the changes of mNDS (Spearman r2 = 0.489, p = 0.024) (B).

A positive linear correlation was found between the CD16/32 expression by Iba-1⁺ cells and increased neurological deficit score at day 6 after stroke ($r^2 = 0.530$, $p = 0.017$), (Figure 3.26). There was no correlation between the M1 marker expression and mNDS at day 14 after stroke.

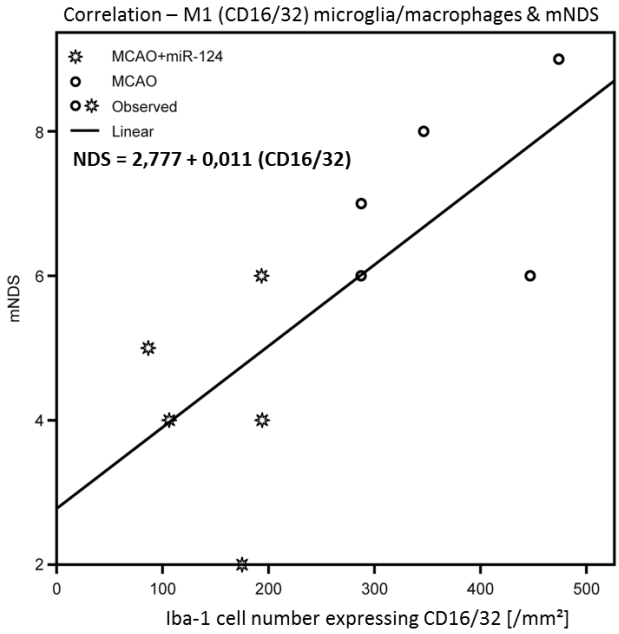

Figure 3.26 Correlation between M1 marker expression and mNDS. The graph shows the correlation between CD16/32 expression and mNDS of the groups of the first experimental protocol. n=5 mice in each group. Changes of CD16/32 expression by Iba-1⁺ cells within the ischemic hemisphere were linearly correlated with the changes of neurological deficit scores in the ischemic mice (Spearman $r^2 = 0.530$, $p = 0.017$).

3.4 Correlation between the expression of M1/M2 markers by Iba-1+ cells and neuronal survival

The Spearman correlation analysis was performed between the M1/M2 markers expressed by Iba-1⁺ cells and the NeuN⁺ cells number (Figure 3.27). Liposomated miR-124 treatment resulted in an increased neuronal survival at day 6 after MCAO, which was paralleled by the observation of decreased M1 marker, CD16/32, and increased M2 markers, CD206 and Arg-1, expression by microglia and macrophages.

A positive linear correlation was found between CD206 expression by Iba-1⁺ cells and increased NeuN⁺ cell number at day 6 after stroke (r^2 = 0.450, p = 0.034), (Figure 3.27 A). Also, a positive linear correlation was found between Arg-1 expression by Iba-1⁺ cells and increased NeuN⁺ cells number at day 6 after stroke (r^2 = 0.709, p = 0.002), (Figure 3.27 B). There was no correlation between both M2 markers and NeuN⁺ cells number at day 14 after stroke.

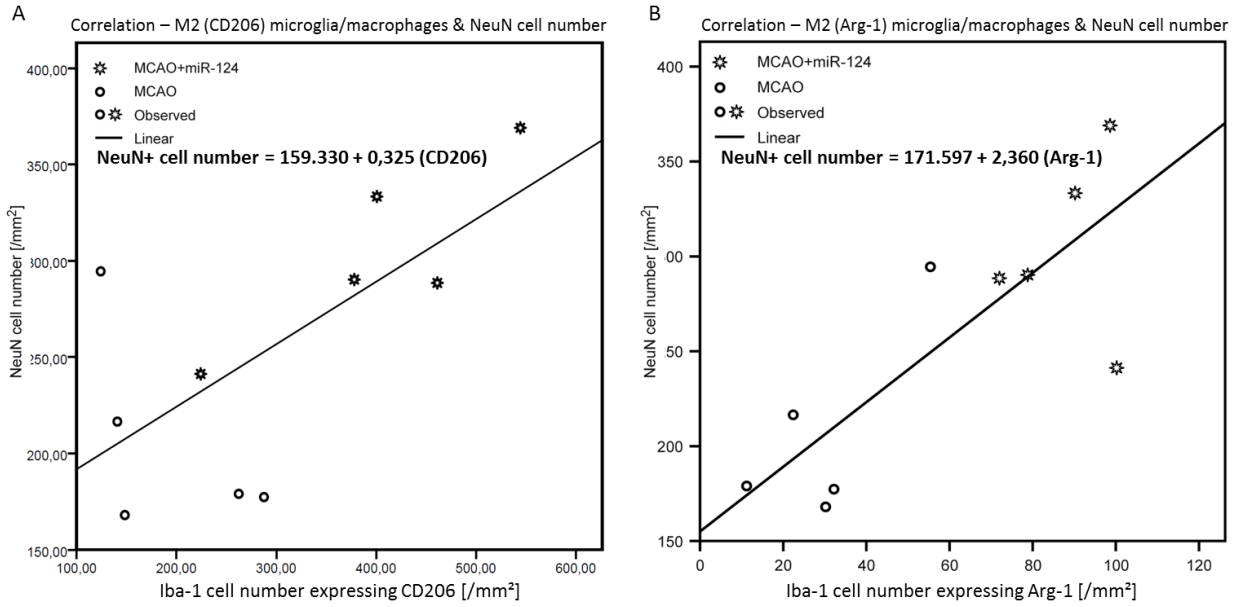

Figure 3.27 Correlation between M2 marker expression and NeuN⁺ cell number. The graphs show the correlation between CD206 expression and NeuN⁺ cell number (A), and Arg-1 expression and NeuN⁺ cell number (B) of the groups of the first experimental protocol. n=5 mice in each group. Changes of CD206 expression within the ischemic hemisphere were linearly correlated to the changes of neuronal survival (Spearman r2 = 0.450, p = 0.034) (A). Changes of Arg-1 expression within the ischemic hemisphere were linearly correlated to the changes of neuronal survival (Spearman r2 = 0.709, p = 0.002) (B).

Correlation analysis showed a negative linear relation between the CD16/32 expression by Iba-1⁺ cells and increased NeuN⁺ cells number at day 6 after stroke (r^2 = 0.454, p = 0.033), (Figure 3.28). There was no correlation between M1 marker and the number of NeuN⁺ cells at day 14 after stroke.

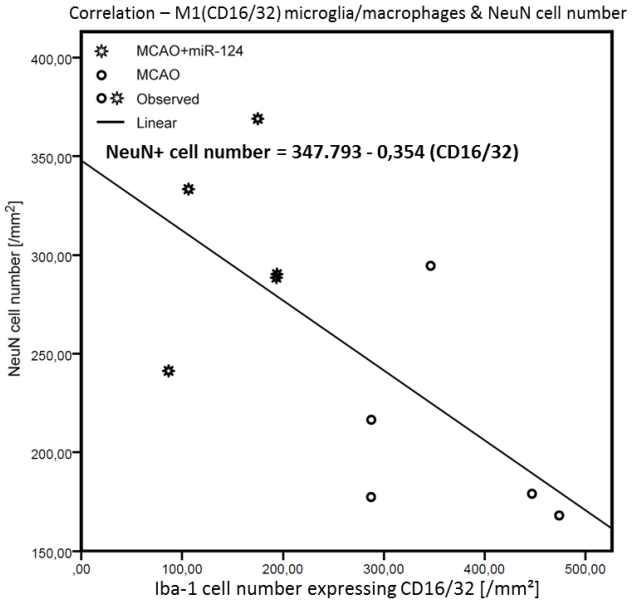

Figure 3.28 Correlation between M1 marker expression and NeuN⁺ cells number. The graph shows the correlation between M1 marker and NeuN⁺ cells number of the groups of the first experimental protocol. n=5 mice in each group. Changes of M1 expression within the ischemic hemisphere were inversely correlated with neuronal survival changes in the ischemic mice (Spearman r^2 = 0.454, *p* = 0.033) (C).

Chapter 4

Discussion

4. Discussion

Our findings demonstrated that miR-124 serves as a promising molecule for immunomodulation and neuroprotection after ischemic stroke. Intracranial injection of miR-124 improved functional recovery after stroke. The number of Iba-1$^+$ immune cells expressing pro-inflammatory M1 marker was positively correlated to the neurological deficit scores whereas expression of anti-inflammatory M2 markers correlated negatively. The immunomodulatory effect of miR-124 was sufficient to shift the M1:M2 ratio towards the functional improvement-relevant M2 phenotype. Administration of miR-124 had a direct neuroprotective effect and accelerated the glial scar formation around the ischemic lesion.

4.1 miR-124 modulates the polarization of microglia and macrophages in the sub-acute phase of ischemic stroke

4.1.1 The effect of the early administration of miR-124

During the last decade, the traditional view regarding the role of the microglia and macrophages in neurodegenerative disorders as detrimental modulators has been changed. The recent studies point toward both protective and destructive roles of these cells after CNS injury. Time dependent polarization of microglia and macrophages toward different phenotypes might account for this dual role. Thus, the importance of precise adjustment of microglia and infiltrating macrophage cells in CNS injury has been highlighted recently, instead of comprehensive suppression of these immune cells. In order to control the phenotypic shift of microglia and macrophages in the sub-acute phase of an ischemic stroke, we have presented a previously unreported approach using the brain specific miR-124.

We revealed that miR-124 administration before the pro-inflammatory peak after stroke did not only change the M1/M2 balance toward a more anti-inflammatory phenotype, but also improved functional recovery in the first week after middle cerebral artery occlusion. The early miR-124 administration at day 2 after stroke increased the number of Iba-1$^+$ cells expressing the M2 markers CD206 and Arginase-1, while the number of Iba-1$^+$ cells expressing the M1 marker CD16/32 decreased. These modulations were

more pronounced in the ischemic border regions, highlighting the protective role of miR-124 in the penumbra. The effect of early administration of liposomated miR-124 on modulating the M1/M2 polarization gradually decreased from day 6 to day 14 in our experiment. Interestingly, we found that the ratio of pro-inflammatory (M1) to anti-inflammatory (M2) phenotype of microglia and macrophages in the miR treated group was significantly lower even after two weeks, confirming the persisted anti-inflammatory effect of the miR-124 still at day 14 after stroke.

MiR-124 is almost especially detected in CNS and is of special interest for stroke studies. In general, the expression profiles of several miRNA are mainly changed during the acute phase after stroke ((Dharap et al., 2009), (Tan et al., 2009), (Saugstad, 2010)). The miR-124 levels were found to be increased within the first 24-48 hours after reperfusion in rodent stroke models ((Weng et al., 2011), (Sun et al., 2013), (Liu et al., 2013)). However, reports on the exact temporal profile are inconsistent ((Weng et al., 2011), (Jeyaseelan et al., 2008), (Zhu et al., 2014)). In human stroke, miR-124 was reported to decrease in the first 24 hours and to be negatively correlated to the infarct size (Liu et al., 2015b). In a mouse model of ischemic stroke, miR-124 was significantly decreased 7 days after stroke (Liu et al., 2011). Thus, finding the effects of miR-124 regulation could be a key aspect for new therapeutic strategy in stroke.

In general following CNS injury, microglia and macrophages display various changes in their morphology, gene expression and function over time. On the one hand, the activated microglia and macrophages promote tissue recovery by clearing debris, adjusting local inflammation and releasing multiple trophic factors ((Hanisch and Kettenmann, 2007), (Thored et al., 2009), (Miron et al., 2013)). On the other hand, these cells could extend tissue damage and prohibit CNS repair ((Ekdahl et al., 2003), (Liu et al., 2007)). Correspondingly, these cells react dynamically to ischemic injury over time. In the acute phase of stroke the majority of recruited microglia and macrophages are M2-dominant, thus providing protective functions. However, the M1 phenotype becomes dominant by about 1 week after injury (Kigerl et al., 2009; Perego et al., 2011; Wang et al., 2013). Recently, it has been shown that the mRNA expression of the M2 phenotype markers (CD206, Arg-1, Ym1/2, IL-10, and TGF-β) peaks between days 3 to day 5 post injury. The M1 phenotype

relevant genes (iNOS, CD16, CD32) continuously increase over time from day 3 on and remain elevated until day 14 after stroke ((Hu et al., 2012), (Pan et al., 2015)). This is in agreement with the expression peak of IRF-4 at day 3, a key transcription factor of M2 polarization (Guo et al., 2014). Notably, a long-term maintenance of the M2 phenotype could result in adverse effect such as tumorigenesis (Komohara et al., 2008). Furthermore, the complete suppression of M1 could end in losing the beneficial effects of the M1 phenotype, such as synaptic remodeling and CNS repair ((Hu et al., 2015), (Hanania et al., 2012)).

In this thesis, miR-124 prolonged the M2 phase while reducing the number of Iba1+ cells with M1 phenotype. The improved functional outcome is in line with the results by Ponomarev (Ponomarev et al., 2011), who reported that administration of miR-124 during the preclinical stage of encephalomyelitis substantially decreased the disease symptoms and enhanced the recovery. Ponomarev showed that bone marrow-derived macrophage cells, transfected with liposomated miR-124, downregulated the expression of the M1 markers TNF-α and inducible nitric oxide synthase (iNOS) and simultaneously upregulated the expression of the M2 markers TGF-β1, Arg1 and FIZZ1. In their study, miR-124 directly suppressed the C/EBP-α and its downstream target PU.1, resulting in a modulation of the activated phenotype of microglia and macrophages (Ponomarev et al., 2011). A similar shift in the M1:M2 ratio of microglia and macrophages in the spinal cord was achieved via intrathecal injection of liposomated miR-124 in an IL-1β induced hyperalgesia model, leading to reduced inflammatory reactions and neuropathic pain (Willemen et al., 2012). A microinjection of miR-124/chitosan particles was also shown to reduce the inflammation in a rat model of spinal cord injury. The expression of TNF-α and iNOS, 2 major substances of the M1 phenotype, was reduced via transfecting the primary microglia with miR-124/chitosan complex particles (Louw et al., 2015). On the contrary, the knockdown of miR-124 via a miR-124 antisense oligonucleotide activated the microglia and macrophages with upregulated MHC class II and CD45. In addition, the development of ramified morphology of the immune cells was inhibited (Ponomarev et al., 2011).

The M1/M2 modulating effect of liposomated miR-124 decreased from day 6 to day 14 in our experiments. The cell numbers of CD206, Arginase-1 and CD16/32 expressing Iba-1^{+}

cells in the miR treated group were no longer significantly different from the corresponding cell numbers of both control groups. However, a clear difference of lower M1:M2 ratio was still observed in the miR treated group (See Figure 3.12 B). We suggest that the time dependent decrease of the immunomodulatory effect of miR-124 can be explained by the short half-life of microRNAs of a few days (Gantier et al., 2011), (Krol et al., 2010). In addition, the liposome approach, in which a lipofection agent delivers the RNA through an endosomal pathway into the cytosol, is limited ((Opanasopit et al., 2011), (Wrobel and Collins, 1995)). The main advantages of the cationic liposomes are less cytotoxicity and more compatibility with different cell types. On the other hand, low transfection efficiency due to the degradation in lysosomes must also be considered (Cortesi et al., 1996). Thus, different delivery strategies for miR-124 are required to achieve long-term effects. As Doeppner et al reported that viral vector-mediated miR-124 delivery leads to persistent neuroprotection, ameliorated motor coordination and improved memory capacity up to 56 days after stroke (Doeppner et al., 2013).

4.1.2 The effect of late administration of miR-124

It has been described that the M1 polarization of microglia and macrophages is gradually enhanced from day 3 after stroke onward (Hu et al., 2012). Therefore, the question was addressed, whether a delayed administration of miR-124 is still efficient to shift the M1:M2 ratio. The results of this study showed that the intracerebral injection of liposomated miR-124 at day 10, after the peak of the M1 phase, still had substantial influence on the microglia and macrophages. The late phase application of miR-124 only decreased the pro-inflammatory M1 phenotype, while by the early application in parallel the M2 phenotype was enhanced and M1 was decreased. Administration of miR-124 at the late stage could not improve the neurological deficits. The idea of modulating neuroinflammation to improve the outcome of neurological disorders is quite novel (Xia et al., 2015). This study is so far the first to demonstrate the therapeutic effect of miRNA on polarization shift of microglia and macrophages.

In our present protocol, administration of miR-124 considerably decreased the M1 marker expression of Iba-1^{+} cells particularly in the border and core regions of the striatal lesion (See figure 3.13), the vicinity of injection channel. In an alternative immunomodulatory approach, Keller and colleagues treated mice with minocycline, a selective inhibitor of M1 microglia (Kobayashi et al., 2013), in an amyotrophic lateral sclerosis (ALS) model. They found that treatment after disease onset could not prolong the survival time, although pre-symptomatic administration was protective (Keller et al., 2011). Administration of minocycline at the M2 phase of ALS showed a potent suppressive effect on the M1 marker expression and no effect on the M2 marker expression (Kobayashi et al., 2013). On the other hand in a stroke model, application of minocycline at day 4 after ischemia improved neurogenesis and functional recovery (Liu et al., 2007). In a carrageenan-induced inflammatory hyperalgesia model, intrathecal injection of liposomated miR-124 during the peak of the pro-inflammatory process (the first 15 hours) reduced the expression of M1 surface markers and attenuated the resistant thermal hyperalgesia (Willemen et al., 2012). These results suggest that targeting the correct phenotype of immune cells at the right time of neurodegenerative disorders is important to achieve therapeutic effects.

4.2 miR-124 exerts a neuroprotective effect after ischemic stroke

In this study, the early administration of liposomated miR-124 after ischemic stroke effectively protected neurons, as seen by the number of preserved $NeuN^+$ cells. Administration of miR-124 at day 2 after stroke resulted in a noticeable increase of $NeuN^+$ cells, in addition to the substantial modulation of M1/M2 polarization of CNS resident microglia and infiltrating macrophage cells. However, this neuroprotective effect was only visible within the first week after stroke and no neuroprotective effect was found any longer at the second week. A former study reported a neuroprotective effect of miR-124 up to 56 days after stroke by using a viral vector-mediated miR-124 delivery (Doeppner et al., 2013). This change in the delivery system demonstrated that a constant level of miR-124 could protect neurons over longer times. Other studies reported a short-term effect of miR-124 as well. For example, intravenous injection of miR-124 directly before MCAO onset decreased the apoptotic cell death in mice 24 h after MCAO, while blockage of miR-124 increased the lesion size (Sun et al., 2013). We suggest that the limited, temporary neuroprotective effects of miR-124 in our study can be explained by the fast turnover of microRNAs in immune cells and neurons ((Gantier et al., 2011), (Krol et al., 2010)) or by the efficacy of different delivery systems.

Several mechanisms involved in the neuroprotective effect of miR-124 have already been reported. Exogenous application of miR-124 was neuroprotective in a mice stroke model by increasing the anti-apoptosis proteins Bcl-2 and Bcl-xl (Sun et al., 2013). Also, it has been shown that the neuroprotective effect of miR-124 was mediated by an Usp14-dependent degradation of REST, resulting in an increased survival rate of neurons (Doeppner et al., 2013). Furthermore, administration of Cy3-labeled miR-124 in the striatum of a Huntington's disease model in mice improved functional recovery and neuronal survival via up-regulating the expression of BDNF and down-regulating the expression of SOX9 (Liu et al., 2015a). Wang et al. showed that exogenous delivery of miR-124 in a Parkinson's disease model in mice mediated the neuroprotection via targeting the Bim, an essential protein regulating the apoptosis and autophagy process of the substantia nigra pars compacta of the basal ganglia neurons (Wang et al., 2015). Also it has been shown that Valproic acid, an anti-convulsant drug, induced its neuroprotective effects

through a miR-124 dependent pathway by activating cAMP and increasing BDNF (Oikawa et al., 2015). In addition, decreased levels of miR-124 by disruption of Rncr3 (retinal non-coding RNA 3), the dominant source of miR-124, resulted in reduced survival of neurons of the hippocampal dentate gyrus and the retinal cones via targeting the transcription factor Lhx2 (Sanuki et al., 2011).

In the present experiment, the increased neuronal survival was more pronounced in the ischemic border region of the cortical lesion. It is worth to note that the increase of Arg-1 in Iba-1^{+} cells, as one of the important M2 mediators, was more prominent in the cortical region, too. Evidences for the neuroprotective role of Arg-1, among the M2 markers, had been reported earlier already (Cherry et al., 2015)). Lange et al. showed that exogenous Arg-1 was capable of protecting the neurons against several apoptotic factors upon oxidative stress (Lange et al., 2004). Estevez et al. presented that the exogenous administration of Arg-1 increased the survival rate of trophic factor-deprived motor neurons in vitro by competing with iNOS for the metabolization of L-arginine (Estevez et al., 2006). Furthermore, Arg-1 increases the production of polyamines and collagen, important for cell proliferation and tissue regeneration, respectively ((Munder, 2009), (Caldwell et al., 2015)).

Since now, no one has studied the effect of miR-124 on the relation between M2 microglia and macrophages and neuronal survival. The results of our present study show for the first time that the neuroprotective effect of the miR-124 treatment can be attributed to the modulation of immune cells toward the M2 phenotype. The importance of alternatively M2 activated microglia and macrophages for neuroprotection is reflected by the highly significant correlation between M2 microglia and macrophages and neuronal survival. Alternatively M2 activated microglia and macrophages do not only contribute to the resolution of the inflammation by the secretion of anti-inflammatory substrates, but also prepare a suitable environment for regeneration by the secretion of several trophic factors, important for neuronal survival (Hu et al., 2015).

Beside the neuroprotective effect, it has been found that several miRNAs (miR-9, miR-124a/b, miR-135, miR-153, miR-183 and miR-219) were specifically expressed in differentiating neurons, suggesting that these miRNAs act as remarkable effectors in

neuronal processes (Sempere et al., 2004). The involvement of miR-124 in the regulation of neurogenesis was reported and it was also shown that miR-124 is progressively up-regulated during embryonic neurogenesis, mostly in the SVZ ((Cheng et al., 2009), (Makeyev et al., 2007)). For the results presented here, enhanced neurogenesis did not play a major role, because days 6 and 14 after stroke were analyzed and formation of the $NeuN^+$ cells takes 2-4 weeks at least.

It seems that miR-124 administration has different effects at different time points after stroke. Recently, a research objecting the neuroprotective effects of miR-124 has been reported as well. In that study, miR-124 application immediately after MCAO suppressed the regeneration processes by inhibiting the DNA repair proteins (Ku70) and downregulating the anti-apoptosis proteins (iASPP) 24 hours after cerebral ischemia, but on the other hand, it did not increase the infarct volume either (Liu et al., 2013).

4.3 miR-124 performs its neuroprotective effect via affecting the glial scar after ischemic stroke

In our present investigations, miR-124 was able to modulate the reactive astrogliosis and scar formation. The early intracranial injection promoted an accelerated infiltration of reactive astrocytes into the lesion core and the formation of a tighter glial scar over time. This result is of particular interest as there is a tight interaction between neurons, astrocytes and immune cells in general and the role of the glial scar for stroke tissue regeneration is believed to be two sided in particular.

The glial scar prevents the spread of the inflammation via forming a physical barrier (Rolls et al., 2009). Moreover, the reactive astrocytes have been reported to be important for providing trophic support for neurons, preventing excitatory neurotoxicity by taking up excessive glutamate and protecting neurons from nitric oxide toxicity (Rolls et al., 2009). Based on the protective function of reactive astrocytes, especially their function as a barrier, a fast development of the glial scar after stroke is described as an efficient neuroprotective mechanism ((Li et al., 2008), (Sofroniew, 2009), (Pekny et al., 2014)). In this line, inhibiting reactive astrocytes leads to synaptic loss, a decreased resistance of the CNS tissue (Hol and Pekny, 2015), increased vasogenic edema (Sofroniew, 2009), larger lesions, local tissue disruptions and demyelination ((Rolls et al., 2009), (Choudhury and Ding, 2016)).

It has been shown that miR-124 resolves the glial scar at 28 and 56 days after stroke (Doeppner et al., 2013). However, it is not clear if this was the result of an early or late astroglial response. The data presented here, show for the first time the potential of miR-124 to up-regulate the astroglial proliferation in favor of protecting the ischemic tissue.

The molecular regulation of the neuron-astrocyte communication unit is mainly undetermined. Interestingly, in an effort to analyze the neuron-to-astrocyte signaling, Morel et al. have revealed that exosomes isolated from the neuron-conditioned medium of the cortical neuronal cell cultures contain numerous microRNAs and small RNAs, in particular miR-124. In that study, they showed that the transfer of the neuronal exosomal miRNA, especially miR-124, into astrocytes led to increased GLT1 protein expression (Morel et al.,

2013), which is responsible for more than 90% of glutamate clearance (Fischer et al., 2013). Moreover, they presented that exogenous delivery of miR-124 significantly prevented further pathological loss of GLT1 proteins in the end stage in a mouse model of ALS. Taken together, their study indicated a new neuron-to-astrocyte communication pathway involving the role of microRNAs, especially miR-124 (Morel et al., 2013). Although in their study the effect of miR-124 on the glial scar formation has not been detected, but their results confirm that miR-124 strongly affects astrocytes. Those results confirm our data that the effects of miR-124 are driven by paracrine interaction of microglia and macrophages with local neighboring cells.

It is worth to note that various cytokines and chemokines secreted by M2 polarized microglia and macrophages are able to modulate reactive astrocytes as well. In our study, administration of miR-124 increased the expression of Arg-1 and CD206 in microglia and macrophages. In Ponomarev et al. study, the expression of TGF-ß in microglia and macrophages increased following administration of miR-124 (Ponomarev et al., 2011). An increased Arg-1 expression was reported to be directly correlated to an increased GFAP expression (Quirie et al., 2013). It was shown that TGF-ß1 is effective in the formation of reactive astrocytes into the glial scar (John et al., 2003). Therefore, the accelerated formation of the glial scar might be attributed to the polarization effect of miR-124 on microglia and macrophages, by secretion of M2 associated cytokines/chemokines. Last but not the least, it was found that M2 polarized monocyte derived macrophage cells in murine models of spinal cord injury could significantly resolve inflammation as well as the glial scar ((Shechter et al., 2011), (Raposo and Schwartz, 2014)), indicating a tight astrocyte–immune cell interplay.

Summary:

In this dissertation, we have demonstrated that miR-124 performs as a multifactorial molecule providing immunomodulation and neuroprotection after ischemic stroke (Figure 4.1). The early intracranial injection of miR-124 resulted in a remarkable reduced pro-inflammatory (M1) to anti-inflammatory (M2) ratio. The increased number of M2-like polarized microglia and macrophages were positively correlated to increased neuronal survival. Moreover, administration of miR-124 decreased the lesion core area, determined by reactive astrocytes, over time and directly increased neuronal survival. All these changes led to improved functional recovery (sensory and motor performance).

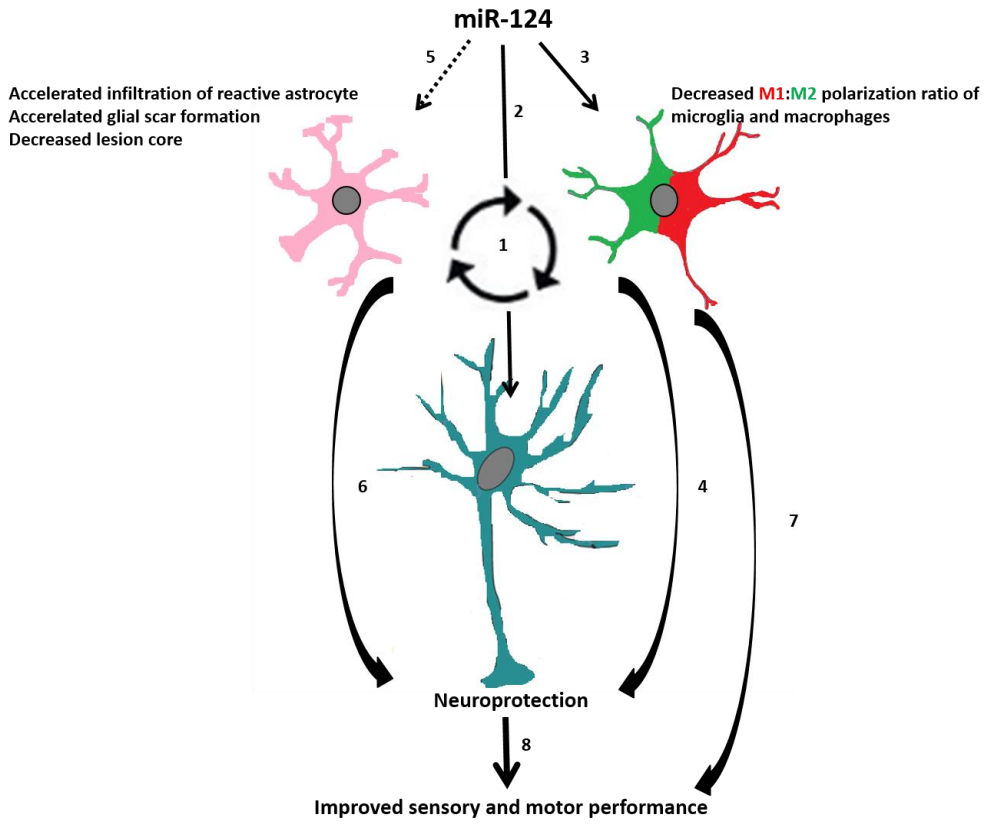

Figure 4.1. **Multifactorial effect of miR-124 on improved functional recovery.** Administration of miR-124 improved the functional recovery after stroke via direct and indirect pathways. (1) There is a close interaction between neurons, astrocytes and immune cells in the CNS. (2) miR-124 directly increased the number of surviving neurons. (3) miR-124 modulated the neuro-inflammation process from the destructive phenotype (M1) to the more protective phenotype (M2), (4) which was correlated to increased neuronal survival. (5) miR-124 decreased the lesion core, which was separated with reactive astrocytes, although the direct effect of miR-124 on modulation of reactive astrocytes is still unknown. (6) A decreased lesion core emphasizes the neuroprotective effect. (7-8) All these changes resulted in improved functional recovery.

Conclusion and outlook

In this dissertation, the immunomodulatory and neuroprotective effects of miR-124 after ischemic stroke were investigated. To achieve these objectives, the short-term and the long-term effects of miR-124 administration at day 2 after stroke induction were monitored. This early treatment was proven to be neuroprotective through modulation of the neuroinflammation from the destructive phenotype (M1) to the protective phenotype (M2). Furthermore, improved functional recovery was observed by miR-124 administration that was correlated with the increased number of M2-like polarized microglia and macrophages. This improved functional recovery highlights the importance of further studies of brain mapping, in order to find the relation between improved sensory and motor performance and brain circuit rewiring after stroke.

The early miR-124 administration seemed not to have long lasting therapeutic effects. However, the immunomodulatory effect of miR-124 did not completely disappear and the M1:M2 ratio remained lower, compared to both control groups, even after two weeks of stroke induction. A challenge here is to enhance the long-term efficacy of miR-124. One possibility would be to use another delivery system, such as carbon nanotubes (CNTs) alone or in combination with liposomes. It has been demonstrated that CNTs can reach the cell nucleus and have higher uptake efficiency in cells than the liposomal delivery system. Alternatively, repeated injections of miR-124 could be done. However, associated side effects with high amount of miR should be considered.

As most of the patients miss the narrow therapeutic window of the acute stage after stroke, finding an effective therapy is demanding. For this purpose, the effect of late administration of miR-124, 10 days after stroke induction, was also investigated in this dissertation. This late treatment resulted in a decreased pro-inflammatory M1 phenotype and subsequently reduced the M1:M2 ratio. However, it could not improve the neurological deficits and neuronal survival. The precise determination of the optimum administration time of miR-124 is crucial, considering the peak of the M1 phenotype of microglia and macrophages at about 1 week after stroke.

References

Adamczak, J.M., G. Schneider, M. Nelles, I. Que, E. Suidgeest, L. van der Weerd, C. Lowik, and M. Hoehn. 2014. In vivo bioluminescence imaging of vascular remodeling after stroke. *Frontiers in cellular neuroscience* 8:274.

Akama, K.T., and L.J. Van Eldik. 2000. Beta-amyloid stimulation of inducible nitric-oxide synthase in astrocytes is interleukin-1beta- and tumor necrosis factor-alpha (TNFalpha)-dependent, and involves a TNFalpha receptor-associated factor- and NFkappaB-inducing kinase-dependent signaling mechanism. *The Journal of biological chemistry* 275:7918-7924.

Amantea, D., G. Micieli, C. Tassorelli, M.I. Cuartero, I. Ballesteros, M. Certo, M.A. Moro, I. Lizasoain, and G. Bagetta. 2015. Rational modulation of the innate immune system for neuroprotection in ischemic stroke. *Frontiers in neuroscience* 9:147.

Amantea, D., G. Nappi, G. Bernardi, G. Bagetta, and M.T. Corasaniti. 2009. Post-ischemic brain damage: pathophysiology and role of inflammatory mediators. *The FEBS journal* 276:13-26.

Aswendt, M., E. Gianolio, G. Pariani, R. Napolitano, F. Fedeli, U. Himmelreich, S. Aime, and M. Hoehn. 2012. In vivo imaging of inhibitory, GABAergic neurons by MRI. *NeuroImage* 62:1685-1693.

Bazzoni, F., M. Rossato, M. Fabbri, D. Gaudiosi, M. Mirolo, L. Mori, N. Tamassia, A. Mantovani, M.A. Cassatella, and M. Locati. 2009. Induction and regulatory function of miR-9 in human monocytes and neutrophils exposed to proinflammatory signals. *Proceedings of the National Academy of Sciences of the United States of America* 106:5282-5287.

Beers, D.R., J.S. Henkel, W. Zhao, J. Wang, A. Huang, S. Wen, B. Liao, and S.H. Appel. 2011. Endogenous regulatory T lymphocytes ameliorate amyotrophic lateral sclerosis in mice and correlate with disease progression in patients with amyotrophic lateral sclerosis. *Brain : a journal of neurology* 134:1293-1314.

Benakis, C., L. Garcia-Bonilla, C. Iadecola, and J. Anrather. 2014. The role of microglia and myeloid immune cells in acute cerebral ischemia. *Frontiers in cellular neuroscience* 8:461.

Beutner, C., K. Roy, B. Linnartz, I. Napoli, and H. Neumann. 2010. Generation of microglial cells from mouse embryonic stem cells. *Nature protocols* 5:1481-1494.

Biggs, J.E., V.B. Lu, M.J. Stebbing, S. Balasubramanyan, and P.A. Smith. 2010. Is BDNF sufficient for information transfer between microglia and dorsal horn neurons during the onset of central sensitization? *Molecular pain* 6:44.

Biswas, S.K., and A. Mantovani. 2010. Macrophage plasticity and interaction with lymphocyte subsets: cancer as a paradigm. *Nature immunology* 11:889-896.

Boche, D., V.H. Perry, and J.A. Nicoll. 2013. Review: activation patterns of microglia and their identification in the human brain. *Neuropathology and applied neurobiology* 39:3-18.

Bouhlel, M.A., B. Derudas, E. Rigamonti, R. Dievart, J. Brozek, S. Haulon, C. Zawadzki, B. Jude, G. Torpier, N. Marx, B. Staels, and G. Chinetti-Gbaguidi. 2007. PPARgamma activation primes human monocytes into alternative M2 macrophages with anti-inflammatory properties. *Cell metabolism* 6:137-143.

Burda, J.E., and M.V. Sofroniew. 2014. Reactive gliosis and the multicellular response to CNS damage and disease. *Neuron* 81:229-248.

Caldwell, R.B., H.A. Toque, S.P. Narayanan, and R.W. Caldwell. 2015. Arginase: an old enzyme with new tricks. *Trends in pharmacological sciences* 36:395-405.

Chen, G.Y., and G. Nunez. 2010. Sterile inflammation: sensing and reacting to damage. *Nature reviews. Immunology* 10:826-837.

Chen, J., P.R. Sanberg, Y. Li, L. Wang, M. Lu, A.E. Willing, J. Sanchez-Ramos, and M. Chopp. 2001. Intravenous administration of human umbilical cord blood reduces behavioral deficits after stroke in rats. *Stroke; a journal of cerebral circulation* 32:2682-2688.

Cheng, L.C., E. Pastrana, M. Tavazoie, and F. Doetsch. 2009. miR-124 regulates adult neurogenesis in the subventricular zone stem cell niche. *Nature neuroscience* 12:399-408.

Cherry, J.D., J.A. Olschowka, and M.K. O'Banion. 2015. Arginase 1+ microglia reduce Abeta plaque deposition during IL-1beta-dependent neuroinflammation. *Journal of neuroinflammation* 12:203.

Choudhury, G.R., and S. Ding. 2016. Reactive astrocytes and therapeutic potential in focal ischemic stroke. *Neurobiology of disease* 85:234-244.

Cortesi, R., E. Esposito, E. Menegatti, R. Gambari, and C. Nastruzzi. 1996. Effect of cationic liposome composition on in vitro cytotoxicity and protective effect on carried DNA. *Int J Pharm* 139:69-78.

David, S., and A. Kroner. 2011. Repertoire of microglial and macrophage responses after spinal cord injury. *Nature reviews. Neuroscience* 12:388-399.

Deb, P., S. Sharma, and K.M. Hassan. 2010. Pathophysiologic mechanisms of acute ischemic stroke: An overview with emphasis on therapeutic significance beyond thrombolysis. *Pathophysiology : the official journal of the International Society for Pathophysiology / ISP* 17:197-218.

Dharap, A., K. Bowen, R. Place, L.C. Li, and R. Vemuganti. 2009. Transient focal ischemia induces extensive temporal changes in rat cerebral microRNAome. *Journal of cerebral blood flow and metabolism : official journal of the International Society of Cerebral Blood Flow and Metabolism* 29:675-687.

Dimou, L., and M. Gotz. 2014. Glial cells as progenitors and stem cells: new roles in the healthy and diseased brain. *Physiological reviews* 94:709-737.

Ding, S. 2014. Dynamic reactive astrocytes after focal ischemia. *Neural regeneration research* 9:2048-2052.

Dirnagl, U., C. Iadecola, and M.A. Moskowitz. 1999. Pathobiology of ischaemic stroke: an integrated view. *Trends in neurosciences* 22:391-397.

Doeppner, T.R., M. Doehring, E. Bretschneider, A. Zechariah, B. Kaltwasser, B. Muller, J.C. Koch, M. Bahr, D.M. Hermann, and U. Michel. 2013. MicroRNA-124 protects against focal cerebral ischemia via mechanisms involving Usp14-dependent REST degradation. *Acta neuropathologica* 126:251-265.

Durafourt, B.A., C.S. Moore, D.A. Zammit, T.A. Johnson, F. Zaguia, M.C. Guiot, A. Bar-Or, and J.P. Antel. 2012. Comparison of polarization properties of human adult microglia and blood-derived macrophages. *Glia* 60:717-727.

Durukan, A., and T. Tatlisumak. 2007. Acute ischemic stroke: overview of major experimental rodent models, pathophysiology, and therapy of focal cerebral ischemia. *Pharmacology, biochemistry, and behavior* 87:179-197.

Ekdahl, C.T., J.H. Claasen, S. Bonde, Z. Kokaia, and O. Lindvall. 2003. Inflammation is detrimental for neurogenesis in adult brain. *Proceedings of the National Academy of Sciences of the United States of America* 100:13632-13637.

Estevez, A.G., M.A. Sahawneh, P.S. Lange, N. Bae, M. Egea, and R.R. Ratan. 2006. Arginase 1 regulation of nitric oxide production is key to survival of trophic factor-deprived motor neurons. *The Journal of neuroscience : the official journal of the Society for Neuroscience* 26:8512-8516.

Farina, C., F. Aloisi, and E. Meinl. 2007. Astrocytes are active players in cerebral innate immunity. *Trends in immunology* 28:138-145.

Fatahzadeh, M., and M. Glick. 2006. Stroke: epidemiology, classification, risk factors, complications, diagnosis, prevention, and medical and dental management. *Oral surgery, oral medicine, oral pathology, oral radiology, and endodontics* 102:180-191.

Faulkner, J.R., J.E. Herrmann, M.J. Woo, K.E. Tansey, N.B. Doan, and M.V. Sofroniew. 2004. Reactive astrocytes protect tissue and preserve function after spinal cord injury. *The Journal of neuroscience : the official journal of the Society for Neuroscience* 24:2143-2155.

Fischer, K.D., A.C. Houston, and G.V. Rebec. 2013. Role of the major glutamate transporter GLT1 in nucleus accumbens core versus shell in cue-induced cocaine-seeking behavior. *The Journal of neuroscience : the official journal of the Society for Neuroscience* 33:9319-9327.

Freilich, R.W., M.E. Woodbury, and T. Ikezu. 2013. Integrated expression profiles of mRNA and miRNA in polarized primary murine microglia. *PloS one* 8:e79416.

Gantier, M.P., C.E. McCoy, I. Rusinova, D. Saulep, D. Wang, D. Xu, A.T. Irving, M.A. Behlke, P.J. Hertzog, F. Mackay, and B.R. Williams. 2011. Analysis of microRNA turnover in mammalian cells following Dicer1 ablation. *Nucleic acids research* 39:5692-5703.

Ginhoux, F., M. Greter, M. Leboeuf, S. Nandi, P. See, S. Gokhan, M.F. Mehler, S.J. Conway, L.G. Ng, E.R. Stanley, I.M. Samokhvalov, and M. Merad. 2010. Fate mapping analysis reveals that adult microglia derive from primitive macrophages. *Science* 330:841-845.

Ginsberg, M.D. 2003. Adventures in the pathophysiology of brain ischemia: penumbra, gene expression, neuroprotection: the 2002 Thomas Willis Lecture. *Stroke; a journal of cerebral circulation* 34:214-223.

Gomez-Nicola, D., and V.H. Perry. 2015. Microglial dynamics and role in the healthy and diseased brain: a paradigm of functional plasticity. *The Neuroscientist : a review journal bringing neurobiology, neurology and psychiatry* 21:169-184.

Gracias, D.T., and P.D. Katsikis. 2011. MicroRNAs: key components of immune regulation. *Advances in experimental medicine and biology* 780:15-26.

Graff, J.W., A.M. Dickson, G. Clay, A.P. McCaffrey, and M.E. Wilson. 2012. Identifying functional microRNAs in macrophages with polarized phenotypes. *The Journal of biological chemistry* 287:21816-21825.

Gravanis, I., and S.E. Tsirka. 2008. Tissue-type plasminogen activator as a therapeutic target in stroke. *Expert opinion on therapeutic targets* 12:159-170.

Guo, S., Z.Z. Li, D.S. Jiang, Y.Y. Lu, Y. Liu, L. Gao, S.M. Zhang, H. Lei, L.H. Zhu, X.D. Zhang, D.P. Liu, and H. Li. 2014. IRF4 is a novel mediator for neuronal survival in ischaemic stroke. *Cell Death and Differentiation* 21:888-903.

Hanania, R., H.S. Sun, K. Xu, S. Pustylnik, S. Jeganathan, and R.E. Harrison. 2012. Classically activated macrophages use stable microtubules for matrix metalloproteinase-9 (MMP-9) secretion. *The Journal of biological chemistry* 287:8468-8483.

Hanisch, U.K., and H. Kettenmann. 2007. Microglia: active sensor and versatile effector cells in the normal and pathologic brain. *Nature neuroscience* 10:1387-1394.

Haupt, C., O.W. Witte, and C. Frahm. 2007. Up-regulation of Connexin43 in the glial scar following photothrombotic ischemic injury. *Molecular and cellular neurosciences* 35:89-99.

Hayakawa, K., T. Nakano, K. Irie, S. Higuchi, M. Fujioka, K. Orito, K. Iwasaki, G. Jin, E.H. Lo, K. Mishima, and M. Fujiwara. 2010. Inhibition of reactive astrocytes with fluorocitrate retards neurovascular remodeling and recovery after focal cerebral ischemia in mice. *Journal of cerebral blood flow and metabolism : official journal of the International Society of Cerebral Blood Flow and Metabolism* 30:871-882.

Hol, E.M., and M. Pekny. 2015. Glial fibrillary acidic protein (GFAP) and the astrocyte intermediate filament system in diseases of the central nervous system. *Current opinion in cell biology* 32:121-130.

Hu, X., R.K. Leak, Y. Shi, J. Suenaga, Y. Gao, P. Zheng, and J. Chen. 2015. Microglial and macrophage polarization-new prospects for brain repair. *Nature reviews. Neurology* 11:56-64.

Hu, X., P. Li, Y. Guo, H. Wang, R.K. Leak, S. Chen, Y. Gao, and J. Chen. 2012. Microglia/macrophage polarization dynamics reveal novel mechanism of injury expansion after focal cerebral ischemia. *Stroke; a journal of cerebral circulation* 43:3063-3070.

Iadecola, C., and J. Anrather. 2011. The immunology of stroke: from mechanisms to translation. *Nature medicine* 17:796-808.

Jang, E., J.H. Kim, S. Lee, J.H. Kim, J.W. Seo, M. Jin, M.G. Lee, I.S. Jang, W.H. Lee, and K. Suk. 2013. Phenotypic polarization of activated astrocytes: the critical role of lipocalin-2 in the classical inflammatory activation of astrocytes. *Journal of immunology* 191:5204-5219.

Jeyaseelan, K., K.Y. Lim, and A. Armugam. 2008. MicroRNA expression in the blood and brain of rats subjected to transient focal ischemia by middle cerebral artery occlusion. *Stroke; a journal of cerebral circulation* 39:959-966.

Jin, R., G. Yang, and G. Li. 2010. Inflammatory mechanisms in ischemic stroke: role of inflammatory cells. *Journal of leukocyte biology* 87:779-789.

John, G.R., S.C. Lee, and C.F. Brosnan. 2003. Cytokines: powerful regulators of glial cell activation. *The Neuroscientist : a review journal bringing neurobiology, neurology and psychiatry* 9:10-22.

Jurkin, J., Y.M. Schichl, R. Koeffel, T. Bauer, S. Richter, S. Konradi, B. Gesslbauer, and H. Strobl. 2010. miR-146a is differentially expressed by myeloid dendritic cell subsets and desensitizes cells to TLR2-dependent activation. *Journal of immunology* 184:4955-4965.

Keller, A.F., M. Gravel, and J. Kriz. 2011. Treatment with minocycline after disease onset alters astrocyte reactivity and increases microgliosis in SOD1 mutant mice. *Experimental neurology* 228:69-79.

Kho, W. 2015. Modulation of the immune response after experimental stroke. In.

Kigerl, K.A., J.C. Gensel, D.P. Ankeny, J.K. Alexander, D.J. Donnelly, and P.G. Popovich. 2009. Identification of two distinct macrophage subsets with divergent effects causing either neurotoxicity or regeneration in the injured mouse spinal cord. *The Journal of neuroscience : the official journal of the Society for Neuroscience* 29:13435-13444.

Kobayashi, K., S. Imagama, T. Ohgomori, K. Hirano, K. Uchimura, K. Sakamoto, A. Hirakawa, H. Takeuchi, A. Suzumura, N. Ishiguro, and K. Kadomatsu. 2013. Minocycline selectively inhibits M1 polarization of microglia. *Cell death & disease* 4:e525.

Komohara, Y., K. Ohnishi, J. Kuratsu, and M. Takeya. 2008. Possible involvement of the M2 anti-inflammatory macrophage phenotype in growth of human gliomas. *The Journal of pathology* 216:15-24.

Koralov, S.B., S.A. Muljo, G.R. Galler, A. Krek, T. Chakraborty, C. Kanellopoulou, K. Jensen, B.S. Cobb, M. Merkenschlager, N. Rajewsky, and K. Rajewsky. 2008. Dicer ablation affects antibody diversity and cell survival in the B lymphocyte lineage. *Cell* 132:860-874.

Koscso, B., B. Csoka, E. Kokai, Z.H. Nemeth, P. Pacher, L. Virag, S.J. Leibovich, and G. Hasko. 2013. Adenosine augments IL-10-induced STAT3 signaling in M2c macrophages. *Journal of leukocyte biology* 94:1309-1315.

Krausgruber, T., K. Blazek, T. Smallie, H. Lockstone, N. Sahgal, S. Alzabin, T. Hussell, M. Feldmann, and I. Udalova. 2011. Irf5 Promotes Inflammatory Macrophage Polarization and Th1/Th17 Response. *Rheumatology* 50:54-54.

Kriz, J. 2006. Inflammation in ischemic brain injury: timing is important. *Critical reviews in neurobiology* 18:145-157.

Krol, J., V. Busskamp, I. Markiewicz, M.B. Stadler, S. Ribi, J. Richter, J. Duebel, S. Bicker, H.J. Fehling, D. Schubeler, T.G. Oertner, G. Schratt, M. Bibel, B. Roska, and W. Filipowicz. 2010. Characterizing light-regulated retinal microRNAs reveals rapid turnover as a common property of neuronal microRNAs. *Cell* 141:618-631.

Kwon, M.J., J. Kim, H. Shin, S.R. Jeong, Y.M. Kang, J.Y. Choi, D.H. Hwang, and B.G. Kim. 2013. Contribution of macrophages to enhanced regenerative capacity of dorsal root ganglia sensory neurons by conditioning injury. *The Journal of neuroscience : the official journal of the Society for Neuroscience* 33:15095-15108.

Lange, P.S., B. Langley, P. Lu, and R.R. Ratan. 2004. Novel roles for arginase in cell survival, regeneration, and translation in the central nervous system. *The Journal of nutrition* 134:2812S-2817S; discussion 2818S-2819S.

Lau, L.T., and A.C. Yu. 2001. Astrocytes produce and release interleukin-1, interleukin-6, tumor necrosis factor alpha and interferon-gamma following traumatic and metabolic injury. *Journal of neurotrauma* 18:351-359.

Li, C., R. Zhao, K. Gao, Z. Wei, M.Y. Yin, L.T. Lau, D. Chui, and A.C. Yu. 2011. Astrocytes: implications for neuroinflammatory pathogenesis of Alzheimer's disease. *Current Alzheimer research* 8:67-80.

Li, L., A. Lundkvist, D. Andersson, U. Wilhelmsson, N. Nagai, A.C. Pardo, C. Nodin, A. Stahlberg, K. Aprico, K. Larsson, T. Yabe, L. Moons, A. Fotheringham, I. Davies, P. Carmeliet, J.P. Schwartz, M. Pekna, M. Kubista, F. Blomstrand, N. Maragakis, M. Nilsson, and M. Pekny. 2008. Protective role of reactive astrocytes in brain ischemia. *Journal of cerebral blood flow and metabolism : official journal of the International Society of Cerebral Blood Flow and Metabolism* 28:468-481.

Li, T., S. Pang, Y. Yu, X. Wu, J. Guo, and S. Zhang. 2013. Proliferation of parenchymal microglia is the main source of microgliosis after ischaemic stroke. *Brain : a journal of neurology* 136:3578-3588.

Liu, T., W. Im, I. Mook-Jung, and M. Kim. 2015a. MicroRNA-124 slows down the progression of Huntington's disease by promoting neurogenesis in the striatum. *Neural regeneration research* 10:786-791.

Liu, X., F. Li, S. Zhao, Y. Luo, J. Kang, H. Zhao, F. Yan, S. Li, and X. Ji. 2013. MicroRNA-124-mediated regulation of inhibitory member of apoptosis-stimulating protein of p53 family in experimental stroke. *Stroke; a journal of cerebral circulation* 44:1973-1980.

Liu, X.S., M. Chopp, R.L. Zhang, T. Tao, X.L. Wang, H. Kassis, A. Hozeska-Solgot, L. Zhang, C. Chen, and Z.G. Zhang. 2011. MicroRNA profiling in subventricular zone after stroke: MiR-124a regulates proliferation of neural progenitor cells through Notch signaling pathway. *PloS one* 6:e23461.

Liu, Y., J. Zhang, R. Han, H. Liu, D. Sun, and X. Liu. 2015b. Downregulation of serum brain specific microRNA is associated with inflammation and infarct volume in acute ischemic stroke. *Journal of clinical neuroscience : official journal of the Neurosurgical Society of Australasia* 22:291-295.

Liu, Z., Y. Fan, S.J. Won, M. Neumann, D. Hu, L. Zhou, P.R. Weinstein, and J. Liu. 2007. Chronic treatment with minocycline preserves adult new neurons and reduces functional impairment after focal cerebral ischemia. *Stroke; a journal of cerebral circulation* 38:146-152.

Lourbopoulos, A., A. Erturk, and F. Hellal. 2015. Microglia in action: how aging and injury can change the brain's guardians. *Frontiers in cellular neuroscience* 9:54.

Louw, A.M., M.K. Kolar, L.N. Novikova, P.J. Kingham, M. Wiberg, J. Kjems, and L.N. Novikov. 2015. Chitosan polyplex mediated delivery of miRNA-124 reduces activation of microglial cells in vitro and in rat models of spinal cord injury. *Nanomedicine : nanotechnology, biology, and medicine*

Macrez, R., C. Ali, O. Toutirais, B. Le Mauff, G. Defer, U. Dirnagl, and D. Vivien. 2011. Stroke and the immune system: from pathophysiology to new therapeutic strategies. *The Lancet. Neurology* 10:471-480.

Makeyev, E.V., J. Zhang, M.A. Carrasco, and T. Maniatis. 2007. The MicroRNA miR-124 promotes neuronal differentiation by triggering brain-specific alternative pre-mRNA splicing. *Molecular cell* 27:435-448.

Mammele, S., K. Frauenknecht, S. Sevimli, K. Diederich, H. Bauer, J. Minnerup, W.R. Schabitz, and C.J. Sommer. 2015. Prevention of an increase in cortical ligand binding to AMPA receptors may represent a novel mechanism of endogenous brain protection by G-CSF after ischemic stroke. *Restorative neurology and neuroscience*

Miron, V.E., A. Boyd, J.W. Zhao, T.J. Yuen, J.M. Ruckh, J.L. Shadrach, P. van Wijngaarden, A.J. Wagers, A. Williams, R.J. Franklin, and C. ffrench-Constant. 2013. M2 microglia and macrophages drive oligodendrocyte differentiation during CNS remyelination. *Nature neuroscience* 16:1211-1218.

Mitsios, N., J. Gaffney, P. Kumar, J. Krupinski, S. Kumar, and M. Slevin. 2006. Pathophysiology of acute ischaemic stroke: an analysis of common signalling mechanisms and identification of new molecular targets. *Pathobiology : journal of immunopathology, molecular and cellular biology* 73:159-175.

Mizutani, M., P.A. Pino, N. Saederup, I.F. Charo, R.M. Ransohoff, and A.E. Cardona. 2012. The fractalkine receptor but not CCR2 is present on microglia from embryonic development throughout adulthood. *Journal of immunology* 188:29-36.

Morel, L., M. Regan, H. Higashimori, S.K. Ng, C. Esau, S. Vidensky, J. Rothstein, and Y. Yang. 2013. Neuronal exosomal miRNA-dependent translational regulation of astroglial glutamate transporter GLT1. *The Journal of biological chemistry* 288:7105-7116.

Moskowitz, M.A., E.H. Lo, and C. Iadecola. 2010. The science of stroke: mechanisms in search of treatments. *Neuron* 67:181-198.

Mosser, D.M., and J.P. Edwards. 2008. Exploring the full spectrum of macrophage activation. *Nature reviews. Immunology* 8:958-969.

Munder, M. 2009. Arginase: an emerging key player in the mammalian immune system. *British journal of pharmacology* 158:638-651.

Napoli, I., K. Kierdorf, and H. Neumann. 2009. Microglial precursors derived from mouse embryonic stem cells. *Glia* 57:1660-1671.

O'Neill, L.A., F.J. Sheedy, and C.E. McCoy. 2011. MicroRNAs: the fine-tuners of Toll-like receptor signalling. *Nature reviews. Immunology* 11:163-175.

Oikawa, H., W.W. Goh, V.K. Lim, L. Wong, and J.C. Sng. 2015. Valproic acid mediates miR-124 to down-regulate a novel protein target, GNAI1. *Neurochemistry international* 91:62-71.

Opanasopit, P., O. Paecharoenchai, T. Rojanarata, T. Ngawhirunpat, and U. Ruktanonchai. 2011. Type and composition of surfactants mediating gene transfection of polyethylenimine-coated liposomes. *International journal of nanomedicine* 6:975-983.

Paixao, S., and R. Klein. 2010. Neuron-astrocyte communication and synaptic plasticity. *Current opinion in neurobiology* 20:466-473.

Pan, J., J.L. Jin, H.M. Ge, K.L. Yin, X. Chen, L.J. Han, Y. Chen, L. Qian, X.X. Li, and Y. Xu. 2015. Malibatol A regulates microglia M1/M2 polarization in experimental stroke in a PPARgamma-dependent manner. *J Neuroinflammation* 12:51.

Paxinos, G.F.K. 2001. The Mouse Brain in Stereotaxic Coordinates. *Academic press*

Pekny, M., U. Wilhelmsson, and M. Pekna. 2014. The dual role of astrocyte activation and reactive gliosis. *Neuroscience letters* 565:30-38.

Perego, C., S. Fumagalli, and M.G. De Simoni. 2011. Temporal pattern of expression and colocalization of microglia/macrophage phenotype markers following brain ischemic injury in mice. *Journal of neuroinflammation* 8:174.

Polfliet, M.M., P.J. Zwijnenburg, A.M. van Furth, T. van der Poll, E.A. Dopp, C. Renardel de Lavalette, E.M. van Kesteren-Hendrikx, N. van Rooijen, C.D. Dijkstra, and T.K. van den Berg. 2001. Meningeal and perivascular macrophages of the central nervous system play a protective role during bacterial meningitis. *Journal of immunology* 167:4644-4650.

Ponomarev, E.D., T. Veremeyko, N. Barteneva, A.M. Krichevsky, and H.L. Weiner. 2011. MicroRNA-124 promotes microglia quiescence and suppresses EAE by deactivating macrophages via the C/EBP-alpha-PU.1 pathway. *Nature medicine* 17:64-70.

Ponomarev, E.D., T. Veremeyko, and H.L. Weiner. 2013. MicroRNAs are universal regulators of differentiation, activation, and polarization of microglia and macrophages in normal and diseased CNS. *Glia* 61:91-103.

Popovich, P.G., and W.F. Hickey. 2001. Bone marrow chimeric rats reveal the unique distribution of resident and recruited macrophages in the contused rat spinal cord. *Journal of neuropathology and experimental neurology* 60:676-685.

Quirie, A., C. Demougeot, N. Bertrand, C. Mossiat, P. Garnier, C. Marie, and A. Prigent-Tessier. 2013. Effect of stroke on arginase expression and localization in the rat brain. *The European journal of neuroscience* 37:1193-1202.

Ransohoff, R.M. 2011. Microglia and monocytes: 'tis plain the twain meet in the brain. *Nature neuroscience* 14:1098-1100.

Ransohoff, R.M., L. Liu, and A.E. Cardona. 2007. Chemokines and chemokine receptors: multipurpose players in neuroinflammation. *International review of neurobiology* 82:187-204.

Ransohoff, R.M., and V.H. Perry. 2009. Microglial physiology: unique stimuli, specialized responses. *Annual review of immunology* 27:119-145.

Raposo, C., and M. Schwartz. 2014. Glial scar and immune cell involvement in tissue remodeling and repair following acute CNS injuries. *Glia* 62:1895-1904.

Ricci, G., L. Volpi, L. Pasquali, L. Petrozzi, and G. Siciliano. 2009. Astrocyte-neuron interactions in neurological disorders. *Journal of biological physics* 35:317-336.

Ritzel, R.M., A.R. Patel, J.M. Grenier, J. Crapser, R. Verma, E.R. Jellison, and L.D. McCullough. 2015. Functional differences between microglia and monocytes after ischemic stroke. *Journal of neuroinflammation* 12:106.

Rolls, A., R. Shechter, A. London, Y. Segev, J. Jacob-Hirsch, N. Amariglio, G. Rechavi, and M. Schwartz. 2008. Two faces of chondroitin sulfate proteoglycan in spinal cord repair: a role in microglia/macrophage activation. *PLoS medicine* 5:e171.

Rolls, A., R. Shechter, and M. Schwartz. 2009. The bright side of the glial scar in CNS repair. *Nature reviews. Neuroscience* 10:235-241.

Sanuki, R., A. Onishi, C. Koike, R. Muramatsu, S. Watanabe, Y. Muranishi, S. Irie, S. Uneo, T. Koyasu, R. Matsui, Y. Cherasse, Y. Urade, D. Watanabe, M. Kondo, T. Yamashita, and T. Furukawa. 2011. miR-124a is required for hippocampal axogenesis and retinal cone survival through Lhx2 suppression. *Nature neuroscience* 14:1125-1134.

Saugstad, J.A. 2010. MicroRNAs as effectors of brain function with roles in ischemia and injury, neuroprotection, and neurodegeneration. *Journal of cerebral blood flow and metabolism : official journal of the International Society of Cerebral Blood Flow and Metabolism* 30:1564-1576.

Saugstad, J.A. 2015. Non-Coding RNAs in Stroke and Neuroprotection. *Frontiers in neurology* 6:50.

Schilling, M., M. Besselmann, C. Leonhard, M. Mueller, E.B. Ringelstein, and R. Kiefer. 2003. Microglial activation precedes and predominates over macrophage infiltration in transient focal cerebral ischemia: a study in green fluorescent protein transgenic bone marrow chimeric mice. *Experimental neurology* 183:25-33.

Schwartz, M., and R. Shechter. 2010. Systemic inflammatory cells fight off neurodegenerative disease. *Nature reviews. Neurology* 6:405-410.

Sempere, L.F., S. Freemantle, I. Pitha-Rowe, E. Moss, E. Dmitrovsky, and V. Ambros. 2004. Expression profiling of mammalian microRNAs uncovers a subset of brain-expressed microRNAs with possible roles in murine and human neuronal differentiation. *Genome biology* 5:R13.

Shaham, S. 2005. Glia-neuron interactions in nervous system function and development. *Current topics in developmental biology* 69:39-66.

Shechter, R., A. London, C. Varol, C. Raposo, M. Cusimano, G. Yovel, A. Rolls, M. Mack, S. Pluchino, G. Martino, S. Jung, and M. Schwartz. 2009. Infiltrating blood-derived macrophages are vital cells playing an anti-inflammatory role in recovery from spinal cord injury in mice. *PLoS medicine* 6:e1000113.

Shechter, R., C. Raposo, A. London, I. Sagi, and M. Schwartz. 2011. The glial scar-monocyte interplay: a pivotal resolution phase in spinal cord repair. *PloS one* 6:e27969.

Shichita, T., M. Ito, and A. Yoshimura. 2014. Post-ischemic inflammation regulates neural damage and protection. *Frontiers in cellular neuroscience* 8:319.

Smith, A.M., and M. Dragunow. 2014. The human side of microglia. *Trends in neurosciences* 37:125-135.

Sofroniew, M.V. 2009. Molecular dissection of reactive astrogliosis and glial scar formation. *Trends in neurosciences* 32:638-647.

Sofroniew, M.V., and H.V. Vinters. 2010. Astrocytes: biology and pathology. *Acta neuropathologica* 119:7-35.

Sun, Y., H. Gui, Q. Li, Z.M. Luo, M.J. Zheng, J.L. Duan, and X. Liu. 2013. MicroRNA-124 protects neurons against apoptosis in cerebral ischemic stroke. *CNS neuroscience & therapeutics* 19:813-819.

Taganov, K.D., M.P. Boldin, K.J. Chang, and D. Baltimore. 2006. NF-kappaB-dependent induction of microRNA miR-146, an inhibitor targeted to signaling proteins of innate immune responses. *Proceedings of the National Academy of Sciences of the United States of America* 103:12481-12486.

Tan, K.S., A. Armugam, S. Sepramaniam, K.Y. Lim, K.D. Setyowati, C.W. Wang, and K. Jeyaseelan. 2009. Expression profile of MicroRNAs in young stroke patients. *PloS one* 4:e7689.

Tennstaedt, A., M. Aswendt, J. Adamczak, U. Collienne, M. Selt, G. Schneider, N. Henn, C. Schaefer, M. Lagouge, D. Wiedermann, P. Kloppenburg, and M. Hoehn. 2015. Human neural stem cell intracerebral grafts show spontaneous early neuronal differentiation after several weeks. *Biomaterials* 44:143-154.

Thored, P., U. Heldmann, W. Gomes-Leal, R. Gisler, V. Darsalia, J. Taneera, J.M. Nygren, S.E. Jacobsen, C.T. Ekdahl, Z. Kokaia, and O. Lindvall. 2009. Long-term accumulation of microglia with proneurogenic phenotype concomitant with persistent neurogenesis in adult subventricular zone after stroke. *Glia* 57:835-849.

Tili, E., J.J. Michaille, A. Cimino, S. Costinean, C.D. Dumitru, B. Adair, M. Fabbri, H. Alder, C.G. Liu, G.A. Calin, and C.M. Croce. 2007. Modulation of miR-155 and miR-125b levels following lipopolysaccharide/TNF-alpha stimulation and their possible roles in regulating the response to endotoxin shock. *Journal of immunology* 179:5082-5089.

Wang, G., J. Zhang, X. Hu, L. Zhang, L. Mao, X. Jiang, A.K. Liou, R.K. Leak, Y. Gao, and J. Chen. 2013. Microglia/macrophage polarization dynamics in white matter after traumatic brain injury. *Journal of cerebral blood flow and metabolism : official journal of the International Society of Cerebral Blood Flow and Metabolism* 33:1864-1874.

Wang, H., Y. Ye, Z. Zhu, L. Mo, C. Lin, Q. Wang, H. Wang, X. Gong, X. He, G. Lu, F. Lu, and S. Zhang. 2015. MiR-124 Regulates Apoptosis and Autophagy Process in MPTP Model of Parkinson's Disease by Targeting to Bim. *Brain pathology*

Weng, H., C. Shen, G. Hirokawa, X. Ji, R. Takahashi, K. Shimada, C. Kishimoto, and N. Iwai. 2011. Plasma miR-124 as a biomarker for cerebral infarction. *Biomedical research* 32:135-141.

Willemen, H.L., X.J. Huo, Q.L. Mao-Ying, J. Zijlstra, C.J. Heijnen, and A. Kavelaars. 2012. MicroRNA-124 as a novel treatment for persistent hyperalgesia. *Journal of neuroinflammation* 9:143.

Wrobel, I., and D. Collins. 1995. Fusion of cationic liposomes with mammalian cells occurs after endocytosis. *Biochimica et biophysica acta* 1235:296-304.

Xia, C.Y., S. Zhang, Y. Gao, Z.Z. Wang, and N.H. Chen. 2015. Selective modulation of microglia polarization to M2 phenotype for stroke treatment. *International immunopharmacology* 25:377-382.

Yilmaz, G., T.V. Arumugam, K.Y. Stokes, and D.N. Granger. 2006. Role of T lymphocytes and interferon-gamma in ischemic stroke. *Circulation* 113:2105-2112.

Young, A.R., C. Ali, A. Duretete, and D. Vivien. 2007. Neuroprotection and stroke: time for a compromise. *Journal of neurochemistry* 103:1302-1309.

Yu, J.Y., K.H. Chung, M. Deo, R.C. Thompson, and D.L. Turner. 2008. MicroRNA miR-124 regulates neurite outgrowth during neuronal differentiation. *Experimental cell research* 314:2618-2633.

Zhu, F., J.L. Liu, J.P. Li, F. Xiao, Z.X. Zhang, and L. Zhang. 2014. MicroRNA-124 (miR-124) regulates Ku70 expression and is correlated with neuronal death induced by ischemia/reperfusion. *Journal of molecular neuroscience : MN* 52:148-155.

Appendix

List of abbreviations

ANOVA	Analysis of variance
Arg-1	Arginase-1
ATP	Adenosine-tri-phosphate
BBB	Blood-brain-barrier
Bcl-2/Bcl-xl	B-cell lymphoma
BDNF	Brain-derived neurotrophic factor
BMDM	Bone marrow derived macrophage
CBF	Cerebral blood flow
CCA	Common carotid artery
CD	Classification determinant
cm2	Square centimetre
CNS	Central nervous system
CSPGs	Chondroitin sulphate proteoglycans
DAMPs	Damage-associated molecular pattern molecules
DC	Dendritic cells
DNA	Deoxyribonucleic acid
EAE	Experimental autoimmune encephalomyelitis
ECM	Extracellular matrix
FID	Free induction decay
FOV	Field of view
g	Gram
GFAP	Glial fibrillary acidic protein
h	Hour
iASPP	Inhibitor of apoptosis-stimulating protein of p53
Iba-1	Ionized calcium-binding adapter molecule 1
I.V	Intravenous

IFN-ϒ	Interferon gamma
IGF-1	Insulin-like growth factor 1
IHC	Immunohistochemistry
IL	Interleukin
iNOS	Inducible nitric oxide synthase
KCL	Potassium chloride
KPBS	potassium phosphate buffered saline
KH2PO4	Potassium dihydrogen orthophosphate
LPS	Lipopolysaccharide
MCA	Middle cerebral artery
MCAO	Middle cerebral artery occlusion
µg	Microgramme
min	Minute
miR	MicroRNA
miRNA	MicroRNA
ml	Milliliter
µl	Microliter
ML	Medial-lateral
mNDS	Modified neurological deficit score
MRI	Magnetic resonance imaging
mRNA	Messenger RNA
ms	Millisecond
MSME	Multi-slice multi-echo
N2O	Nitrous oxide
NaCl	Sodium chloride
NaOH	Sodium hydroxide
NDS	Normal donkey serum

NeuN	Neuronal nuclear antigen
NGF	Nerve growth factor
NO	Nitric oxide
O2	Oxygen
OGD	Oxygen glucose deprivation
PBS	Phosphate-buffered saline
PFA	Paraformaldehyde
pO2	Partial pressure of oxygen
REST	RE1-silecing transcription facto
ROI	Region of interest
RT	Room temperature (20°C)
s	second
SD	Standard deviation
STAT3	Signal transducer and activator of transcription 3
TE	Echo time
TGF-β	Transforming growth factor-beta
TNF-α	Tumor necrosis factor-alpha
TR	Repetition time
tPA	Tissue plasminogen activator
Usp-14	Ubiquitin carboxyl-terminal hydrolase 14

List of Figures

Figure 1.1: Different types of stroke……11

Figure 1.2: Events after cerebral ischemia……12

Figure 1.3: Interactions between neurons, microglia and astroctyes……13

Figure 1.4: Time dependent recruitment of inflammatory cells into the brain following focal cerebral ischemia……14

Figure 1.5: Embryonic origins of macrophages and microglia……15

Figure 1.6: The microglia and macrophages interplay after CNS injury……16

Figure 1.7: Polarization of microglia and macrophages……18

Figure 1.8: Dynamic reactive astrocytes in the penumbra at different stages after stroke……20

Figure 1.9: Astrocyte reactions after CNS injury……20

Figure 1.10: Factors involved in the polarization of microglia and macrophages……22

Figure 1.11: The role of miRNAs in the regulation of immune reactions……23

Figure 1.12: The role of miR-124 on modulating the polarization of microglia……24

Figure 2.1: Timelines of the experimental protocols……28

Figure 2.2: Middle cerebral artery occlusion model……29

Figure 2.3: Schematic representation of the mouse brain in stereotaxic coordinates.. ……30

Figure 2.4: Schematic representation of glial scar and lesion size area……36

Figure 3.1: Characterization of the development of ischemic lesion after MCAO……39

Figure 3.2: Comparison of ΔT2 time in three experimental protocols at day 2, 6 and 14 after MCAO……40

Figure 3.3: Comparison of T2 lesion volume in three experimental protocols at day 2, 6 and 14 after MCAO……41

Figure 3.4: Different morphology and kinetics of microglia and macrophages after stroke……43

Figure 3.5: Dynamic proliferation of Iba-1^{+} cells after intracranial injection of miR-124 in stroke model……45

Figure 3.6: Effect of miR-124 on M2 phase of Microglia and macrophages……48

Figure 3.7: Effect of miR-124 on M2 phase of microglia and macrophages……49

Figure 3.8: Effect of miR-124 on M1 phase of microglia and macrophages……..……..……..50

Figure 3.9: Effect of miR-124 on M2 phase of microglia and macrophages at day 14 after stroke of second experimental protocol……..……..……5
3

Figure 3.10: Effect of miR-124 on M2 phase of microglia and macrophages at day 14 after stroke of second experimental protocol……..……..……..……..54

Figure 3.11: Effect of miR-124 on M1 phase of microglia and macrophages at day 14 after stroke of second experimental protocol……..……..55

Figure 3.12: Effect of delayed miR-124 injection on M2 phenotype of microglia and macrophages..57

Figure 3.13: Effect of delayed miR-124 injection on M1 phenotype of microglia and macrophages..58

Figure 3.14: Effect of miR-124 on the M1:M2 ratio of microglia and macrophages in the border region of striatal lesion……..60

Figure 3.15: Effect of miR-124 on the M1:M2 ratio of microglia and macrophages in the border region of cortical lesion……60

Figure 3.16: Different morphology of NeuN positive cells after stroke……..61

Figure 3.17: Effect of early intracranial injection of miR-124, day 2 after MCAO, on neuronal survival……..63

Figure 3.18: The effect of early intracranial injection of miR-124, at day 2 after MCAO, on neuronal survival at day 6 after MCAO……..64

Figure 3.19: The effect of late intracranial injection of miR-124, 10 days after MCAO, on neuronal survival……..……65

Figure 3.20: Reactive astrogliosis and the scar formation over time……66

Figure 3.21: The effect of miR-124 on reactive astrocytes and the glial scar development……..67

Figure 3.22: The effect of miR-124 on reactive astrocytes and the glial scar development……..68

Figure 3.23: The effect of early intracranial injection of miR-124 on functional recovery after stroke..
……69

Figure 3.24: The effect of late intracranial injection of miR-124 on functional recovery after stroke..
……..70

Figure 3.25: Correlation between M2 markers expression and mNDS……..71

Figure 3.26: Correlation between M1 marker expression and mNDS……..……..72

Figure 3.27: Correlation between M2 marker expression and NeuN$^+$ cell number……..……..73

Figure 3.28: Correlation between M1 marker expression and NeuN$^+$ cells number……..74

Figure 4.1: Multifactorial effect of miR-124 on improved functional recovery……..86

List of publication

1) **Hamzei Taj S,** Kho W, Riou A, Wiedermann D, Hoehn M. 2016. MiRNA-124 induces neuroprotection and functional improvement after focal cerebral ischemia. Biomaterials 91: 151-165

2) **Hamzei Taj S,** Kho W, Aswendt M, Collmann F , Hefeneger C, Adamczak J, Tennstaedt A, Hoehn M. Dynamic modulation of microglia/macrophage polarization by miR-124 after focal cerebral ischemia. (In preparation)

Acknowledgement

First of all, I would like to express my sincere appreciation and thanks to my advisor Prof. Dr. Mathias Hoehn for the continuous support of my Ph.D study, for his patience, insightful comments, and extensive knowledge and expertise.

Besides my advisor, I would like to thank all members of the In-vivo-NMR group for the pleasant working atmosphere and for their support. I have been fortunate to work with Widuri Kho, who her master thesis was a part of my study. Our teamwork contributed to the completion of my work. I would like to thank Melanie Nelles for teaching me the histology and Andreas Beyrau for teaching me the MCAO procedure. I also like to thank Ulla Uhlenküken, who helped me with the arrangement of the graphics. I particularly thank Stefanie Vogel for her great help to write the ''Zusammenfassung''.

My sincere thanks also goes to my PhD colleagues in my lab at the Max Planck Institute in Cologne, Markus, Joanna, Annette, Adrien, Claudia, Franzi, Marion, Stephie, Luam, and Anuka. Thank you for sharing ideas, stimulating discussions and experiences.

I really appreciate the financial support of Ministry of Health & Medical Education of Islamic Republic of Iran for the first 4 years of my Ph.D study.

Last but not the least, I would like to thank my family: my lovely mother and my brothers and sister for supporting me spiritually throughout my study and my life. My thanks to my beloved husband Reza for supporting me during all the times of my Ph.D study. At the end I would like to dedicate my dissertation to my father to keep his spirit alive.